

THE CHARGE TRANSPORT IN LIQUID SULPHUR

AND

FLUORESCENCE OF THE SOLID

A thesis submitted to the

University of Leicester

by

P. K. Ghosh, M. Sc.,

For the degree of

Doctor of Philosophy

UMI Number: U622418

All rights reserved

INFORMATION TO ALL USERS

The quality of this reproduction is dependent upon the quality of the copy submitted.

In the unlikely event that the author did not send a complete manuscript and there are missing pages, these will be noted. Also, if material had to be removed, a note will indicate the deletion.



UMI U622418

Published by ProQuest LLC 2015. Copyright in the Dissertation held by the Author.
Microform Edition © ProQuest LLC.

All rights reserved. This work is protected against
unauthorized copying under Title 17, United States Code.



ProQuest LLC
789 East Eisenhower Parkway
P.O. Box 1346
Ann Arbor, MI 48106-1346

X75299582X

546.723
335378
30-5-68



CONTENTS

	Page
<u>Acknowledgements</u>	v
<u>Abstract</u>	vi
<u>Chapter 1 : Introduction</u>	1
<u>Chapter 2 : Review of Charge Transport in Molecular</u>	
<u>Liquids</u>	3
Hexane -----	5
Pyrene -----	9
Benzene -----	9
Rare - Gas Liquids -----	12
Concluding Remarks -----	13
<u>Chapter 3 : Properties of Solid and Liquid Sulphur</u>	17
3.1 : Transport Properties of Solid Sulphur ----	17
Small Polaron Theory -----	18
Hopping Transport of Electrons in Sulphur -	20
Band Structure of Orthorhombic Sulphur ---	23
3.2 : Physical Properties of Liquid Sulphur ---	24
Polymerisation of Liquid Sulphur -----	25
<u>Chapter 4 : Experimental Methods</u>	27
4.1 : Principle of Drift Mobility Measurements -	27
4.2 : General Description of Apparatus for Measuring	
Drift Mobility -----	32
Experimental Procedure -----	33
4.3 : Specimen Chamber -----	34

	Page
4.4 : Preparation of Electrodes -----	36
Gold Electrodes -----	37
Nesa Electrodes -----	37
Platinum Electrodes -----	38
4.5 : Light Sources -----	39
4.6 : Detection -----	41
4.7 : Field Unit -----	41
4.8 : Growth of Sulphur from Solution -----	43
4.9 : Growth of Sulphur from the Melt -----	43
4.10: Growth of Sulphur from Vapour Phase -----	45
<u>Chapter 5 : Experimental Results</u>	46
5.1 : Introduction -----	46
5.2 : Laboratory Reagent Sulphur -----	46
Hole and Electron Mobilities in the	
Crystalline Solid -----	47
Charge Transport in the Laboratory Reagent	
Liquid -----	49
Anomalous Field Dependence of $1/t_t'$ -----	50
Field Transient in the Liquid -----	51
5.3 : Liquid Ultrapure Sulphur -----	52
Negative Charge Transport in the Ultrapure	
Liquid Below 160°C -----	53
Negative Charge Transport in the Ultrapure	
Liquid Above 160°C -----	54

Positive Charge Transport in the Ultrapure Liquid Below 160°C -----	55
Positive Charge Transport in the Ultrapure Liquid Above 160°C -----	55
Effect of Heating on Charge Transport in the Ultrapure Liquid -----	56
5.4 : Supercooled Liquid Sulphur -----	57
5.5 : Re - solidified Sulphur -----	57
5.6 : Space Charge Characteristics of Liquid Sulphur	58
Probe Measurements -----	58
Dark Current Measurements -----	60
5.7 : Solid - Liquid Transition of Dark Conductivity	63
5.8 : Efficiency of Carrier Generation in Liquid Sulphur -----	64
Carrier Recombination Lifetime -----	66
<u>Chapter 6 : Discussion</u>	68
6.1 : Introduction -----	68
6.2 : The Nature of Charge Transport in Liquid Sulphur	68
The Nature of Negative Charge Carriers ---	69
The Nature of Positive Charge Carriers ---	73
The Possibility of a Mixed Electronic and Ionic Motion -----	73
6.3 : Charges in the Dark -----	75
6.4 : Charge Transport in Liquid Sulphur Above 160°C	76

	Page
6.5 : Anomalous Behaviour of Photogenerated Charges in Liquid Sulphur -----	79
<u>Chapter 7 : Fluorescence of Sulphur</u>	84
7.1 : Introduction -----	84
7.2 : Experimental Methods and Results -----	87
7.3 : Quantum Yield of Fluorescence -----	90
7.4 : Discussion -----	94
<u>Chapter 8 : Conclusions</u>	97
<u>Tables</u>	100
<u>Appendix I</u>	101
<u>References</u>	102
<u>Figures</u>	

ACKNOWLEDGEMENTS

The author would like to express his thanks to Professor E. A. Stewardson for the opportunity to work in his department. He is greatly indebted to Dr. W. E. Spear for suggesting the research problem and for his generous help and guidance given continuously throughout the investigation. Thanks are due to Professor R. C. Jarnagin for helpful discussion on some aspects of this work.

The author wishes to express his gratitude to the Xerox Corporation of Rochester, U. S. A. for support during this work.

ABSTRACT

Specimens of liquid sulphur were obtained by melting orthorhombic sulphur crystals or ultrapure granules of sulphur. Between the melting point (119°C) and 160°C , liquid sulphur is composed of puckered S_8 ring molecules bound by weak van der Waal forces as in the solid. Above 160°C , polymerisation of ring molecules takes place. Drift mobility techniques have been used to study the charge transport during melting and in the liquid up to about 200°C . The specimen cell consisted of two parallel quartz discs separated by glass spacers, 50 to 700 microns thick. Transparent electrodes were applied to the inner surfaces of the discs. Charge carriers were generated close to one of the electrodes by a fast ultraviolet light pulse (~ 10 microsecond duration), and carriers of one polarity were drawn across the specimen in the applied field. Their transit time was measured giving a value for the drift mobility. The results showed that the charge transport is due to both negative and positive charges which move in the liquid by means of phonon - assisted random hopping between neighbouring molecules. From a detailed discussion of the results it is concluded that we are dealing here with an electronic, rather than an ionic charge transport. The electron and hole mobilities at the melting point are 1.0×10^{-4} and 5.5×10^{-5} $\text{cm}^2/\text{volt sec}$ respectively. ^{The} Electron mobility which is ^a hopping transport in the solid, shows a drop of a factor of 30 during change of state. This has been attributed to a decrease of overlap J by a fac-

tor of 5.5. Between 119°C and 160°C the electron mobility increases in the liquid with increasing temperature with an activation energy of 0.15 ± 0.03 ev. Holes have the same activation energy within a larger experimental error. Above 160°C both electron and hole mobilities decrease slowly with increasing temperature. This has been attributed to a decrease in the hopping probability resulting from a loss of ring molecules by polymerisation.

Dark current measurements on liquid sulphur suggested that in less pure specimens impurity ions set up a space charge near each electrode of opposite polarity to that of the electrode which modifies the current in accordance with Thomson's model of conduction in gases.

The measurement of the efficiency of carrier generation in liquid sulphur has been carried out at an applied field of 33 K volt/cm, considerably less than the saturation value. The results show that the ultraviolet photoconductivity reaches a peak at about 2600 \AA with a generation efficiency of 10^{-2} . The recombination lifetime of generated carriers has been estimated to be about 10^{-7} sec.

The visible emission of solid sulphur under x - ray excitation has been studied. The observed emission has an estimated efficiency between $10^{-4} - 10^{-6}$. Three emission peaks at 4900, 5300 and 5700 \AA have been detected. The emission is thought to be due to λ transitions from a molecular excited state, 2.7 ev above the ground state, to the singlet ground state of λ S_8 molecule.

CHAPTER 1

1

INTRODUCTION

In recent years there has been a growing interest in the electrical transport properties of organic molecular liquids. However, very few investigations have been made in both solid and liquid state. Such studies should be of particular interest in molecular systems such as sulphur in which the interactions between molecules are of the weak van der Waals type. The reason is that a considerable amount of information has recently become available for charge transport in solid sulphur and one would expect much of its transport characteristics should be retained in the molecular liquid. It is the purpose of the present work to investigate the transport properties of sulphur on melting and in the liquid and in particular to correlate the results with the thoroughly understood behaviour of the solid. It is a difficult problem to distinguish experimentally between ionic and electronic transport. It will be shown that the anomalous viscous properties of liquid sulphur are particularly useful in this respect.

Surprisingly little knowledge exists in the field of charge transport in molecular liquids. Chapter two of this thesis gives a short review of previous work. Chapter three discusses the transport properties of solid sulphur. One section has been devoted to the theory of 'hopping transport', as this mechanism is relevant in the interpretation of the results obtained. Chapter three also includes a review of relevant

physical properties, such as viscosity and polymerisation, of liquid sulphur.

In chapter four, the experimental methods used in this work are described. The experimental results are presented in chapter five and the interpretation is discussed in chapter six.

A preliminary investigation of the visible emission spectrum of solid sulphur is also included in this thesis (chapter seven).

Chapter eight summarises the conclusions.

REVIEW OF CHARGE TRANSPORT IN MOLECULAR LIQUIDS

Until comparatively recently much of the interest in dielectric liquids derived from their use as practical insulators. It is clear, however, that the complete explanation of phenomena such as breakdown and conduction in technical liquids and simple hydrocarbons requires much more fundamental information about charge transfer as a whole. The main problem in work on technical liquids is to identify the charge carriers and to analyse the transport mechanism. The interpretation of such measurements is often difficult because of the predominant effects of space charge and impurities.

A wide range of measurements of carrier mobilities in hydrocarbons, paraffins and silicones were reported by Adamczewski ⁽¹⁾ on behalf of a group of workers in Poland. This group has largely concentrated on the properties of carriers formed by x-ray irradiation of the liquid. The room temperature mobilities are of the correct order of magnitude for ions: about 10^{-3} - 10^{-4} cm²/volt sec in normal hydrocarbons and paraffins, falling to 10^{-5} - 10^{-6} cm²/volt sec in highly viscous liquids. The temperature variation shows that the mobilities of the negative carriers are inversely proportional to the viscosity of the liquid as expected for ions obeying Walden's rule (see below). However, the smaller mobilities of the positive carriers vary more rapidly with temperature; this has been taken as an indication that this ion is possibly not a stable entity.

Walden's rule ⁽²⁾ is an empirical principle which states that, for ions in solution, the product of ion mobility and solvent viscosity is a constant independent of temperature. The theoretical basis ⁽³⁾ of Walden's rule is well understood. The aqueous solutions of a wide range of liquids follow this behaviour closely. This rule can be derived simply from Stokes' law ⁽⁴⁾ as follows. For a spherical body of radius r moving through a medium of viscosity η , Stokes showed that the drag force on the sphere due to the viscosity of the liquid is,

$$F = 6 \pi \eta r v \quad \text{-----}(2.1)$$

where v is the terminal velocity of the sphere. For a spherical ion of radius r and charge q moving with a velocity v under the influence of an applied field E , $F = qE$ and $v = \mu E$, where μ is the ionic mobility. Eq.(2.1) can now be written as,

$$\mu \eta = \frac{q}{6 \pi r} = \text{constant} \quad \text{-----}(2.2)$$

which is Walden's rule. For a sphere the value of the constant is $q/6 \pi r$. It will, however, be modified by the shape of the ion ⁽⁴⁾.

The predicted ionic mobility is thus,

$$\mu = \frac{q}{6 \pi \eta r} \quad 10^7 \text{ cm}^2/\text{volt sec} \quad \text{-----}(2.3)$$

where q is in coulombs, r in cm and η in poise.

Caravajal et al. ⁽⁵⁾ have shown that in some organic solvents the mobility of ions whose radius was greater than about 5 \AA could be reliably estimated from Stokes' law. For smaller ions or in polar sol-

utions, Stoke's relation is a poorer estimate and one should use an effective radius for the ions. deGroot, Gary and Jarnagin (6) made an estimate of the effective ion radius using a simple electrostatic model. It appears that the effective radius is larger due to solvent molecules attaching themselves to the ion.

Hexane

Among the hydrocarbons and other liquids, the $C_n H_{(2n+2)}$ family of saturated hydrocarbons has been most extensively studied. The negative and positive carrier mobilities in hexane ($n = 6$) at $20^\circ C$ as obtained by several authors are shown in Table 2.1. It is interesting to review LeBlanc's results in some detail.

The mobility of negative charge carriers in hexane as measured by LeBlanc is 1.4×10^{-3} cm²/volt sec at $27^\circ C$. Furthermore, the mobility varies exponentially with temperature and is given by,

$$\mu = A \exp(-E/kT) \quad \text{-----}(2.4)$$

where $A = 0.3 \pm 0.2$ cm²/volt sec and E , the activation energy, is 0.14 ± 0.02 ev. From the activation energy ^{of viscosity} quoted by him to be 0.073 ev, it appears that the product of mobility and the liquid viscosity is anomalous with respect to Walden's rule. LeBlanc also measured the mobility ratio of negative charges in hexane and heptane; this is 1.1 ± 0.2 . If the charge carriers in the two liquids were homologous

* Forster quotes a value of 0.1 ev for the viscosity activation energy (18)

negative molecular ions, then this ratio should be larger. This evidence points against an ionic transport mechanism. LeBlanc therefore proposed an alternative model according to which the excess carrier is an electron which travels some distance before being trapped temporarily on an impurity molecule. ('Trapping' is used here in a different sense from that in a solid. In the liquid, a molecule traps a carrier and becomes charged; the ion thus formed can move under the influence of an applied field. The motion of the charge is therefore a mixed motion of ions and electrons and the drift velocity is $v = v_{\text{ion}} + v_{\text{electron}}$. It is possible to talk about trapping in liquids if $v_{\text{electron}} \gg v_{\text{ion}}$). If the average time spent by the electron in such a trap is τ_t and that spent between trapping events is τ_{free} , then the effective electron drift mobility is given by

$$\mu = \mu_0 \frac{\tau_{\text{free}}}{\tau_t + \tau_{\text{free}}} \quad \text{-----} (2.5)$$

where μ_0 is the electron mobility in the absence of trapping. Furthermore, if in the range of temperature investigated $\tau_t \gg \tau_{\text{free}}$, then

$$\mu = \mu_0 \frac{\tau_{\text{free}}}{\tau_0} \exp(-\epsilon_t/kT) \quad \text{-----} (2.6)$$

as the probability of thermal release is equal to $\tau_0^{-1} \exp(-\epsilon_t/kT)$.

The activation energy of mobility of negative charges in hexane has been identified with ϵ_t and interpreted as the average trapping energy for electrons. According to LeBlanc some evidence for the above model has been provided by Crowe's measurements in hexane (12).

Crowe, making measurements in saturated hydrocarbons at breakdown fields, obtained a value of $9 \times 10^{-3} \text{ cm}^2/\text{volt sec}$ for the negative charge mobility in hexane at a field of $1.5 \times 10^6 \text{ volt/cm}$. This is a factor of 6.5 larger than LeBlanc's value. Crowe's method of measuring mobility was, however, different in that the transit time of an electron was assumed to be the same as the 'formative time lag' of breakdown discharge. (This is the time required between an electron emission by the cathode and the appearance of a spark due to 'collision ionisation' caused by the electron). Crowe also found that the formative time lag[‡] (or the mobility) was approximately the same for a wide variety of liquids of different molecular weight and viscosity. He concluded that the mobility calculated from the data was that of an electron or an avalanche of electrons in hexane. It was suggested that the low value of mobility was due to the electrons in the liquid spending part of the time being trapped or attached to neutral molecules and occasionally breaking away under the influence of the intense applied field to cause ionisation.

To explain Crowe's results, LeBlanc proposed that at high fields in the region of breakdown the voltage drop across a trap of molecular dimensions will be an appreciable fraction of the trapping energy (ϵ_t). This will lead to a significant increase in the rate of escape from traps. Considering classical processes only (i.e., neglecting tunneling effects

[‡] A formative time lag ten times smaller than Crowe's value in hexane has been obtained by Lewis and Ward (13).

which may be important at breakdown fields) and treating the traps as square wells of radius δ one finds instead of Eq.(2.6) that the drift mobility should vary with the field strength as,

$$\mu = A \exp \left[-(\epsilon_t - eE\delta) / kT \right] \quad \text{-----}(2.7)$$

where A, the pre-exponential factor in Eq.(2.6), is obtainable from experiment (see Eq.(2.4)). Taking $\mu = 9 \times 10^{-3} \text{ cm}^2/\text{volt sec}$ at $E = 1.5 \times 10^6 \text{ volt/cm}$, and $\mu = 1.4 \times 10^{-3} \text{ cm}^2/\text{volt sec}$ at $E = 0$. LeBlanc obtained a value of about 3 \AA for δ ; thus the traps appear to be of molecular dimension.

Secker and Lewis⁽¹¹⁾ have also measured the mobilities of positive and negative charge carriers in hexane. Unlike the other authors (Table 2.1), however, they obtained a large scatter of experimental results of about 200 %. They used x-ray excitation to inject excess electrons into the liquid. The average values of both positive and negative carriers were about twice those reported previously. They also made some measurements of the space charge limited currents and found it much lower than the theoretical value below a field of 1 Kvolt/cm. To explain these observations they postulated that the liquid moves at a velocity v , in the same direction as the field induced charge motion. Provided the mobile charges are ions, such liquid motion could be set up by two processes: first by momentum transfer from the injected photoelectrons (energy $\sim 20 \text{ K ev}$) into the liquid, and secondly, by the interaction of the charges and the liquid molecules throughout the transit time of the former between the electrodes. Although from their published data it is difficult to see the validity of their interpretation, such

liquid motion has been observed by Gary and Lewis (14).

Pyrene

It would appear that more complete information could be obtained from measurements in both the solid and the liquid state of the same material. Such measurements in molecular systems have so far been made only in pyrene by LeBlanc (15);

LeBlanc's measurements are, however, very preliminary and no definite conclusions as to the nature of charge transport can be made from them. He observed a drop in hole mobility by a factor of 10^3 at the melting point (149°C) from 0.3 to about $3 \times 10^{-4} \text{ cm}^2/\text{volt sec}$. In the solid LeBlanc's results agree with those of Bepler's (16);

Benzene

So far we have essentially been discussing the properties of charge carriers introduced in liquids by external radiation. Intrinsic (dark or natural) conductivity can also give some useful informations regarding charge transport.

The lowest conductivities of 10^{-19} - $10^{-20} \text{ ohms}^{-1} \text{ cm}^{-1}$ have been obtained in highly purified paraffins (17) and it is possible that even this residual conduction is due to dissociated impurities or other extrinsic causes. On the other hand, the relatively high conductivity ($10^{-14} \text{ ohms}^{-1} \text{ cm}^{-1}$) of benzene measured by Forster (18) is thought to be an intrinsic property of the liquid and this was confirmed by Nowak (17).

Systematic changes in the conductivity of a series of related hydrocarbons were described by Forster ^{(19),(20)}, and from these it appears that the intrinsic conduction is associated with the presence of π -electrons in the molecules. Because of the higher activation energy of conductivity in unsaturated hydrocarbons, Forster suggests that the conduction in these liquids involves a π -electron jumping process which is independent of the presence of trace impurities and does not occur in saturated substances.

In most insulating liquids the current is found to decrease with time following the application of the field, and this effect is thought to be partly due to a build up of space charge layers on the surfaces of the test cell. The rest is a genuine time dependence which is probably caused by the removal of non-equilibrium carriers from the bulk of the liquid, although it is not certain whether these are discharged at the electrodes or how much they contribute to the build up of space charge layers there. Probe measurements of the potential distribution in benzene and other hydrocarbons by Forster ^{(18),(19),(20)} have directly confirmed that there is a considerable space charge near the electrodes. This is shown in Fig.2.1 for benzene. In saturated hydrocarbons the space charge is predominantly near the cathode, but in unsaturated hydrocarbons it occurs mostly near the anode. This is probably due to different types of carriers in the two cases.

To explain the existence of space charge layers near the electrodes and the resulting non-ohmic current in these organic liquids, Silver ⁽²¹⁾ proposed a theoretical model for conduction in insulating liquids based

on a theory originally formulated by J. J. and G. P. Thomson ⁽²²⁾ for the space charge distribution in a gas between plane parallel electrodes. This theory, which does not distinguish between electronic and ionic conduction and is thus applicable to both type of conduction, is in reasonable agreement with the experimental results for benzene. It suggests that the measurement of the potential distribution may be a useful tool for obtaining transport parameters in liquids.

Thomson's theory should be applicable to insulating liquids with a slow generation rate of carriers regardless of generation mechanism. The electrodes are assumed to be non - injecting. The theory shows that the liquid may be considered to consist of two space charge limited regions near the electrodes in series with an intrinsic region in the bulk; this is in agreement with Forster's result as shown in Fig. 2.1. An interesting consequence of this theory is that the current (I) versus voltage (V) relationship has the form

$$V = C_1 I d + C_2 I^2 \text{ -----(2.8)}$$

where d denotes the electrode separation. C_1 and C_2 are constants depending upon the charge transport properties of the liquid. Eq.(2.8) agrees well with the results obtained for benzene by Forster. (It is interesting to note in passing that Wilson ⁽²³⁾ obtained an expression similar to Eq. (2.8) in his theory for the conduction in flames which has been verified experimentally).

As indicated by Silver, the important advantage of the above theory is that, from the experimentally obtained value of the potential drops (V_n and V_p , Fig. 2.1) at the electrodes and the widths of the space

charge regions (d_n and d_p , Fig.2.1) one can calculate parameters such as the mobility of charges responsible for the dark conduction in the liquid, the density of carriers, and the generation and recombination coefficients. One can then compare these with the corresponding parameters of the excess charges generated by external radiation. No drift mobility data for the excess charge carriers are available for benzene, but Silver obtained a value of about 10^{-6} cm²/volt sec for the mobility of both positive and negative charges in benzene, from the analysis of Forster's data.

Rare - Gas Liquids

Owing to the complicated shapes of hydrocarbon molecules it is unlikely that there will ever be a detailed theory of charge transport in these liquids. Comparison with Stokes' law etc., can only give a very crude interpretation of the results. Only in the case of the rare-gas liquids has this problem been more successfully resolved. The investigations with liquified noble gases are significant for the understanding of the nature of charge transport with regard to its dependence on applied field, correlation, temperature and pressure, since the experimental results lend themselves to detailed theoretical treatment.

For example, for positive ions the mobilities ⁽²⁴⁾ were: 6×10^{-4} cm²/volt sec for argon at 5 atm and 90°K, 6.8×10^{-4} cm²/volt sec for krypton at 22.7 atm and 145°K and 2.85×10^{-4} cm²/volt sec for xenon at 7.5 atm and 184.2°K. It was suggested that in these fluids the charge species were Ar₂⁺, Kr₂⁺ and Xe₂⁺ respectively. Negative charges, thought

to be due to oxygen or nitrogen impurities, have also been observed⁽²⁶⁾ to have about the same mobilities as the positive ions. It was shown by Davis, Rice and Meyer^{(24),(25)} that the observed mobilities and their temperature dependence were in qualitative agreement with the theory developed by Rice and Allnatt⁽²⁶⁾ and by Barker⁽²⁷⁾.

The rare-gas liquids are unique also in that electrons have been observed to have a mobility higher by a factor of about 10^6 than the ions. Miller, Spear and Howe⁽²⁸⁾ have measured the drift mobility of carriers generated by electron bombardment over a range of applied field from 10 volt/cm to 100 Kvolt/cm. Near the triple point, the 'low field electron mobility' in liquid argon, krypton and xenon were found to be 475, 1800 and 2200 $\text{cm}^2/\text{volt sec}$ respectively, about one half of the mobility found in the corresponding solids. It is remarkable that no significant change in the scattering mechanism occurs on melting of the solid rare-gases. In fact, pronounced 'hot electron' effects were observed in drift velocity versus field curves for both the liquids and the corresponding solids, and their fit to Shockley's 'hot electron theory' has been shown to be satisfactory.

Concluding Remarks

In the absence of a complete theory applicable to the hydrocarbons and other liquids with complicated molecular structure, one can but resort to a crude interpretation of the charge transport behaviour in such liquids in terms of Stokes' law or Walden's rule. On the assumption that the charge carriers in liquids are ions, Adamczewski derived

some empirical relationships between different parameters such as the mobility, viscosity, recombination coefficient, etc. He included in his investigations those charge species which do not obey Walden's rule, considering them as unstable ionic species. It, however, seems unlikely that in non-polar media, in a small temperature range, this should be the case.

The charges, which do not obey Walden's rule, are more likely to be electronic, as LeBlanc's investigations show. These may be trapped during their motion through the liquid and consequently move with a very low drift mobility for a part of their transit. LeBlanc's experiments, however, give no information concerning the nature of such 'traps'. In his measurements, different liquid samples yielded the same value of mobility; it is therefore unlikely that residual polar impurities furnish the trap sites. A trapping mechanism similar to that in an amorphous solid was suggested. According to Fowler ⁽²⁹⁾, electron trapping in amorphous solids arises from discontinuities in the electron conduction band at crystalline boundaries. The same picture might also apply to liquids, which can be visualized as consisting of a large number of randomly orientated, crystal-like regions of submicroscopic size.

However, the main objections to LeBlanc's model are as follows. First, the type of field dependence described by Eq.(2.7) has not been observed. The studies of the field dependence of negative carrier mobility were made by Chong and Inuishi ⁽⁹⁾ for pure hexane at fields up to 500 Kvolts/cm and for benzene up to 120 Kvolt/cm and by Terlecki ⁽³⁰⁾ for pure hexane, octane and decane up to 300 Kvolt/cm. They have not

found a field dependence of mobility. Secondly, Crowe's interpretation of breakdown phenomenon on which LeBlanc apparently based his trapping model is rather doubtful in view of the recent work on dielectric breakdown in liquids (17). It is now increasingly realised that breakdown may not be an intrinsic property of the liquid and that it can frequently be explained in terms of bubble or cavity formation which is different from collision ionisation process in that it does not need a high energy electron to initiate breakdown.

LeBlanc himself is inclined to reject such a model in view of his work on pyrene. He felt that it was unlikely that a trap controlled transport should be predominant in the liquid and completely absent in the solid. He therefore suggested that the transfer of charges from one trap (impurity or defect) to the next makes only a small contribution to the overall motion and that the main effect is that the electron is almost permanently 'self-trapped' in the polarisation field of its surroundings (see 'small polaron theory', next chapter). The lack of long range order will possibly enhance the probability of this polarisation 'self-trapping' and effective localisation of the electron on each molecule it encounters. Subsequent transfer to an adjacent site can then occur only with the absorption and emission of phonons and will therefore be temperature activated.

Such a theory, as tentatively suggested by LeBlanc, now exists in a comprehensive form for solids due to Holstein, Yamashita and Kurosawa and others (next chapter). This has been successfully applied to electron transport ('hopping transport', next chapter) in orthorhombic sul-

phur. No precise investigation of charge transport in liquids exists in the light of this theory. Liquid sulphur appears to be best suited for this purpose in view of the already available data for the solid.

In the liquid, the charge motion will be complicated by ions. Since, a molecule on which a carrier is 'self-trapped' can also move as an ion. If the ionic mobility is comparable to that of the electrons or larger it may be difficult to distinguish the two component mobilities.

PROPERTIES OF SOLID AND LIQUID SULPHUR3.1 Transport Properties of Solid Sulphur

Crystalline sulphur exists in two stable allotropic forms. Orthorhombic sulphur (S_{α}) is stable below 96°C . If heated slowly above this temperature, it changes to the monoclinic (S_{β}) form. Both the allotropes are molecular crystals consisting of puckered S_8 ring molecules; the molecules are bound together in the lattice by weak van der Waals forces.

A detailed investigation of the temperature dependence of the hole and electron transport in orthorhombic sulphur crystals has been carried out by Spear and co-workers (31), (32), (33), (34) using drift mobility techniques (chapter 4). As shown in Fig. 3.1, holes possess a room temperature mobility of up to $10\text{ cm}^2/\text{volt sec}$. At the lower temperatures the hole drift mobility is an activated process, and during transit through the specimen the holes interact with a level of centres 0.19 eV (E_t) above the valence band. With increasing temperature a transition to a lattice controlled transport takes place. The transition between the two mechanisms is expressed by the following relation,

$$\mu_h = \mu_L \left[1 + (N_t/N_v) \exp(E_t/kT) \right]^{-1} \quad (3.1)$$

where μ_h is the measured mobility, μ_L is the lattice mobility, N_v denotes the effective density of states in the valence band and N_t the density of shallow traps. The solid curves in Fig. 3.1 were fitted according to this relation corresponding to the given values of N_t .

The results for the electron mobility is shown in Fig. 3.2. The

transport is an activated process throughout the temperature range leading to a drift mobility of $\mu_e = (6.2 \pm 0.6) \times 10^{-4} \text{ cm}^2/\text{volt sec}$ at 21°C and an activation energy of $E_a = 0.167 \pm 0.005 \text{ eV}$ in all principal directions of the crystal. The remarkable consistency of the results, which is in complete contrast to the hole results, together with the low value of the mobility, led the above authors to exclude a trap controlled transport. They fitted the results to the small polaron theories of Holstein (35) and of Yamashita and Kurosawa (36). In the following these theories are discussed in detail since they introduce a new transport mechanism applicable to highly localised carriers as opposed to a description of transport in terms of delocalised Bloch functions. As shown by the results in this thesis such a theory could well be applicable to the transport of charge carriers in liquid sulphur.

Small Polaron Theory

Consider an excess electron in a molecular crystal, such as sulphur, characterised by an extremely low electron mobility. Because of the small wavefunction overlap between electron states on neighbouring molecules, the electron may remain in the region of a lattice site for a time long compared with the period of molecular vibrations. The electron will polarise the surrounding lattice and neighbouring molecules will be displaced to new equilibrium positions corresponding to a reduction of the total energy of the system. The induced lattice distortion will thus produce a potential well for the electron and the electron will be essentially 'self - trapped' with a binding energy E_p .

The electron with its region of lattice distortion is known as a polaron. The term 'small polaron' is used for non - polar media where the lattice distortion is fairly localised.

The main condition for the formation of small polaron is $E_b \gg J$, where J is the overlap energy between neighbouring electron states. The transport has been investigated theoretically by Holstein and by Yamashita and Kurosawa. The general results of these theories are that essentially two mechanisms can occur, described with reference to Fig. 3.3 which shows the $\mu - 1/T$ curve calculated for the case of sulphur.

(a) At temperatures below T_c (The transition temperature between the two mechanisms), the transport of the polaron between neighbouring molecules occurs without absorption and emission of phonons i. e., the polaron quantum number remains unchanged during the transition. In this case the polaron will move as a whole and one describes its transport in terms of Bloch functions. It can be seen from the Fig. 3.3 that in the low temperature region the mobility decreases with increasing temperature, consistent with transport in a band. With increasing temperature scattering becomes more intense and the scattering relaxation time τ will decrease. T_c is the temperature for which the polaron bandwidth $w = \frac{\hbar}{\tau}$. This means that the uncertainty in energy after a scattering event will be equal to the polaron bandwidth and the band description breaks down.

(b) For $T > T_c$, the transition of the polaron between molecules will be accompanied by absorption and emission of phonons

and the polaron will 'break up'. The transport is then a random diffusion process by a series of uncorrelated, phonon assisted site jumps and referred to as 'hopping' transport. The limiting conditions for the occurrence of this transport mechanism have been discussed by various authors (37), (38), (39) and it was shown that for carrier mobilities below about $0.1 \text{ cm}^2/\text{volt sec}$ hopping conduction should in principle occur.

Although hopping transport is likely to play a part in a fairly wide range of organic and inorganic molecular solids, there still exists a lack of really conclusive experimental evidence for hopping conduction in these materials. The work of Spear, Adams and Gibbons has led to the conclusion that the electron transport in orthorhombic crystals of sulphur represents a good example of an intermolecular hopping mechanism. Hole transport, on the other hand, exhibits the features of a polaron band type motion.

Hopping Transport of Electrons in Sulphur

The small polaron theories lead to expressions for the probability P of a carrier making a transition to a neighbouring site which can be related to the experimental data by

$$\mu_e = \frac{e a^2}{k T} P \quad \text{-----(3.2)}$$

where e is the electronic charge and ' a ' represents the spacing between molecular sites. Eq.(3.2) follows directly from elementary diffusion theory and from Einstein's relation between diffusivity and mobility.

With an average value of 'a' = 5.95 Å for $\sqrt[3]{S_\alpha}$ lattice, the experimental results lead to $P = 4.4 \times 10^9 \text{ sec}^{-1}$ at 21°C. Re-plotting the data of Fig. 3.2, the temperature dependence of P can be expressed over the whole range by

$$P = P_0 \exp(-\epsilon_p/kT) \quad \text{-----}(3.3)$$

where $P_0 = 5.1 \times 10^{12} \text{ sec}^{-1}$ and $\epsilon_p = 0.18 \text{ ev}$, somewhat larger than the activation energy associated with the mobility. It can be seen that for all temperatures below the melting point (368°K) the electron will be localised on a molecule for several periods of molecular vibration. The intermolecular transition is most likely to occur by tunneling, when as a result of vibrational interaction the two electron states are in energy coincidence.

Yamashita and Kurosawa used time dependent perturbation theory to calculate this transition probability,

$$P_y = \frac{2\pi}{\hbar^2 \omega_0} J^2 \exp \left[-2\gamma (2S+1) \right] \times I_0 \left\{ 4\gamma \left[S(S+1) \right]^{1/2} \right\} \quad \text{---}(3.4)$$

where J is the intermolecular exchange energy (a measure of the overlap between intermolecular orbitals), I_0 the modified zero order Bessel function and $1/S = \exp(\hbar\omega_0/kT) - 1$. The dimensionless electron - lattice parameter γ is defined as

$$\gamma = \frac{E_b}{\hbar\omega_0} \quad \text{-----}(3.5)$$

where E_b denotes the polaron binding energy and the localized electron is assumed to interact predominantly with a molecular vibrational frequency ω_0 (i. e., dispersion neglected).

The corresponding expression obtained by Holstein is,

$$P_h = \frac{J^2}{\hbar^2 \omega_0} \left[\frac{2\pi}{2\gamma \operatorname{cosech} \frac{\hbar \omega_0}{2kT}} \right]^{1/2} \exp \left[-2\gamma \tanh \frac{\hbar \omega_0}{4kT} \right] \quad (3.6)$$

Eqs. (3.4) and (3.6) were used by Gibbons and Spear to compute $P \times (2\pi)^{-1/2} (\hbar E_b / \gamma J^2)$ for a number of γ values, and the results were plotted, as shown in Fig. 3.4, as a function of $E_b/2kT$. For $\gamma \gg 5$, the values deduced from the two theories are in remarkably good agreement. On the basis of Eq.(3.3), which satisfies the experimental data over the temperature range , a lower limit of γ was set to be 15. For a given value of γ greater than 15, the value of E_b in the abscissa of Fig. 3.4 was adjusted until the gradient of the line was equal to the experimental value, ϵ_p . Having obtained E_b , $\hbar \omega_0$ was calculated from Eq.(3.5) and J was found from the scaling factor. The results of the curve fitting are summarised in Table 3.1. The four most prominent fundamental peaks of the molecular vibrational spectrum lie above the limiting value of γ in the range between $\gamma = 17$ and 27. The wave number and assignment according to Scott et al. ⁽⁴⁰⁾ are included in Table 3.1. The average value of E_b corresponding to these modes is 0.48 ev; the value of J derived from the analysis is about 0.05 ev not unreasonable for a molecular crystal such as sulphur.

As discussed above, Holstein predicts that with decreasing temperature there should be a transition to band type motion, and gives the low temperature limit (T_c) for the occurrence^{re} of a hopping transport as

$$\frac{\hbar \omega_0}{2kT} \leq 1$$

For the lowest temperature used in the experiment of Gibbons and Spear this condition is fulfilled for

$$\hbar\omega_0 \leq 0.034 \text{ eV}$$

so that all the values in Table 3.1 fall within the hopping range. There are several subsidiary conditions given by Holstein which involve E_b , and J . With one exception, these are satisfied for the group of fundamental vibrations.

Electron lifetime measurements were made by the above authors and are consistent with the hopping model.

Band Structure of Orthorhombic Sulphur

The electronic structure of orthorhombic sulphur has been examined by Gibbons ⁽⁴¹⁾ in terms of molecular orbital theory. The Bloch tight binding scheme was employed to estimate the width of electron and hole bands by an approximate method.

The bonding between atoms in a ring is described in terms of $3sp^3$ hybrid orbitals. Two orbitals per atom are occupied by lone pairs and the remaining two are engaged in forming two single covalent bonds with neighbouring sulphur atoms on the ring. The lone pair orbitals interact weakly to give rise to a π -system of molecular orbitals round the ring, the energies of which are very close to those of the lone pairs in the isolated atom. The overlap between the bonding orbitals lead to σ -bonds and the strong interaction between these orbitals gives rise to widely separated bonding and anti-bonding states. This is illustrated in Fig. 3.5. It can be seen that the 4s outer shell

electrons in the molecule fill the σ , π and π^* molecular orbitals and leave the σ^* system of levels unoccupied. In the solid, interactions between molecules will slightly broaden the molecular energy bands. Since these interactions are very small indeed, the identity of the molecular configuration will largely be preserved.

Electrons in the σ^* band are in highly localised levels in antibonding states situated between neighbouring atoms in the ring. The excess electron is likely to interact strongly with the molecular vibrations of the bonds leading to the formation of a polaron. From the geometrical configuration of the various orbitals it can be seen that the overlap between neighbouring molecules in the solid of the π and π^* states is very much larger than that of the σ and σ^* states. The hole band should therefore be considerably wider than the electron band. These tentative conclusions have been confirmed by calculations of the intermolecular overlaps and bandwidths, and strongly support the interpretation of the experimental data.

3.2 Physical Properties of Liquid Sulphur

Orthorhombic sulphur melts at 113°C , while monoclinic sulphur melts at 119°C . Since orthorhombic sulphur changes only slowly to the monoclinic form, even near the melting point, it is possible to melt it before any appreciable amount of monoclinic sulphur is formed.

Liquid sulphur at the melting point is a light yellow, transparent liquid of low viscosity (~ 0.1 poise). Its most interesting property is the variation of viscosity with temperature, as shown in

Fig.3.6 (42). This has been well established as being connected with the molecular structure of the liquid. As the temperature is increased from the melting point, the liquid becomes deep orange in hue and its viscosity decreases. Above 160°C , the viscosity increases by four orders of magnitude as the ring molecules break up into chains which then polymerise. At 180°C , the viscosity reaches a maximum and the liquid is intensely coloured to be nearly opaque. Above 180°C , it again acts as a normal liquid as the long chain molecules break up into short ones, the viscosity falling with increasing temperature. At atmospheric pressure it boils at 444°C . Small amount of impurities greatly reduces the viscosity maximum at 180°C . The viscosity changes of the pure liquid is perfectly reversible (42).

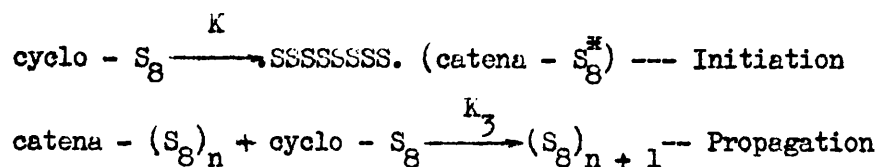
Liquid sulphur, even though relatively impure, supercools easily. Small droplets may even be cooled to room temperature and kept in the liquid state indefinitely, the duration depending upon their size. Fanelli showed that the viscosity versus temperature curve of the supercooled liquid is an unbroken continuation of the normal liquid curve (43).

Throughout the whole temperature range of the solid and the liquid the density is a slowly decreasing function of temperature, as shown in Fig. 3.7 (44), and there is no marked change in density at the melting point.

Polymerisation of Liquid Sulphur

Theoretical attempts to describe the physical properties of liquid sulphur on the basis of an equilibrium between S_8 rings and

chains were made by Powell and Eyring (45) and by Gee (46). Their attempts were partially successful because they used only one equilibrium constant. The approach by Tobolsky and Eisenberg (47), (48) utilising two equilibrium constants, one for initiation and one for propagation, proved to be more successful over the whole temperature range. According to them the equilibrium polymerisation of sulphur can be represented as follows,



Symbolically cyclooctasulphur is designated as M (monomer) and catenaoctasulphur as $M_n^{\#}$ (polymer). The theory relates the experimental observables such as the concentration of M in equilibrium with the polymer and the number - average degree of polymerisation P (average number of S_8 units per chain) of the polymer with the theoretical constants K, K_3 and M_0 . M_0 is the moles of S_8 unit (whether monomeric or polymeric) per kilogram and is a constant at all temperature, namely 3.9. Tobolsky's theory is in good agreement with the experiments as shown by Figs. 3.8 and 3.9 representing the functional dependence of M and P on temperature.

EXPERIMENTAL METHODS4.1 Principle of Drift Mobility Measurements

Drift mobility is measured directly by timing the transit of generated carriers across a specimen of known thickness. The carriers may be generated by bombarding the specimen by high energy electrons or by shining light on it. To confine the generated carriers in a narrow layer the exciting radiation should be non - penetrating and its duration should be sufficiently short. The pulsed electron beam technique developed by Spear ^{(49),(50),(51)} has been used to measure drift mobilities in Se, CdS ^{(52),(53)} , sulphur and, solid and liquid rare gases. In the present investigation optical excitation by short light flashes was used throughout.

The transit time can be measured by essentially two methods. Charge integration is the most sensitive method for transit times below about ten microseconds. On the other hand, the display of current pulses may be used for the measurement of longer transit times. A brief description of the principles of the two methods is given in the following.

Shockley ⁽⁵⁴⁾ has given a very general derivation of the current that flows in a given system of grounded conductors due to the motion of a point charge. This can be applied to the case of a sheet of charge q moving with a constant velocity v between two plane parallel electrodes separated by a distance d , as illustrated in Fig.4.1. v is thus the drift velocity in a uniform applied field E . The total displacement

current is given by,

$$i = q \frac{v}{d} = \frac{q}{t_t} \quad \text{----- (4.1)}$$

where t_t is the transit time. If a resistive load R is inserted in the lead from the collecting electrode S to ground, the potential developed across the load during transit is,

$$V_s = i R = q \frac{v}{d} R$$

The total capacity C from S to ground including the specimen capacitance can be used to integrate the current by making R so large that $RC \gg t_t$. Then the potential between $t = 0$ and $t = t_t$ will rise linearly and is given by

$$V_s = \frac{q}{C d} x(t)$$

For $RC \gg t \gg t_t$,

$$V_s = \frac{q}{C}$$

Under ideal conditions the current pulse ($RC < t_t$) and the integrated signal ($RC \gg t_t$) will be ^{as} shown in Fig.4.2. In the case of the current pulse V_s drops sharply to zero after a time t_t when the charge sheet reaches S , whereas with an integrated signal V_s becomes constant. Both lead to an experimental value for the transit time

$$t_t = \frac{d}{\mu E} \quad \text{----- (4.2)}$$

or,

$$\frac{1}{t_t} = \frac{\mu}{d^2} V$$

since $E = V/d$, where V is the applied potential. Therefore the plot of $1/t_t$ against V should give a straight line passing through the origin. The gradient of this line should yield the drift mobility.

For the observation of ideal traces as illustrated in Fig.4.2 several conditions must be satisfied.

- (a) The applied field E must be uniform. This would be the case if the 'self - field' of the drifting charges is very much smaller than E . That is,

$$\frac{q}{A \epsilon \epsilon_0} \ll E \quad \text{-----}(4.3)$$

where q is in coulombs, ϵ_0 is $3.36 \times 10^{-14} \text{ F cm}^{-1}$ and ϵ is the relative dielectric constant of the sample, and A the electrode area.

- (b) The accuracy to which μ can be determined depends largely upon the sharpness of the discontinuity at $t = t_t$. To work under optimum conditions it is essential that $t_t \gg t_p$, where t_p is the duration of the excitation pulse, and that $d_p \ll d$, where d_p is the average depth of penetration of ^{the} incident light.

- (c) $t_t < \tau$, the lifetime of carriers with respect to traps. Let τ_r be the release time associated with such traps. If $\tau_r > t_t$ the traps are termed 'deep traps' in the following.

- (d) The dielectric relaxation time τ_d of the specimen must be longer than t_t of the charge cloud, which represents a deviation from charge neutrality ^{and} will tend to become compensated by carrier injection. Thus $\tau_d = \epsilon \epsilon_0 \rho \gg t_t$, where ρ is the effective resistivity of the specimen at a particular

value of the applied field.

Although it is evident from condition (c) above that difficulties will arise if $\tau < t_t$, it has been found possible to study drift mobility and lifetime when $\tau \sim t_t$. Under this condition the pulse shapes are shown in Figs. 4.3 and 4.4.

In the presence of a uniform volume distribution of deep traps⁽⁵⁵⁾

$$q(t) = q_0 \frac{\tau}{t_t} \left[1 - \exp(-t/\tau) \right] \quad (4.4)$$

It can be shown that for charge integration

$$t' = \tau \left[1 - \exp(-t_t/\tau) \right] \quad (4.5)$$

where t' is defined by the intersection of the tangents to the pulse at $t = 0$ and $t = t_t$, as shown in Fig. 4.3.

From Eq.(4.4),

$$\frac{dq}{dt} = \frac{q_0}{t_t} \exp(-t/\tau) \quad (4.6)$$

Therefore,

$$i(t) = i_0 \exp(-t/\tau) \quad (4.7)$$

The current pulse is shown in Fig. 4.4. The initial current will decrease exponentially due to bulk trapping until a reduced charge sheet arrives at the signal electrode. At t_t

$$i(t_t) = i_0 \exp(-t_t/\tau)$$

For $\tau < t_t$, $i(t_t)$ may become so small that no discontinuity at t_t is detectable, as shown in Fig. 4.5. So that ~~transit time measurements~~ are not possible in such cases. Using Eq.(4.7) it is possible to measure τ from current pulses, since $i(\tau) = 1/3 i_0$.

Trapping becomes complicated when the trap distribution is non-uniform or when different types of centres involve more than one lifetime.

An additional difficulty may arise from carrier diffusion and the statistical nature of trapping and release. These cause the charge cloud to broaden during transit giving rise to a tail at the end of the signal (Fig. 4.4). If the tail is due to diffusion alone, t_t is the average time of arrival of the charges and is measured up to the middle of the tail. An estimate of the width of the tail due to the diffusive broadening is given below. If, however, the tail is longer due to trap release and other causes (for example, in the liquid, the tail may occur due to slow moving ions trailing behind the main sheet of charge), measurement of t_t up to the middle of the tail is not meaningful. The transit time is therefore measured up to the beginning of the tail (t_t^a), as shown in Fig. 4.4.

It is of interest to make an estimate of the broadening of the charge sheet due to the finite width of the excitation pulse and diffusion. The initial width of the sheet, assuming a mobility of 10^{-4} cm² volt⁻¹ sec⁻¹ and a light flash duration of 10^{-5} sec, is about 6×10^{-4} cm for an applied potential of 400 volts across a specimen of 200 microns thickness. (This neglects the penetration depth of light which is less than 10^{-4} cm). The diffusion coefficient D given by Einstein's formula ($\mu kT/e$) is about 4×10^{-6} cm²/sec at 400°K. Therefore the diffusion length during a transit time of 10^{-2} sec is

$$L = \sqrt{D t_t} \quad \text{----(4.8)}$$

The total diffusion length in the direction of travel is $2L$, so that the width of the charge sheet should be less than 10^{-3} cm, at the end of transit. This corresponds to a tail of about 5 per cent of the transit time which lies well within the experimental error.

4.2 General Description of Apparatus for Measuring Drift Mobility

In this section the complete experimental arrangement will be briefly discussed with reference to the block diagram in Fig.4.6, while the more detailed description of the various parts of the equipment is left to the following sections.

The specimen chamber is a small oven which contains the sample. A thermocouple and a potentiometer measure the temperature of the sample. Light from the flash unit is focussed by a lens and mirror arrangement on to the sample. The potential to be applied across the sample is provided by the field unit, which could be pulsed electronically, or operated manually by a microswitch.

It can be shown that for maximum sensitivity in both current pulse and charge integration methods, it is necessary to keep the specimen capacity and input capacity of the detecting apparatus as small as possible. The signal is therefore fed directly on to the grid of the cathode follower. The load R which is a switched bank of resistors, was included in the cathode follower unit. The output signal is observed in a Tektronix 541 A oscilloscope after suitable amplification by a preamplifier.

The oscilloscope is triggered externally from the light flash by an OCP 71 phototransistor triggering unit connected to the 'scope.

To reduce 'pick - up' from the light source, the specimen chamber and the associated units shown in Fig.4.6 are placed inside an earthed wire - cage, the light source being placed outside it. Mains ac 'pick - up' is reduced by careful filtering of the mains supply. A filtering unit is included in the cage for this purpose.

Experimental Procedure

The sulphur specimens were melted in air at atmospheric pressure in the specimen chamber between two plane parallel electrodes. Negative and positive charge pairs were generated in the specimen close to the generation electrode G (Fig.4.1) by a short pulse of light. Depending on the polarity of the applied field either generated negative or positive charges were drawn across the specimen towards the signal electrode S. The signal voltage V_s was displayed on the 'scope. The current pulse has an initial spike due to one type of carriers being drawn out by the generation electrode. This is shown in Fig. 4.7. This spike is however very fast and can be eliminated by reducing the risetime of the detecting system.

During a transit, some of the carriers may be trapped in the bulk of the sample. The resulting polarisation, if large, may affect the transit of subsequent carriers. The space charge was neutralised by shorting out the specimen. This was done by shorting the output of the field unit to ground by a small resistance in the 'off' posi-

tion of the unit. The neutralisation of the space charge was often aided by several light flashes between voltage pulses. These light flashes are therefore called 'discharge pulses'.

Capacitive coupling across the specimen produces a large transient signal voltage at the beginning of the field pulse. This must have time to decay before the light excitation pulse occurs, to prevent its interference with the photocarrier signal. In the case of liquid sulphur the field transient has added characteristics, which are discussed in chapter five (sec.5.6.)..

The sequence of actions in the procedure of transit time measurements is described with reference to Fig.4.8 which shows the different pulses observed in the 'scope. First the field is switched on and there is a corresponding transient at $t = 0$. After a delay of t_d during which the transient current has decayed to a constant value, the light is flashed. This initiates the transit signal. The field is then switched off, producing a corresponding transient in the opposite direction. After a few 'discharge pulses' the procedure is repeated.

4.3 Specimen Chamber

Fig.4.9 shows the experimental cell which contained the liquid sample. It comprised an oven A made of a heavy hollowed out brass cylinder of high thermal capacity which was heated by means of a heating coil C wound on the outside.

The quartz discs Q_1 , Q_2 and Q_3 were placed inside a thin - walled brass tube D resting coaxially on a shoulder inside A. The bore of

smaller diameter at the bottom of A and D provided a passage for for the illuminating radiation.

The sample S_1 under investigation was melted between discs Q_2 and Q_3 . The thickness of the sample was determined by glass spacers of predetermined thickness. These were permanently fixed on to the bottom quartz disc Q_3 .

There was a second sample S_2 , the reference sample, enclosed by discs Q_1 and Q_2 . The hot junction of a chromel - alumel thermocouple was embedded in it for accurate temperature measurement.

The whole quartz disc assembly was tightly pressed together by a coil spring W. The electrical lead to the bottom electrode was taken out through a ceramic tube, which fitted in a hole drilled off - axis in A and projected out. The lead was soldered at this end to a wire in steel tube H insulated from the wire by a ceramic tube. A BNC - connector was fitted to H for electrical connection. The oven was supported vertically by the rod G.

The electrical lead for the upper electrode was taken out through another ceramic tube enclosed in the steel tube F. F was brazed vertically to E, the lid of the specimen chamber. E had a central hole to bring out the thermocouple. The upper end of F had an UHF - connector fixed to it.

The heating coil C was made of a wire tape of low resistance. It was wound on the cell over a layer of asbestos tape to insulate it from the cell body. It was further coated with a heat resistant mixture of alumina powder and slightly diluted water - glass. The

mixture hardened after a short period of dehydration; it was then cured slowly in an oven at a moderate temperature. The heater control comprised a 100 volts dc supply, a coarse and a fine rheostat, and an ammeter.

The temperature of the hot junction of the thermocouple was measured to within a degree centigrade by a potentiometer.

4.4 Preparation of Electrodes

Figs. 4.10 (a) and (b) show the shape of the electrodes. The central circular region was the electrode proper in contact with the specimen. A limb stretched out of this to the periphery of the disc where electrical connection was made with the lead. The lead was pushed from the other side of the disc through an ultrasonically drilled hole, Fig. 4.10 (c). The junction B was made with Pt - paste, aqua- (or alcohol) dag or silver paste. The former was preferred because it led to better electrical behaviour. These substances possess poor mechanical strength and it was essential to bond leads to the quartz discs with araldite. The lower disc Q_3 was fitted with a short ceramic tube J which was used to locate the disc with respect to D and A (Fig.4.9). It also prevented any movement of D with respect to the cell body and thereby reduced the possibility of damage of the lead and its shorting to earth.

Three different materials were used for the electrodes. These were deposited on the quartz discs by the methods described below. quartz discs were chosen for their transparency to the ultraviolet

radiation. The choice of the electrode material and electrode preparation were difficult because of the requirement that (a) the lower electrode should be transparent to the radiation of interest and (b) the electrodes should be sufficiently inert not to interact appreciably with liquid sulphur.

Gold Electrodes

Gold was deposited on to the quartz substrate by evaporating gold - wire in a heated filament under a vacuum of about 10^{-5} torr. The evaporation was controlled to give a semi - transparent gold layer with a resistance of about 100 ohm. Such layers had a 50 per cent transmission to near ultraviolet light, and served as the lower electrode. For the upper electrode semi - transparent or thick gold layers were used.

The type of gold electrodes, shown in Fig. 4.10 (a), was also tried. This involved two evaporations in succession, first an annular then a superimposed grid.

Nesa Electrodes

The difficulty with gold electrodes was that they were soft and adhered firmly to sulphur after the solidification of the liquid. Any attempt to remove the sulphur damaged the electrodes as well. Each sample preparation necessitated therefore the cleaning of the substrates and the deposition of a new electrode. This was overcome by using nesa electrodes. Once prepared, they adhered firmly to the

substrates and even scraping with metal would not remove them. Also, nesa was nearly 100 per cent transparent to ultraviolet and visible radiation.

Nesa is essentially a layer of tin oxide. The starting material is a solution of several inorganic and organic compounds. The constituents and their proportions in which they were used are as follows: 1 gm of SbCl_3 , 10 cc of conc. HCl, 75 gm of SnCl_2 , 50 cc of absolute alcohol and 50 cc of distilled water.

First, the SbCl_3 was dissolved in HCl. The solution was kept cool in an ice - bath. The SnCl_2 was then added slowly in a fume chamber. The solution was then well mixed with water and alcohol was added slowly. A grade 54 filter paper was used finally to filter the mixture and a clear nesa solution was obtained.

The actual deposition of nesa on quartz consisted of heating the disc in an oven up to a temperature of about 600°C , and then spraying the solution on to it. After a rough calibration with trial layers, the resistance could be judged from the reflected white light fringes. Layers of 500 - 1000 ohm were easily obtained after several seconds of spraying. A mask was used on the substrate to confine the layer to the desired shape (Fig. 4.10 (b)).

Platinum Electrodes

Pt was preferred to the other electrode materials for low electrical noise at high applied fields. It was cathode sputtered on to quartz substrates in an argon atmosphere. The arrangement is shown

in Fig. 4.11. The chamber was an inverted glass funnel F placed on a vacuum baseplate B which was at a positive potential. The disc Q was enclosed in a metal mask M and placed on B. A thin Pt disc D was suspended horizontally inside the chamber from a wire. The wire was sealed in at the top of the funnel and carried the terminal T connected to the negative potential. The baseplate carried a needle valve V which joined the chamber to an argon cylinder.

The chamber was first evacuated and argon let in. The pressure was adjusted so that the cathode glow was near the Pt disc and the substrate in a dark space. The current was adjusted by the applied voltage supply, for an optimum rate of deposition.

Semi-transparent Pt layers were rather difficult to obtain and were of high resistance. So thick layers were prepared, and the lower electrode was carefully scratched in fine parallel lines for light transmission leaving a continuous annular portion on the outside (Fig. 4.10 (a)).

Pt layers prepared in this way, although very much harder than gold, tended to deteriorate gradually through repeated sample removal. The old layer was simply removed by leaving the disc in conc. chromic acid for few hours. The removal of nesa was, however, not so easy and an efficient way of doing it has not yet been found.

4.5 Light Sources

Light flashes were obtained from an Osram X1E - type xenon - mercury tube. Fig. 4.12 shows the associated circuitry. (a) is the

power pack which applied a potential of 1 K volts across a 4μ F charging capacitor in parallel with the tube, as shown in (b). A short trigger voltage was derived from a car ignition coil and carried to the trigger electrode 3 of the tube. The breakdown of the gas in the tube discharged the capacitor through the tube producing the flash. This flash was extremely rich in ultraviolet radiation and had a width of about 10 microseconds.

The triggering circuit is shown in (b). When the microswitch m. s. was closed the mercury relay was energised and contacts 1 and 2 closed. This produced the H. T. impulse in the car ignition coil.

At the instant of closing m. s. a signal was available for synchronisation of the pulsed field unit described in sec.4.7. There was a 5 milliseconds delay between this signal and the light flash. The mercury relay could also be energised from an outside source, e.g., a multivibrator.

When a faster flash was necessary, an adjustable spark gap was used for the light source. This is shown in Fig. 4.13. The condenser was charged from a 10 K volts transformer through a 300 M ohm resistor and the breakdown discharged the condenser. The rate of this discharge could be controlled by the Variac. The whole assembly was enclosed in a metal box with a hole in front of the spark gap for the light, which was reflected off a front surfaced mirror and focussed on to the specimen. The duration of the spark was about 100 nanoseconds.

4.6 Detection

The signal V_s is developed across the resistance of the cathode follower shown in Fig. 4.14. A provision was made for including a mercury wetted relay to gate the input. The input capacitance, including the specimen chamber, was 45 pF, and the stage gain 0.85.

The output signal from the cathode follower was fed through a coaxial cable to an amplifier. Two types of amplifier were used, a Levell type - TA 60 low frequency amplifier (bandwidth 1c/sec - 3 Mc/sec) and a Keithley low noise ac amplifier (bandwidth 0.1 c/sec - 100 c/sec), both having a maximum gain of 60 db.

4.7 Field Unit

In most experiments a battery box was used, fitted with a polarity reversal switch and a microswitch for short manual operation of the field. The voltage was provided by a bank of 9, 45 and 90 volts dry batteries. Four selector switches connected to the battery tapings covered the range ^{from} ~~between~~ 0 to [±]990 volts in 1.5 volts steps. A stabilised electronic power pack supplying potentials of up to [±] 1000 volts in 10 volts steps was also used. This was also fitted with a microswitch.

In earlier experiments with gold electrodes polarisation effects and increased noise were observed after a prolonged application of the steady field, so that a pulsed field appeared essential. In a number of experiments an electronic field pulse unit was tried, as shown by the block diagram in Fig. 4.15.

The pulse unit consisted of a Schmitt trigger, multivibrator and a relay drive. In case gating was required to short out field transients, the gating relay in the cathode follower unit was driven by another multivibrator. Sometimes a delay was necessary between the field pulse and gating pulse and a delay multivibrator was therefore included.

The signal for the Schmitt trigger was derived by a variety of ways. A low frequency oscillator was used for pulsed measurements at a constant rate. For single shot measurements the signal was either obtained from the light flash unit (sec. 4.5) or from a microswitch discharging a capacitor.

Synchronisation of the light flash was achieved easily when the trigger signal was derived from the flash unit, provided the right amount of delay could be obtained between the trigger and the flash from the unit. When the gating was used it was essential for the flash to occur within the gating pulse, as shown in Fig. 4.15. Because of this, when the delay between the gating and field pulses was large, the light flash was triggered by the delay multivibrator. The Schmitt trigger in this case received its signal from the microswitch or a signal generator.

The pulse technique was rather difficult to use because of the nature of the field transients which made it necessary that the delay should be large. As shown in Fig. 4.8, the transient has a width comparable to the photocarrier transit. For thick specimens and at low fields this became too large. Manual operation of the field

was therefore preferred. This choice was helped by the fact that polarisation effects were negligible in liquid sulphur with the use of Pt and nesa electrodes.

4.8 Growth of Sulphur from Solution

Some of the starting material in the experiments on liquid sulphur was crystalline. These were grown from solution of sulphur in CS_2 . Laboratory grade (BDH, see Appendix I) reagents were used.

Slow evaporation of a saturated solution in a glass trough or beaker gave crystals of orthorhombic sulphur growing in the bi - pyramid habit. Specimens were prepared from these by grinding them parallel to the natural (111) faces. For this special 'jigs' were used as described by Adams⁽⁵⁶⁾. The grinding process involved the successive use of finer grinding powders, and finally, the ground surfaces were polished with diamond paste of appropriate grade. Special polishing cloths were used.

The thickness of the specimen was measured with an optical lever thickness gauge as described by Spear et al.⁽⁵⁷⁾

4.9 Growth of Sulphur from the Melt

Attempts have been made to grow pure crystals from the melt and from ^{the} vapour phase as it seems possible that the crystals grown from solution might contain CS_2 and other solvent impurities.

Bridgeman's method was tried for growth from the melt. The arrangement is shown in Fig.4.16. A cylindrical furnace F with a heating

* Koch - light ultrapure sulphur was used (see Appendix I for details)

coil W was supported vertically by a retort stand. A glass tube R, which could move freely along the axis of F, was fixed to the polystyrene disc P. P was kept afloat on water contained in a polythene vessel C. The level of water in C determined the position of R in the furnace. R supported the tube T containing the specimen. The position of T inside F was shown by the indicator N and scale S fixed to the retort stand.

The heating coil W consisted of two sections A and B. The current in the coils could be controlled to maintain a steady temperature. A and B were kept just above and below the melting point of sulphur respectively. The temperature profile was measured by means of a chromel - alumel thermocouple. C was filled with water to raise R so that the top end was in the upper section of A. Water was allowed to flow out slowly at a rate controlled by a tap. T moved down and molten sulphur crystallised as it passed from A to B. The rate of this passage was varied from 0.5 cm - 2 cm per hour.

It was essential to cool T slowly before taking it out of the furnace. The section B was therefore lengthened to ensure a more gradual decrease in temperature and the current through the coils reduced slowly after the specimen had passed into B.

It was difficult in spite of the precautions to prevent the cracking of the specimen due to unequal thermal expansions of sulphur and glass. The cracking was large along the axis of T. The configuration of the furnace and the cell was therefore changed to rectangular, as shown in Fig. 4.16 (b) and (c).

Specimens obtained from the rectangular geometry were much better. They were clear with a small amount of visible defect structure and large specimens could be obtained if the cell was taken apart carefully. Drift mobility experiments on these specimens, however, proved unsuccessful because of 'deep - trapping' by defects.

4.10 Growth from Vapour Phase

Fig. 4.17 shows the arrangement used. A pyrex tube was rounded at one end and joined to a narrower tube at the other. The tube was cleaned and dried under vacuum and ultrapure sulphur granules were put in. It was then evacuated and sealed off under vacuum of about 7×10^{-4} torr. The sulphur was then melted and solidified at the sealed end. The tube was then supported vertically at the other end on an aluminium heat sink through which water at room temperature was passed. The assembly was placed in a furnace and the temperature controlled between 80° and 100° C to give a sustained rate of crystallisation.

Crystals were formed at the cold end of the tube. The process was very slow. The crystals were very thin and fragile, about 1 cm in length and 1 to 2 mm in width. The thickness lay between 50 - 100 microns. Most of the crystals were opaque. A few of the thinner ones were transparent, but reverted to the opaque form at room temperature. This was thought to be due to the monoclinic form of sulphur changing to the orthorhombic. Runs were performed with a furnace temperature below 96° C, but without any change of this behaviour.

EXPERIMENTAL RESULTS5.1 Introduction

In the next four sections the results of the mobility of charge carriers in solid and liquid sulphur will be presented. Section 5.2 will deal with the crystalline sulphur grown from laboratory reagent (BDH)* and its melt while the more meaningful results of the liquid ultrapure sulphur (Acocn - Light)** will be presented in section 5.3. The results for the liquid are very complex; all the pulse shapes are therefore summarised in the beginning of the chapter in Figs. 5.1 to 5.7. The results on supercooled liquid sulphur and re - solidified sulphur are given in sections 5.4 and 5.5 respectively.

An attempt has been made to investigate the space charge distribution in liquid sulphur in section 5.6. In section 5.7 the dark conductivity of solid and liquid sulphur ^{are given} and, finally, in section 5.8 the charge generation and recombination lifetime measurements will be presented.

5.2 Laboratory Reagent Sulphur

Crystalline specimens grown from solution with laboratory reagent were prepared with plane parallel faces on which, in some experiments, semi - transparent gold electrodes were evaporated. In the specimen chamber, gold electrodes on the quartz discs were used.

The specimens were heated slowly from room temperature up to the melting point and above, and the changes in the transport properties

* For details see Appendix I.

examined. Monoclinic sulphur in the range from 96°C to 119°C was of particular interest. The temperature was increased in steps and $1/t_t - V$ graphs were obtained from photocarrier transits at each temperature. The mobility values calculated from the gradient of the graphs were plotted logarithmically against $1/T^{\circ\text{K}^{-1}}$.

Specimens with evaporated gold electrodes showed uncertain behaviour in the liquid state. Signals either disappeared completely or were rather noisy. Some specimens also showed strong polarisation effects in the liquid. A noticeable improvement of the general behaviour was observed if gold electrodes were not put on the specimen. However, because of the imperfect contact, in the solid, surface polarisation effects were observed which could only be overcome by careful application of routine discharge pulses.

Hole and Electron Mobilities in the Crystalline Solid

A few hole and electron mobility curves below the melting point have been plotted in figs. 5.8 and 5.9 respectively.

In the temperature range investigated, from room temperature to the melting point, the hole mobility curves show the characteristic features observed by Adams and Spear and discussed in section 3.1 (p.17). At room temperature the hole mobility as given by the present experimental points lies between 0.6 and $3 \text{ cm}^2/\text{volt sec}$.

As the temperature is increased above 96°C the integrated hole transits become rather nonlinear, as indicated by Fig. 4.5 (a). Nevertheless the measurements are sufficiently meaningful to indicate an

appreciable drop in hole mobility in the monoclinic range. Near the melting point it is difficult to integrate the signals and the current pulses are displayed. These are triangular due to carrier loss during transit, as shown in Fig.4.5 (b). No mobility values could therefore be obtained.

Electron transport differs substantially from the hole transport. A large number of specimens has been studied and a few mobility values are plotted in Fig. 5.9. These lie on a single straight line between $5 \times 10^{-4} \text{ cm}^2/\text{volt sec}$ at room temperature and $2.9 \times 10^{-3} \text{ cm}^2/\text{volt sec}$ at the melting point in the region of hopping transport (Fig. 3.2), discussed in section 3.1 (p. 17 and 20).

The monoclinic region was of interest but here also results on electron mobility were difficult to obtain because of deep trapping. In a usual temperature run between 96°C and 119°C lasting less than half an hour the electron mobility goes on increasing up to the melting point where there is a sudden drop of mobility. However, if the temperature is kept steady at a point in this range for several hours a rapid drop in mobility will take place, as shown by the results in Fig.5.10 obtained by Gibbons and Spear (34).

The above observations indicate that under certain conditions a drop in mobility takes place in the monoclinic temperature range. The mobility decreases due to a partial transformation to the monoclinic form. This increases the density of defects which will affect both hole and electron mobility by trapping and impurity scattering. It is also possible that there are regions of earlier melting formed as the

temperature approaches the melting point. This is likely between 113° and 119°C (melting point of orthorhombic and monoclinic sulphur respectively) if the specimen is partially transformed. Gibbons and Spear, however, obtained their results below 113°C .

Charge Transport in the Laboratory Reagent Liquid

In this subsection the mobility results obtained after melting the crystalline samples will be discussed. As the nature of charge carriers in the liquid is by no means obvious these will be referred to in the present chapter as negative and positive charges.

The signals observed for both positive and negative charges have some interesting features, as shown in Fig. 5.1. The current at first drops then rises to produce a rounded cusp after which there is a final slow drop to zero. The tail depicted by the final drop is unusually long. The transit time was measured by drawing tangents at the cusp as shown. For reasons discussed in the next subsection ("Anomalous Field Dependence of $1/t_t'$, p. 50), this may not be the true transit time and is denoted by t_t' .

The results obtained when both the negative and positive carrier mobilities were calculated from the t_t' values are shown in Fig. 5.11. These refer to specimens of 100 to 250 microns thickness. The results show a considerable scatter of experimental points and it was not possible to deduce a value for the activation energy. As shown in the figure, the negative carrier mobility drops to about $1 \times 10^{-4} \text{ cm}^2/\text{volt sec}$ at the melting point and remains near that value up to 160°C . The mobility

of the positive charges appears to be somewhat lower.

A significant fact about these results is that they were derived from $1/t'_t - V$ plots having a large intercept on the V - axis. An example is shown in Fig. 5.12.

Mobility measurements on melted crystals have been carried out with Kesa electrodes on quartz without any apparent improvement of the scatter of experimental results. Fig. 5.13 shows a plot of $\log \frac{\mu}{-ve} - 1/T$ for samples of 150 to 620 microns thickness; the overall scatter is about 400 %. Positive charges show the same general behaviour. Fig. 5.13 also indicates an apparent thickness dependence of mobility.

Above 160°C , photosignals are observable but are 'triangular' as shown in Fig. 4.5 (b). Consequently, no mobility values could be obtained.

Anomalous Field Dependence of $1/t'_t$

As pointed out in the previous subsection, $1/t'_t - V$ plots have large intercepts on the v - axis. It was felt, that much of the uncertainty in the previous results and also the apparent thickness dependence of mobility might be connected with this effect. In Fig. 5.14 the results for a number of specimens of widely different thicknesses have been correlated. In this graph d^2/t'_t has been plotted against V , so that the gradient should give the 'mobility'. On the same graph, line U.P. represents all the results obtained for ultrapure liquid sulphur (see next section, p. 51) which did not show this anomalous behaviour. The interesting fact brought out by this correlation is

that the thinner specimens are in approximate agreement with the U.P. results, whereas the anomalous behaviour sets in for specimens above about 300 microns thickness. These observations will be discussed and explained in section 6.5.

Field Transient in the Liquid

During experiments with pulsed fields, transients were observed simultaneously as the switching on of the field. This is shown in Fig. 4.8 together with the phototransit. The field transient has an apparent transit time t_f which varied with the applied field in the same fashion as t_t' . Calculated 'mobility' values are about $(2 - 4) \times 10^{-4}$ cm²/ volt sec in both directions of applied field for a specimen of 250 microns. Similar transients have been observed by Heilmeyer and Heyman (58) in azobenzene and p - azoxyanisole.

Field transients have also been recorded in subsequent experiments with ultrapure liquid sulphur using Nesa and Pt electrodes. These will, however, not be discussed further until section 5.6. The behaviour of field transients is rather complex and has not been studied extensively. However, from the current - voltage relationship (section 5.6) it was concluded that they are probably due to carrier injection from the electrodes by the applied field.

5.3 Liquid Ultrapure Sulphur

Although the results presented in the previous section brought out the general features of the charge transport in liquid sulphur they were not sufficiently accurate to lead to any more detailed information and understanding. To achieve this a series of experiments using liquid ultrapure sulphur were carried out.

Several granules of Koch - Light ultrapure sulphur were melted on the bottom quartz disc, which was shaken gently for the individual blobs of sulphur to form a continuous layer. The top quartz disc was then pressed on to the molten sample which re - solidified to a micro-crystalline layer of thickness equal to the spacers. Care was taken not to heat the sample for too long or to a temperature appreciably above the melting point. In these experiments only Kesa and Pt electrodes were used.

Negative Charge Transport in the Ultrapure Liquid Below 160°C

Negative carrier transits are well behaved in a fresh ultrapure sample. Typical transits are shown in Fig. 5.2. The tail is still too long to be explained entirely by diffusion of carriers (see estimate in section 4.1, p. 31) but it is shorter than that corresponding to the signals in the laboratory reagent liquid and allows transit time measurements up to the middle of the tail (t_t). However, in most cases with increasing temperature this tail lengthened as shown by the photograph of a trace in Fig. 5.3. For consistency transit time t_t^a was measured in all experiments on the ultrapure liquid. $1/t_t$ or $1/t_t^a$

versus V plots were linear up to the highest applied fields of about 50 K volts/cm; they passed through the origin yielding consistent values of mobility. There was no perceptible variation of mobility with sample thickness up to about 400 microns. Lifetime with respect to deep traps was estimated to be about 60 milliseconds

The mobility results on samples of 60 to 370 microns thickness obtained from the t_t^a values are plotted on a $\log \mu_{-ve} - 1/T$ graph shown in Fig. 5.15. The points lie on a straight line between 1.0×10^{-4} cm²/volt sec at 119°C to 1.5×10^{-4} cm²/volt sec at 160°C. The temperature dependence has the form,

$$\mu_{-ve} = A \exp \left(- \frac{E}{kT} \right)$$

The activation energy E was found to be 0.15 ± 0.03 eV and A to be (0.0088 ± 0.0040) cm²/volt sec. The activation energy is the same for mobility values calculated from t_t , as shown in Fig. 5.16, which was obtained with one specimen where measurement of t_t was possible within the temperature range. The difference in the calculated mobility values for both methods is about 20 %.

Measurements were carried out mostly at sufficiently low light intensities to keep the number of photocarriers as small as possible so that the 'self - field' (section 4.1, p. 29) of the carriers was small. However, because of large 'current noise' in the liquid this was not always possible. Higher light intensities were used in some experiments but no space charge limitation or variation of transit time due to the distortion of the internal field of the specimen

were detected.

Negative Charge Transport in the Ultrapure Liquid Above 160°C

In a few cases transients were observed above 160°C with a marked change in shape as shown in Fig. 5.4. The current decreased exponentially from the instant of photogeneration due to loss of carriers (resulting in ion formation) and the arrival of the reduced charge sheet was depicted by a slight discontinuity at t_t^a . The lifetime was reduced to about 5 milliseconds. This necessitated the application of comparatively high fields which was not always possible because of noise. These signals were first observed with Pt electrodes which, unlike Au or MoS₂ electrodes, showed very little increase of noise at high fields.

The results on several specimens are included in Fig. 5.15. The interesting feature is the absence of any major discontinuity near 160°C, although the mobility seems to decrease slightly above this point. This observation is of importance and will be discussed in section 6.4. It should be mentioned that a period of five or ten minutes was allowed for the polymerisation of sulphur to reach an equilibrium. To confirm the fact that changes observed above 160°C were due to polymerisation, specimens were heated quickly to this temperature and steady runs performed from there. Good agreement with previous results was obtained.

Positive Charge Transport in the Ultrapure Liquid Below 160°C

Positive carriers present a difficult problem even in the ultrapure liquid. Only in few cases, using Pt electrodes, was it possible to make meaningful measurements. The corresponding mobility values lie on a straight line between $5.5 \times 10^{-5} \text{ cm}^2/\text{volt sec}$ at the melting point and $9 \times 10^{-5} \text{ cm}^2/\text{volt sec}$ at 160°C, as shown in Fig. 5.15. The activation energy is remarkably close to that for the negative charges.

In most samples, however, no transits could be observed initially. After a period of heating transits appeared and exhibited the anomalous behaviour mentioned in section 5.2 (subsection at p. 50) and illustrated in Fig. 5.1.

In some specimens transits of the shape shown in Fig. 5.5 were seen on lowering the light intensity. The component of time t_t' was identified with the 'anomalous' signal (p. 50) and $1/t_t'$ varied with the applied field in a nonlinear fashion as shown in Fig. 5.17. In addition there was an indication of a slower component of time t_t'' .

The noise level permitting, at still lower light intensities, the t_t'' component only could be observed as illustrated in Fig. 5.6. $1/t_t''$ -V plots were linear with zero intercept as shown in Fig. 5.17. The corresponding mobility values agree well with those plotted in Fig. 5.15.

Positive Charge Transport in the Ultrapure Liquid Above 160°C

Certain changes occurred in the shape of positive carrier transit above this temperature, as shown by Fig. 5.7. Complications in the

form of components disappeared. There was little carrier loss during transit. However, accurate measurement of transit time was difficult at low fields because of extremely rounded tail of transit. At high fields there was a better definition of t_t^a .

The transport behaviour is again remarkable in that it is similar to that of negative carriers. In addition, there is a significant drop in mobility at 160°C; this is discussed in section 6.2 with reference to Fig. 6.1 which shows this drop clearly. Above 160°C the mobility decreases slowly with increasing temperature.

Effect of Heating on Charge Transport in the Ultrapure Liquid

It was noticed that ultrapure samples were extremely susceptible to heat treatment. This was, however, slow enough to make measurements over the whole of the temperature range possible.

The nature of the change is very complex. So far, the indications are that after this change has been established in a sample, the negative charges behave in the anomalous fashion (p. 50). Component structure as in the case of positive carrier transits have also been observed (p. 55). The term mobility is rather misleading as applied to such signals unless it refers to low fields and low light intensities (i.e., it refers to the slow component which behaves in the normal fashion). In an aged sample, the maximum extent of the change would be a reduction of mobility by 30 %.

For the positive signals the change was such that the slow component of transit was no longer observable.

5.4 Supercooled Liquid Sulphur

It was sometimes possible to cool samples of liquid sulphur below the melting point provided it had been kept above the melting point for a considerable time. Both positive and negative signals were observed down to 70°C. The resulting mobility values lie essentially on the extrapolated $\log \mu - 1/T$ curve. This is shown for negative charges in Fig. 5.11.

5.5 re - solidified sulphur

Only one sample of re - solidified sulphur produced measurable transits. The results for the electron mobility are shown in Fig. 5.9. One set of points (dots enclosed by circles) were obtained on cooling and the other (asterisks) on heating. The points lie within 40 % of that in the crystalline solid and lead to a gradient close to that for the crystal.

Hole signals have also been observed in the same sample and these had extremely nonlinear transit (Fig. 4.5 (a)) due to deep trapping. However, current pulses could be displayed and the mobility at 80°C was calculated to be about $3 \times 10^{-7} \text{ cm}^2/\text{volt sec}$, a factor of ~ 100 less than in the crystal.

It is interesting to note that the effect of destruction of the crystalline periodicity or long range order is different for electrons and holes. Electron transport is essentially unaffected indicating that only short range order is important in this case.

Unfortunately no other specimen produced similar signals because of

excessive deep trapping. This is not difficult to understand since, the destruction of long range order is likely to introduce an increased number of defects.

5.6 Space Charge Characteristics of Liquid Sulphur

The results of the charge carrier mobility in laboratory reagent liquid sulphur (subsection at p. 49) showed a large internal field as indicated by the intercept of $1/t_t' - V$ plots (Fig. 5.12). It was thought to be due to a build-up of a static space charge in the specimen. An attempt was made to obtain some information on the space charge distribution by (a) probe measurements (as discussed in connection with benzene, subsection of chapter 2 at p. 9) and (b) dark current measurements.

Probe Measurements

In this method a metal probe was used in contact with the sample. The following assumptions were implicitly made: (a) the probe does not disturb the potential distribution, and (b) the probe assumes the potential of the dielectric in contact with it.

In liquid or solid media there is no general theory of probes as the Langmuir theory for ionised gases. It is likely that the probe will assume the potential of the dielectric with more difficulty as the resistance of the dielectric increases. Indeed complications may arise if the density of mobile charges is too low in (a) charging the capacitance of the measuring apparatus and (b) supplying the current

through the measuring circuit under steady state conditions.

The present experiment was preliminary in nature. The arrangement is shown by a block diagram in Fig. 5.18. B is a porcelain boat which contains the liquid specimen. Two electrodes, fixed to the boat and separated by a distance d (~ 1 cm), are dipped in the sample with the probe between them. The applied potential across the electrodes is supplied by two power packs in series and providing potentials V_1 and V_2 with respect to earth. The part of the probe outside the liquid sample is well screened and insulated, and is connected through a null detector to earth.

The procedure was to set a value of $V_1 + V_2$ and alter V_1 and V_2 to vary the potential of the probe. The boat was there~~after~~ moved with respect to the probe until a null position of the detector was achieved, indicating that the liquid at that point was at the same potential as the probe. The distance of the probe from either electrode was measured from the initial and final readings of the micrometer.

Fig. 5.19 shows the form of potential distribution obtained in both ultrapure and laboratory reagent samples with gold electrodes and a Pt probe. The low field regions near the electrodes are thought to be due to injection of charge carriers from the electrodes in to the sample. But contrary to this, magnesium and Pt electrodes showed more or less linear potential distribution, as shown in Fig. 5.20. This probably explains the better behaviour of Pt electrodes in charge transport experiments (section 5.3).

The general conclusion is that at $E < 3$ K volts/cm there is no

analogy between the observed potential distribution in liquid sulphur and the results of Forster (Fig. 2.1) described in chapter 2.

Steady currents through the cell were measured and varied linearly with the applied field up to 2 K volt/cm. The conductivity of liquid sulphur was measured to be approximately 10^{-12} ohms⁻¹ cm⁻¹, in agreement with that obtained with Nesa electrodes in dark current measurements.

Dark Current Measurements

The arrangement for the dark current measurements is shown in Fig. 5.21. The power pack supplied the applied field and the current was measured with a Hewlett - Packard ammeter. In these experiments specimens of 150 to 200 microns thickness with Nesa electrodes on quartz discs were used.

When the field was applied the dark current rose to an initial value I_1 within the response time of the detector (~ 1 sec). I_1 then decreased within ten to twenty seconds to a certain value I_2 which represented essentially the steady state value. The dependence of I_1 and I_2 on applied potential is shown in Figs. 5.22 and 5.23 respectively. These results give interesting general information on the properties and behaviour of liquid sulphur in contact with Nesa electrodes.

Fig. 5.22 shows that (a) the initial current I_1 varies as the square of the applied potential and (b) that the results for laboratory and ultrapure liquids are identical. (a) suggests that there

is a free carrier reservoir of electrochemical origin near the sample-electrode interface which is injected by the field under space charge limited conditions. This current could not occur in the presence of a potential distribution given in Fig. 2.1 which certainly would not allow space charge limited current. (b) shows that this would apply to both laboratory reagent and ultrapure liquid sulphur. Very similar behaviour is exhibited by the current i_0^f in the field transient current signal shown in Fig. 4.8 (see also the subsection at p. 51). i_0^f is also plotted against V in Fig. 5.22 for ultrapure sulphur. The laboratory reagent liquid behaves similarly.

On the other hand Fig. 5.23 shows that in the behaviour of the steady current I_2 there is a basic difference between fresh ultrapure and laboratory reagent samples as shown by curves A,B and D,E respectively. Curves A and B for ultrapure sulphur show practically linear current-voltage relationship suggesting that electrodes at all potentials can supply and extract the carriers involved in dark conduction. It is therefore unlikely that appreciable polarisation can build up near the electrodes.

From the different behaviour of laboratory reagent samples as shown by curves D and E a number of valuable conclusions can be drawn. At low applied potentials the current tends towards an ohmic variation with the field. With increasing V , the curves show a sublinear relationship with an exponent between $1/2$ and $1/4$, and at high fields there is a rapid increase of current. Similar behaviour has been observed by Zaky et al.⁽⁵⁹⁾ in liquid hexane. This behaviour at low

and intermediate fields is in agreement with the predictions of the Thomson model (chapter 2, p. 11) for ionic transport in gases.

Thomson's theory, as applied to the liquids by Silver, provides the following relationship

$$V = C_1 I d + C_2 I^2$$

For large interelectrode spacing, d , as in the probe experiments, the ohmic part is predominant. In general, however, the above equation predicts a current - voltage characteristic consisting of an ohmic region at low applied potentials followed by a range in which $I \propto V^{\frac{1}{2}}$. In laboratory reagent sulphur as well as in hexane the exponent is, however, less than $\frac{1}{2}$.

We must therefore conclude that in the steady state, in laboratory ^{reagent} samples, the potential distribution is essentially that given by Thomson model (Fig. 2.1). From the behaviour of ^{the} initial current I_1 in laboratory reagent sulphur it appears that such a distribution could not have been present initially. This strongly suggests that the space charge layers determining the steady state current in laboratory reagent samples are composed of impurity molecules which are either present as ions or are ionised by the initial burst of free carriers. Curve C in Fig. 5.23, which was obtained with an ultrapure sample after half an hour of heating, seems also to indicate that reaction of liquid sulphur with the electrodes produces impurity molecules which ionise and set up space charge layers at the electrodes. It seems unlikely that the space charge layers are formed from S_8 ions, because such layers do not occur in a fresh ultrapure sample.

As the field increases further, the space charge at the electrodes will increase and a stage may be reached, depending upon the electrode material, when the potential drop at the electrodes is large enough to cause injection. The current in this case will rise superlinearly with the applied potential as indicated by curves D and E in Fig. 5.23 and Thomson's theory will no longer hold.

5.7 Solid - Liquid Transition of Dark Conductivity

with the present experimental chamber it was possible to make some preliminary investigation of the changes of dark conductivity of sulphur on melting. The current measurements were taken at one value of the field in the ohmic region for both ultrapure and laboratory reagent samples and the results plotted in Fig. 5.24. Mesa electrodes were used.

It can be seen that the experimental curves for the solid are in reasonable agreement with the conductivity values quoted in the I. C. T. (60). On melting there is no discontinuous change in conductivity. The gradient in the liquid is about the same as in the solid at room temperature.

The significant feature of the liquid curves is the absence of any ~~apparent~~ marked change at 160°C . In ultrapure liquid sulphur there is an increase of current after a slight drop at this temperature. For the laboratory reagent sample this drop is larger.

5.8 Efficiency of Carrier Generation in Liquid Sulphur

Efficiency of carrier generation is defined as the number of carriers produced per incident photon. In the sense used here this is different from the quantum efficiency which is defined as the number of carriers liberated per photon at the saturation field for which every carrier produced is drawn out of the generation region before it has a chance to recombine with a carrier of opposite sign. In the present experiment it was impossible to observe saturation even at the highest field that could be applied before breakdown. The efficiency is therefore specified at a value of the applied field and allows comparison of the generation efficiency at different wavelengths.

To calculate the efficiency at a given wavelength one needs first information on the number of carriers released by the incident light and second, the number of incident photons in the light pulse.

The number of carriers can be obtained from the oscilloscope trace of a carrier transit.

$$\frac{q}{e} = i_0 t_t$$

where i_0 is the initial photocurrent calculated from the initial pulse height (volts), as shown in Fig. 4.4, and the cathode follower input resistance.

The pulse light source was used in conjunction with a high resolution monochromator. The light output was calibrated with a sensitive N. P. L. calibrated photocell (Rank QVA 39) to give the intensity distribution of the spectrum down to 2300 Å.

The current i_c through the standard photocell was measured with a Hewlett - Packard ac microammeter. Light flashes with a repetition rate of 1 to 5 per second were used. The microammeter was not able to follow individual flashes and indicated an average current \bar{i} . Thus,

$$i_c = \bar{i} \frac{T_r}{T_p}$$

where T_p is the pulse width and T_r the interval between adjacent pulses or reciprocal of the pulse rate, as shown in Fig. 5.25. With the help of the photocell calibration in amp/ watt against wavelength this gave the number of ^{photons} per pulse.

The intensity distribution with wavelength of ^{the} light source is shown in Fig. 5.26. The monochromator (C. P. 4 Optica grating monochromator) had a spectral range from 10,000 to 1.800 Å and a spectral bandwidth of 16 Å/ mm slit width. For the present measurements the maximum slit width of 3.6 mm was used (i.e., a bandwidth of 57.6 Å). At this slit width the light output in the sensitive region of the specimen response was only about 10 % of the unmonochromated light. With such limited intensity the measurement of the spectral distribution of the generation efficiency was restricted to the range from 2300 to 3100 Å. Beyond these limits the photosignal to noise ratio was unity. Increasing the light intensity by the use of special filters also failed to show any response above 3100 Å.

Fig. 5.27 shows the spectral dependence of efficiency of photo-generation of both negative and positive carriers in liquid sulphur (ultrapure) at an applied field of 33 k volt/cm. The efficiency levels

off at approximately the same wavelength (2600 \AA) as in the solid. For comparison, the quantum efficiency curve for the solid is included in Fig. 5.27 which shows that the shape is fairly similar. One can conclude that the generation mechanism is not fundamentally different from that of the solid which has an optical 'band - gap' of 4.2 eV ⁽³²⁾.

Carrier Recombination Lifetime

The number of carriers drawn out of the generation region by the applied field per light pulse is given by,

$$q = Q \frac{\tau_R}{t_g}$$

where Q is the total number of carriers generated by the light pulse, τ_R is the recombination lifetime in the generation region, and t_g is the time taken by the carrier under consideration to cross the generation region. The condition for saturation is $\tau_R \gg t_g$. Q is given by

$$Q = \eta f e$$

where η is the quantum efficiency and f the number of incident photons per pulse. q is therefore given by,

$$q = \eta f \tau_R \alpha (\mu_e + \mu_h) E e$$

where α is the absorption coefficient. The photocurrent i_o due to electrons is then,

$$i_o = \frac{q}{t_t} = \eta f \tau_R \alpha (\mu_e + \mu_h) e \frac{\mu_e E^2}{d}$$

$$i_o \propto E^2$$

The validity of the above expression is borne out by the observed square law dependence of the transient photocurrent on the applied potential, as shown in Fig. 5.28. From ^{the equation} above it is also seen that $q \propto f$, which is the case for a monomolecular recombination where τ_R is independent of light intensity. This again agrees with the results of Fig. 5.29.

Either the linear $q - V$ (Fig. 5.30) or $q - f$ plots for a monochromatic radiation could be used to evaluate the parameter $\eta \tau_R$. Both calculations lead to a value of about 10^{-8} sec at 2500 Å. Here the absorption coefficient α at the wavelength concerned has been assumed to be the same as that in the solid ($\sim 10^5 \text{ cm}^{-1}$). The correction for reflection and absorption of light by the lower quartz disc amounted to about 20%. η is likely to be of the order of 10^{-1} (Fig. 5.27) and this would give $\tau_R \sim 10^{-7}$ sec.

DISCUSSION6.1 Introduction

In this chapter the results presented in chapter five will be discussed. In particular the following aspects are of special interest.

Liquid sulphur is unique for its anomalous variation of viscosity with temperature. The study of carrier mobility and of viscosity as a function of temperature provides, therefore, an excellent means of distinguishing electronic and ionic transport mechanisms. This is discussed in section 6.2.

The results of dark current measurements provide useful information regarding the effect of impurities on charge transport in liquid sulphur. Section 6.3 is devoted to this.

An attempt is made in section 6.4 to explain the charge transport behaviour above 160°C and in section 6.5 the far more complicated behaviour of laboratory reagent liquid sulphur is discussed and compared with the ultrapure liquid.

6.2 The Nature of Charge Transport in Liquid Sulphur

The main difficulty in interpreting the results of charge transport in liquids is to decide whether the transport is electronic or ionic, as can be seen from the survey of previous work in chapter two. The present work, however, allows us to make fairly conclusive deductions in this respect concerning the negative charge transport.

(a) Activation energy of mobility between 119° - 160° C

The mobility of negative charge carriers just above the melting point is 1.0×10^{-4} cm²/ volt sec, and up to 160° C it varies with temperature as in the solid :

$$\mu_{-ve} = A \exp(-\epsilon_k/kT) \quad \text{-----}(6.1)$$

where the activation energy ϵ_k is 0.15 ± 0.03 ev, which within the experimental error is the same as in the solid (0.167 ± 0.005 ev).

The negative charge transport in the liquid therefore appears to be closely similar to electron transport in the solid, apart from the fact that there is a drop in mobility by a factor of 30 at the melting point.

For the purpose of illustration the hopping probability P of an electron between neighbouring molecules is written down for the 'high temperature region' for which $\gamma \gg \hbar\omega_0/kT$. This is obtained by suitable expansion of Eqs. (3.4) and (3.6)

$$P = \frac{1}{\hbar} \left(\frac{\pi}{2 E_b kT} \right)^{\frac{1}{2}} J^2 \exp(-E_b/2kT) \text{---}(6.2)$$

It was shown in chapter three that a satisfactory fit was obtained between the experimental temperature dependence of mobility and the theoretical expressions of P through the equation

$$\mu_e = \frac{e a^2}{kT} P \quad \text{-----}(6.3)$$

In the liquid the activation energy of the mobility and therefore E_b is the same as in the solid, but the mobility is smaller by a factor of 30. For Eq (6.3) to be applicable to the liquid, P must

be reduced by the same factor, as 'a' is practically unchanged on going from solid to liquid. According to Eq. (6.2), J must be smaller by a factor of about 5.

J is a measure of the overlap between the relevant molecular orbitals ('Band Structure of Orthorhombic Sulphur', chapter three, p. 23) and therefore depends strongly on the relative orientation of the molecules. There is little change in the density of sulphur on melting (Fig. 3.7), but in the liquid the molecules have now additional degrees of freedom (e.g., rotational and translational). This rather more statistical arrangement of the molecules is very likely to reduce the average J. That is, an excess electron cannot jump to the neighbouring molecule until a favourable orientation of the molecule is achieved.

(b) Stoke's law and Walden's rule below 160°C

In the liquid, however, the molecules are mobile, so one cannot easily disregard the possibility of ionic transport. As mentioned in chapter two, there is no complete theory of ionic transport in liquids with complicated molecular structure. In the present discussion we shall examine the feasibility of an ionic transport in liquid sulphur on the basis of Stoke's law and Walden's rule.

The ionic mobility μ_i is given by Stoke's formula (p.4)

$$\mu_i = \frac{q}{6\pi\eta r} 10^7 \text{ cm}^2/\text{volt sec} \quad \text{-----(6.4)}$$

The molecules in the liquid (S_8) are assumed to be spherical due to their ability to rotate about the centre of gravity; the radius

of the sphere is about 3 \AA . The viscosity near the melting point is 0.12 poise (Fig. 3.6). Then assuming one electronic charge per ion, μ_i is calculated to be $2.5 \times 10^{-5} \text{ cm}^2/\text{volt sec}$, a factor of 4 smaller than the experimental value of the negative carrier mobility. However, as deGroot, Gary and Jarnagin (p.5) have shown, an effective radius should be used for ions having a radius less than 5 \AA . Their theory has been applied successfully to ions of a wide variety.

According to the theory of deGroot et al, the principal contribution to the electrostatic field at a point in a fluid near a charge is assumed to be of Coulomb origin. Then supposing that a neutral molecule remains attached to ionic charge q if the energy per molecule at the distance of approach is greater than kT , an effective radius of the ion is found to be

$$r' = \left[\frac{q^2 M}{32 \pi^2 N_A kT \epsilon \epsilon_0 \rho} \right]^{1/4} \quad \text{-----(6.5)}$$

where, N_A is Avogadro's number, M is the molecular weight and ρ is the density. Eq. (6.5) is in M. K. S. units. It is not clear whether this theory is applicable to liquid sulphur, which is non - polar, but such a correction would decrease the ionic mobility further as the following estimation shows. For liquid sulphur, at 400°K , ϵ is $3.52^{(61)}$ and ρ is $1.76 \times 10^3 \text{ Kg/m}^3$. Therefore, r' is calculated to be 18.4 \AA . The estimated mobility from Stoke's law is then $3.8 \times 10^{-6} \text{ cm}^2/\text{volt sec}$ at the melting point. This is a factor of about 30 smaller than the experimental value.

Another aspect of ionic transport is Walden's rule (p. 4),

$$\begin{aligned} \mu_i \eta &= \text{constant} \\ \mu_i &\propto \exp(-\epsilon_i/kT) \end{aligned} \quad \text{----- (6.6)}$$

where ϵ_i is the activation energy of viscous flow of liquid sulphur which is in fact 0.23 eV between the melting point and 160°C. This value of ϵ_i is about 50 % larger than the activation energy associated with the negative carrier mobility and Walden's rule does obviously not hold for the negative charge transport. This result, together with the estimated ionic mobility of at least a factor of 4 smaller than the observed values suggests strongly that the negative charge transport is electronic rather than ionic.

(c) Stoke's law and Walden's rule above 160°C

The most convincing evidence against ionic transport is provided by the continuation of the mobility curve above 160°C. Although there is a slight decrease in mobility with temperature, it is not nearly as much as Eq.(6.6) would suggest. For example, the viscosity at 164°C is 124 poises. If the charge transport below 160°C were ionic, the mobility should drop by a factor of 10^3 at this temperature. In fact the observed drop in mobility is less than 20 % of the value just below 160°C. It may be argued that the charge species are different below and above 160°C. However, from the smooth transition between the two regions (see Figs. 5.15 and 6.1), this seems unlikely. ~~So~~ ~~that~~ It will be assumed that the same charge species is responsible for the transport throughout the whole temperature range

On the evidence summarised in this subsection, there is little doubt that the negative charge carriers observed in ultrapure liquid sulphur are electrons which move by an intermolecular hopping mechanism.

The Nature of Positive Charge Carriers

The same considerations as for the negative charges apply to the positive charges as well. Apart from the fact that the mobility is a factor of 2 less than the negative carrier mobility, the positive charges behave in a remarkably similar fashion to the negative charges. The magnitude of mobility indicates that unlike the hole transport in the solid (section 3.1, p. 17) holes in the liquid move by means of intermolecular hopping. The intermolecular overlap between the lone pair orbitals would certainly be reduced on melting thereby reducing the hole band width. It is possible that with the loss of long range order, the intramolecular overlap of the lone pair orbitals may increase producing σ - type states where the holes could be localised and thus give rise to a phonon assisted hopping mechanism as in the case of electrons.

The Possibility of a Mixed Electronic and Ionic Motion

At this point one must distinguish between trapping of electrons by neutral molecules to form stable ions and 'self - trapping' (i.e., the localisation leading to hopping transport). When a stable ion is formed by trapping of an electron, it is a permanent state until the ion recombines or is neutralised at the positive electrode. In the case

of 'self - trapping', the electron is able to move between neighbouring molecules by phonon assisted transitions. But since the molecules are mobile, the overall transport is due to both ionic and electronic motion. One can then write, for the observed mobility

$$\mu = \mu_i + \mu_e$$

Just above 160°C , the ionic component μ_i is at least a factor of 10^3 smaller than μ_e . So, one should expect a drop in mobility at this temperature due to the absence of the ionic component in the above equation, even if the electronic part of the transport is somewhat different (section 6.4) from that below this temperature. As shown in Fig. 6.1 (a re - plotted version of Fig. 5.15 in the temperature region of interest), the positive mobility shows such a drop from which an ionic mobility of about $3 \times 10^{-5} \text{ cm}^2/\text{ volt sec}$ at 162°C is deduced. The ionic mobility calculated from Stoke's law and viscosity activation energy is $4.8 \times 10^{-5} \text{ cm}^2/\text{ volt sec}$ at 162°C . Considering the experimental error in measuring the positive carrier mobility the agreement is good. However, the electron mobility shows no equivalent drop, and it appears therefore that the negative ions must have a mobility of not more than about $1 \times 10^{-5} \text{ cm}^2/\text{ volt sec}$ (within the experimental error) at 162°C . It is not entirely clear why the negative and positive ions should have different mobilities. One possibility is that they are different ionic species e.g., impurity and sulphur ions.

6.3 Charges in the Dark

It was seen from the results in section 5.6 (p. 60) that a reservoir of charges is present near the electrodes (field transient current) which are swept away on the application of a steady field until a steady state is reached. The steady state current behaviour is different in the ultrapure and laboratory reagent liquid. In ultrapure samples this is ohmic up to about 50 K volt/cm indicating that charges are being extracted and replenished by the electrodes to preserve the condition of charge neutrality and that there is no appreciable build up of space charge (i.e., the potential distribution is uniform). In laboratory reagent samples the electrodes appear to behave as blocking contacts i.e, there are considerable heteropolar space charge regions near the electrodes. The silver - Thomson model is applicable to this case and the experimental results are in general agreement with predictions based on this model.

The nature of the charges in the surface layers is not known. Nevertheless the results suggest that in the laboratory reagent samples the space charge layers are formed from impurity ions which are not easily extracted by the electrodes. It is unlikely that these layers are composed of S_8^+ or S_8^- ions, because of their absence in a fresh ultrapure sample. However, after prolonged heat treatment ultrapure liquid sulphur shows evidence of space charge layers resulting from impurities which are probably produced by reaction with the electrodes.

As discussed by Rose ⁽⁶²⁾, the striking difference between a metal - electrolyte and a metal - semiconductor contact is that in

the former, up to a few volts, an extremely high capacitance corresponding to a spacing of "plates" of only about 1 \AA is observed. This means that the contact is supporting a field of 10^8 volts/cm, in contrast to maximum fields of about 10^6 volts/cm in solids. The reason the metal - electrolyte can support such high fields is that conduction in the electrolyte is by actual ions themselves rather than electrons. The electrons on the negative ions lie energetically a few volts below the Fermi level in the metal and hence cannot flow into the metal either directly or by tunneling. The negative ions in the electrolyte tend to accumulate at the electrode surface until the electric field is high enough to raise the electrons to the level of the Fermi surface of the metal. The raising of the electrons is also facilitated by chemical reaction.

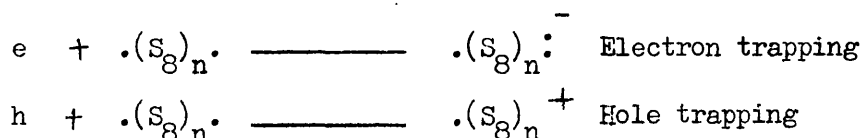
The results of current measurements therefore indicate that the electrons in a fresh ultrapure sample are more loosely bound to sulphur molecules than to an impurity molecule in the laboratory reagent samples, and that their energy is close enough to the Fermi energy of the electrode (Wesa) for them to be easily extracted by the applied field. Similar arguments apply for holes in liquid sulphur.

6.4 Charge Transport in Liquid Sulphur Above 160°C

Although the observed transport behaviour in liquid sulphur above 160°C provides ~~an~~ important evidence against ionic transport, it still remains to explain the slight decrease in mobility with temperature in this range. This effect has been observed in a number of specimens and

appears to be a genuine transport property. Ideally, in the absence of an ionic transport (if it plays any part at all in the normal liquid below 160°C) the gradient of $\log \mu - 1/T$ should remain negative above 160°C, as expected from a phonon assisted hopping transport. But in the case of liquid sulphur, the anomalous change in viscosity is accompanied by polymerisation of the ring molecules as discussed in section 3.2, p. 25. The possibility that polymerisation may decrease the hopping probability will now be discussed.

Suppose the hopping probability P is a function of only the overlap between the ring molecules. Any chain molecule, which may fill the space between neighbouring ring molecules acts only as a deep trap for electrons. The process of trapping by catena molecules $(\cdot(S_8)_n\cdot)$ is as following



(The dots represent an unpaired electron at the chain ends). Evidence for the sudden enhancement of trapping is obtained from the shape of negative transit signals above 160°C (Fig. 5.4).

The mobility in the high temperature region is given by Eqs. (6.2) and (6.3) as

$$\mu_e = \frac{e}{h} \frac{\pi}{kT} \left(\frac{\pi}{2 E_b k T} \right)^{\frac{1}{2}} a^2 J^2 \exp(-E_b/2kT) \quad (6.7)$$

Provided the chain molecules do not assist in the hopping process 'a', the average distance between neighbouring ring molecules, will

increase with the degree of polymerisation. But J , on the other hand, decreases with increasing 'a'. The resulting temperature dependence of mobility will therefore depend on the variation of the product $a(T) J(T)$.

$a(T)$ can be determined from the known temperature dependence of the equilibrium of S_8 ring molecules and catena sulphur chains (or M) shown in Fig. 3.8. The results are plotted in Fig. 6.2. The calculation of the change in the overlap integral J with increasing 'a' is in general a difficult problem. However, in the present case we are only concerned with small changes in 'a' under conditions of very small overlap. The estimate will therefore not be critically dependent on the assumed form of J . As a first approximation we put

$$J = J_0 \exp(-a/a_0) \quad \text{-----}(6.8)$$

where J_0 and a_0 are constants.

If $\mu(T)^{\text{ext}}$ represents the extrapolated electron mobility data beyond about 160°C for constant 'a' and J (curve A in Fig. 6.1), then the observed mobility $\mu(T)^{\text{obs}}$ is given by

$$\frac{\mu(T)^{\text{obs}}}{\mu(T)^{\text{ext}}} = \frac{a(T)^2}{a^2} \exp\left(-\frac{a(T) - a}{a_0}\right) \quad \text{---}(6.9)$$

From the fit to the experimental data $a_0 \sim 10^{-8}$ cm. The calculated curve beyond 158°C is shown in Fig. 6.1 in good agreement with the experimental points. With the given a_0 substitution into Eq. (6.8) gives $J/J_0 = 3 \times 10^{-3}$ for the liquid. This is in reasonable agreement (considering the factor of 5 drop in J in the liquid) with the calculated overlap ratio of 8×10^{-3} in the solid obtained by D. J.

Gibbons (private communication):

The above treatment, although crude, provides therefore a satisfactory explanation for the observed transport behaviour. Also, this model appears to be equally applicable to holes in the liquid.

6.5 Anomalous Behaviour of Photogenerated Charges in Liquid Sulphur

This section will deal in general with the results which show the anomalous behaviour mentioned in section 5.2 (subsection, p. 50) for both negative and positive charges in laboratory reagent liquid sulphur and in section 5.3 (subsection, p. 55) for positive charges in liquid ultrapure sulphur. These results refer to the temperature range between 120° - 160° C and are summarised below.

(a) In a fresh ultrapure sample where the negative signals are well behaved, positive signals are initially 'triangular' (Fig. 4.5 (b)). After prolonged heating, positive 'transits' could be observed and behaved in anomalous fashion (p. 55). This is accompanied by a similar change in the negative signals (subsection, p. 56). Signals of both polarity have now the shape shown in Fig. 5.1 at high light intensities and $1/t_t' - V$ plots are non-linear. At lower light intensities the signals revealed an additional component with a well defined transit time t_t'' (Figs. 5.5 and 5.6); $1/t_t'' - V$ plots are linear with zero intercept (Fig. 5.17). Thus after heating, the transport behaviour in the ultrapure liquid approaches that in the laboratory reagent samples.

(b) In laboratory reagent samples only the component of time t_t' was observed. Both negative and positive charges behaved in the same fashion.

As concluded in section 6.3 it is most likely, that the observed changes in transport behaviour in the ultrapure liquid is due to the formation of impurity ions by prolonged reaction of liquid sulphur with the electrodes.

In this discussion reference will be made to the $d^2/t_t' - V$ plot in Fig. 5.14 obtained with several specimen thicknesses. These results were obtained with laboratory reagent liquid sulphur and represent the general behaviour of the anomalous signal. An interesting feature of these signals is brought out by plotting the true transit time i.e., t_t^a in fresh ultrapure sulphur, against t_t' obtained from Fig. 5.14 for specimens of widely different thickness. This is shown in Fig. 6.3. It can be seen that for thin specimens $t_t' \simeq t_t^a$. With increasing thickness t_t' tends towards a constant value of about 24 milliseconds.

It is suggested that the above behaviour is a result of trapping of fast carriers (electrons or holes) by impurity molecules. Because of their low mobility these form essentially a static ionic space charge during the transit of the remaining carriers. It is suggested that t_t' corresponds not to the true transit time but is an enhancement of current due to the increased resultant field and will occur approximately at $t_t' \simeq \tau$, the lifetime of the carriers with respect to ion formation. This is illustrated in an essentially qualitative way in the following.

If N_0 is the initial number of excess fast carriers generated by light at $t = 0$, the number of fast carriers as a function of time is

$$N(t) = N_0 \exp(-t/\tau)$$

The number of slowly moving generated ions is at any time t given by

$$N'(t) = N_0 [1 - \exp(-t/\tau)]$$

The self-field E' due to this space charge of slow ions will build up in time τ and the remaining fast carrier cloud at $x \approx \mu E \tau$ will be subjected to an additional field E' which is roughly proportional to $N'(\tau)$. The question now arises: will E' be sufficiently large to affect the resultant field E in the specimen?

In Fig. 6.4 curve (a) shows the field distribution $E(x)$ that would be expected in a laboratory reagent specimen (section 5.6 and Fig. 2.1). Soon after switching on of the field part of the surface charge Q is screened from the interior of the specimen by the ionic space charge layer Q_i of opposite polarity. This will reduce E to an approximate value $(Q - Q_i)/\epsilon E_0$. From the geometrical capacity (~ 1 pf) of specimen it is estimated that $Q = 2 \times 10^9 e$ for a specimen of 500 microns in thickness and an applied potential of 400 volts. Q_i might be about $0.5 \times 10^9 e$ so that the internal field is reduced to about $\frac{3}{4}$ of the expected value. With the comparatively high intensities of flash illumination used in these experiments the initial current height leads to a value of $N_0 = 10^9$ generated carriers per flash. $N'(\tau)$ will thus be about 0.7×10^9 ions per flash which will be distributed with decreasing density from $x=0$ to about $x = \mu E \tau$ (150 - 200 microns) as indicated in Fig. 6.4. The significant point is that $eN'(\tau) \approx Q_i$

and the two will always be of opposite polarity. (The case shown in Fig. 6.4 refers to electron generation at $x \neq 0$). The generated negative ions will thus tend to increase the resultant field for $x \gg \mu_E \tau$ by largely compensating the effect of polarisation charge Q_i . At $x \sim 250$ microns E is likely to level out at a higher value than before as indicated by curve (b) in Fig. 6.4. The generated ionic space charge is unlikely to affect the field distribution near the positive electrode to any extent.

The transient current signal measured under these conditions will depend on the product $E(t)N(t)$. The time dependence of both these factors, together with the expected current signal is shown in Fig. 6.5. It is now clear that in the region of decreasing $N(t)$ and increasing $E(t)$, $I(t)$ should go through a maximum which should correspond to the measured value of t_t' . This value should be somewhat larger than the lifetime with respect to ion formation, τ , which might be about 15 - 20 milliseconds in a laboratory reagent specimen. Fig. 6.5 also shows a small 'hump' due to the effect of the large anode field on the remaining carriers. This can be identified with the time t_t'' observed with some specimens. With decreasing light intensity $N'(\tau)$ decreases and the effect of the generated ionic space charge on the transport becomes negligible. This is borne out experimentally by the fact that at low light intensity the maximum at t_t' disappears.

So far the discussion referred to thick specimens (400 - 700 microns) for which $d \gg \mu_E \tau$. For thinner specimens (up to about 250 microns) the field increase takes place closer to the anode and the position of

the current maximum at t_t approaches the true transit time t_t^a . This is clearly shown in Fig. 5.14 and in Fig. 6.3 for $t_t^a < 20$ milliseconds.

In a fresh ultrapure sample the lifetime of generated electrons with respect to ion formation is very long; a roughly estimated value for the lifetime is about 60 milliseconds (section 5.3, p. 53) and the above effect is not expected to occur.

The above model therefore provides a reasonable explanation for the observed behaviour of laboratory reagent sulphur. The decrease of mobility calculated from t_t'' (in ultrapure sulphur) with duration of heating (subsection, p. 56) may also be explained in terms of ionic space charge which collects at the electrodes. It may be shown very generally (Hellyer, F. G., private communication) that any non - uniformity of field distribution will increase the transit time. Since the density of ions increases (section 5.6) with duration of heating, t_t'' will also increase.

FLUORESCENCE OF SULPHUR7.1 Introduction

Fluorescence and phosphorescence are two special cases in the general category of luminescence. When luminescent materials are excited by radiation or cathode rays (electrons), emission may occur during excitation and in some cases, for considerable periods after the excitation has ceased. Fluorescence is the term applied to emission between states of equal multiplicity and usually has a small radiative lifetime. Phosphorescence is the term which is applied to emission between states of differing multiplicity and usually has a long radiative lifetime.

The investigation of the occurrence and characteristics of luminescence of molecular substances has not only increased the general knowledge of such processes but has provided a powerful method of determining electronic structure of molecules.

The occurrence of luminescence can be discussed by means of energy diagrams which represent the normal and excited states of the molecule. A molecule not only possesses electronic energy but also vibrational and rotational energy. These extra degrees of freedom are subject to quantum conditions as in the case of electronic energy.

The upper and lower curves of Fig. 7.1 is a schematic representation of the potential energy configuration of a diatomic molecule in its excited and normal states respectively. Vibrational levels are represented by horizontal lines attributed to each curve. Rotational levels are not included. At ordinary temperatures the unexcited molecule will possess not more than one or

two vibrational quanta. A schematic diagram of the energy state of the same molecule is also shown in Fig. 7.2. Absorption of light causing electronic excitation will raise the molecule into its excited state by transition AA'. Coupling between the electronic and vibrational states of the molecule in the excited condition will lead to deactivation to state B'. A resonance transition A'A taking place is unlikely if coupling is present. After the state B is reached luminescence will occur with transition B'B to the ground state and further loss of energy by coupling with vibrational states so that the initial state A is once more reached. The lifetime of the excited state of the molecule will depend on several factors, including the transition probability for luminescence and the disturbance by external agents. Furthermore, there is always a probability of a non - radiative return to the ground state if the state 'C' is reached (internal quenching). In luminescent molecules the vibrational states will effect such transition at higher temperatures and a formula for the internal quenching has the form

$$\beta = \frac{1}{1 + p^{-1} b \exp(-E/kT)}$$

where β is the luminescence efficiency and p is the probability of optical transition B'B. $b \exp(-E/kT)$ is the probability that the molecule will reach the ground state by the path B'C'CB. E is the energy of transition B'B. In most cases of quenching in organic molecules the above process is obscured by other influences such as, external or collision quenching and photochemical changes (e.g., predissociation).

According to the model discussed, the absorption and emission spectra of molecules will consist of regularly spaced bands corresponding to transitions between vibrational levels of the ground state to those of the excited state. The energy difference between adjacent bands would be expected to correspond to that between the vibrational states. As an example, Fig. 7.3 gives the absorption and emission spectra of solid anthracene ⁽⁶³⁾. A mirror image effect is usually observed between the spectra. Exact correspondence does not occur since the absorption involves transition at a certain temperature from the corresponding vibrational level of the ground state to any of the vibrational levels of the excited state, while emission is due to transitions from the excited state to any of the vibrational levels of the ground state, as shown in Fig. 7.2. The first excited state for anthracene is placed at approximately 3 eV, corresponding to 4000 Å wavelength, where the two spectra coincide. This excited state has a short lifetime and is therefore assigned to be a singlet, since the ground state is also a singlet and the transition between the states are allowed. Phosphorescence is also observed in anthracene corresponding to a triplet to ground state transition, which is forbidden. The emission has a lifetime of the order of milliseconds.

The purpose of the present investigation of emission in sulphur was made to gain some knowledge of the molecular excited states of S_8 in the solid. The study of the optical properties ⁽³²⁾ gives no clear indication of the first excited state of the molecule. The extensive work on the organic molecules show such information should be obtained from

luminescence.

7.2 Experimental Methods and Results

The excitation of emission in sulphur at room temperature has been studied for three kinds of exciting radiation. These were ultraviolet to the visible radiation ($2300 - 4500 \text{ \AA}$), high energy electrons and x - rays. The signal was studied either with small bandwidth filters or when stronger, with a monochromator.

For optical excitation the specimen was mounted at the input of Optica grating monochromator, as shown in Fig. 7.4. An EMI multistage photomultiplier (type 9526 S) was used at the output to detect any signal. The exciting radiation of wavelength from 4500 to 2500 \AA was filtered from a H_2 - lamp, an iodine or a tungsten filament lamp and the longer wavelength region was scanned for the emission signal. An arrangement was also used where the front illuminated surface was studied for the emission. No genuine emission was detected with either arrangement.

Next, high energy electrons from an electron gun were used for the excitation of the sample. Electrons of up to 30 K ev were generated and focussed on to the specimen placed inside the gun, as indicated in Fig. 7.5. The photomultiplier was placed outside the gun in front of the window facing the specimen. Some emission was detected which, however, appeared to originate mainly from other sources such as the window and the photomultiplier envelope. These luminesced under the x - rays generated by the bombarded specimen. It was difficult to perform

a blank experiment where the specimen was absent since most parts of the specimen holder also produced x - rays under electron bombardment.

Excitation by X - Rays

X - rays were generated by ^aPhilips PW 1008 self - rectifying ~~type~~
~~source~~ ^{generator} run by a stabilized power supply. A copper target was used.

X - rays were received by the specimen through a mica - beryllium window which was blocked by a thin black paper to cut out any stray filament light from the tube.

The experimental arrangement was the same as that for optical excitation (Fig. 7.4). The specimen was placed at the input of a monochromator and the photomultiplier placed at its output. Care was taken to eliminate all stray light in the room reaching the experimental arrangement by covering it with black cloth.

Different specimens were used. Crystalline specimens of thickness ranging from 150 to 900 microns were grown from solution and prepared as discussed in chapter four (subsection at p. 43). Melt crystals (subsection, p. 43) were also used. In some experiments a thin layer of re - solidified ultrapure sulphur (Koch - Light, Appendix I) was investigated.

All specimen exhibited an emission in the blue - green region of the optical spectrum, 5900 to 4500 Å. When a thin black card having negligible x - ray absorption was placed in front of the specimen (i.e., between the specimen and monochromator) a background reading could be observed with the photomultiplier. This was thought to be due to lumin-

escence of the internal optics of the monochromator under x -ray irradiation. It was reduced by careful alignment and lead shielding of the monochromator. In all subsequent experiments the background reading which amounted to about 20 %, was subtracted from the emission reading. The maximum signal obtainable with the highest permissible power of the source (40 ma at 40 K volts) was too small for the Optica grating monochromator. A simple prism monochromator was therefore used with a dense flint prism at 1 mm slit width. A pen recorder was used in conjunction with a Hewlett - Packard ammeter, as an amplifier, to record the signal.

Fig. 7.6 shows results obtained from a large number of recorder plots using a moderate source power (30 ma at 35 K volts). The photomultiplier voltage was 800 volts and its response in the region of emission was nearly constant with the number of photons. The spectral resolution at 1 mm slit width was about 100 \AA and is indicated in the figure.

Three emission peaks were detected at 4900, 5300 and 5700 \AA . The average distance between the consecutive peaks are 0.15 ev. Other smaller peaks may be present but they were often masked by the background noise of the photomultiplier and the x - ray source or the lack of spectral resolution.

A preliminary investigation was made of the temperature dependence of the emission. The specimen was cooled down to -70°C from room temperature and an enhancement of the emission by 20 % was observed.

7.3 Quantum Yield of Fluorescence

The quantum yield of emission is defined as following

$$\beta(\nu) = \frac{\text{emitted number of quanta } (\nu)}{\text{absorbed number of quanta } (\nu')}$$

It is difficult to estimate β with any accuracy in the case of x-ray excitation. Part of the incident beam is transmitted by the specimen, the amount depending upon the frequency of the radiation. Of the absorbed x-rays, only a small fraction is utilized in producing emission, the remainder being dissipated in exciting fluorescent x-ray emission and electrons by photoelectric processes. Heating of the specimen may also take place as a part of the dissipative process. The calculation of the amount of absorbed radiation is also made difficult by the existence of characteristic lines in the x-ray beam superimposed on a large continuum from an unmonochromated source, such as used in the present case. A rough estimate could however be made from the knowledge of the average absorption coefficient of sulphur for x-rays, as shown later.

Excitation in the ultraviolet to visible region should be a better method to study the behaviour of high energy bound electrons. Unfortunately solid sulphur did not show any emission under excitation by ultraviolet radiation for which sulphur has a very small absorption depth. It was thought that this might be due to external quenching by impurities in the solid surface. A further attempt to detect the emission on ultraviolet excitation was made on a dilute solution of sulphur which now has a large absorption depth.

Spectroscopic quality ethyl alcohol was used as the solvent. And

for this experiment a spectrofluorometer ("Fluorispec") by Baird Atomic Instruments was used. The solvent was first scanned for indications of impurities. From the positions of absorption and emission peaks, the solvent appeared to contain traces of general impurities of the aromatic hydrocarbon type. Judging from the emission strengths observed in the present apparatus from solutions of known anthracene concentrations and using an effective quantum efficiency of about 0.3, the impurity content of the ethyl alcohol was estimated to be about 10^{-8} - 10^{-9} mole/ litre.

Two solutions were prepared of concentrations, 2×10^{-4} and 2×10^{-5} mole/ litre of S_8 using ultrapure sulphur. These solutions failed to produce any emission in the region of 3000 to 6000 Å on excitation with radiation of wavelength from 2300 to 5000 Å. This result refers to both room temperature and liquid nitrogen temperature. The experiment at liquid nitrogen temperature was performed with the more dilute solution in a quartz tube immersed in liquid nitrogen contained in a quartz dewar. Considerable increase of light scatter was introduced due to nitrogen bubbles produced during irradiation and resulted in a 1/20 th smaller signal - to - noise ratio than for the solution at room temperature.

Table 7.1 (next page) shows the results obtained. From the effective quantum yield of about 0.3⁽⁶⁴⁾ in ethyl alcohol and the estimated detectability of the spectrofluorometer it was concluded that S_8 has no emission whose effective yield exceeds 10^{-4} .

From this result, any impurity in the ultrapure sulphur which

absorbs in the ultraviolet - visible region and emits with 0.3 efficiency would have been detected in the sulphur solutions down to about 10^{-8} to 10^{-9} mole/ litre. Since no emission attributable to other than the solvent sources was observed in the 10^{-4} mole/litre solution, then no emitting impurity was present in the solid sulphur to greater than 10^{-4} to 10^{-5} mole/ litre or 1 - 10 ppm.

Table 7.1 (a)

Detectibility of "Fluorispec"

Yield	Conc.	Abs. Coeff. (average)	Emission strength	Comment
0.3	10^{-7} M Anthr. in EtOH	10^4 litre/mole cm	100	Experimentally demonstrated to be sufficiently dilute, so that signal is proportional to concentration.
0.3^*	10^{-9} M impurity in EtOH	10^4 * litre/mole cm	1	Detectable at a signal-to - noise ratio of 2 or 3.

* Assumed values

Table 7.1 (b)

Efficiency of Sulphur in EtOH

Emission strength	Conc.	Absorption Coefficient (average)	Yield
Undetectable S/N 1	2×10^{-4} M	10^4 litre/mole cm	Therefore $\leq 10^{-4}$
Undetectable S/N 1	2×10^{-5} M	10^4 litre/mole cm	$\leq 10^{-4}$

In the following a rough estimate is given of the emission efficiency for x - ray excitation.

The efficiency of generation of x - rays is given roughly by

$$G = 1.1 \times 10^{-9} Z V$$

where Z is the atomic weight of the target and V the tube voltage. For a copper target Z is 29, G is therefore 0.1 % of the total generated power at 35 K volt. When a current of 30 ma is flowing, the power of generated x - rays is therefore 0.1 watt, which is further reduced by collimation to 10^{-3} watt. This is distributed over a range of wavelength as shown in Fig. 7.7. However, the absorption coefficient for x - rays increases with wavelength and, in the region of 1.5 \AA it is such that the energy absorbed by a specimen of 300 microns (average thickness) is about $0.75 I_0$ where I_0 is the incident energy. It is therefore assumed that nearly a third of the x - ray energy (the longer wavelength side of 1.5 \AA - Cu K_{α} lines) is completely absorbed by the specimen. This corresponds to about 10^{12} x - ray photons per sec, assuming an average wavelength of 2 \AA .

From the photomultiplier calibration with a light source of known intensity distribution (photons per sec), the maximum number of visible photons emitted by sulphur under x - ray irradiation (Fig. 7.6) is estimated to about 10^6 per sec. So the emission yield is about 10^{-6} .

It should be pointed out that the x - ray absorption coefficient is given by

$$\alpha_x = \gamma + \delta + \dots$$

where γ , δ , \dots etc. are the absorption coefficients for various

processes, such as the photoelectric process, Compton scattering, fluorescent x - ray emission and other processes one of which is the emission in the visible region. In the latter process electrons in the higher bound states (valence electrons) are raised to higher states (singlet or triplet states) and produce an emission when they return to the ground state. 10^{-6} is therefore approximately the lowest limit of efficiency of emission of solid sulphur by x - rays.

7.4 Discussion

The emission spectrum obtained experimentally for solid sulphur as shown in Fig. 7.6 bears a close resemblance with that of anthracene (Fig. 7.3). It is therefore tempting to interpret the sulphur spectrum in the same way. One would according to this interpretation, expect the excited state to lie in the region of 4600 \AA , 2.7 ev.

One would also expect the average distance between the vibrational peaks to correspond to the features of the infra - red spectrum of sulphur as shown in Fig. 7.8. It is therefore unlikely that the vibrational interaction takes place in the strong band at 0.11 ev, but there is a smaller peak near 0.15 ev which may be connected with the emission peaks.

The photoconductivity and absorption spectrum are shown in Fig.7.9 together with the emission spectrum. (The weak emission corresponds to weak absorption and no vibrational structure is expected to show up in the absorption spectrum). The interesting fact is that there is a photoconductivity peak centred at 4500 \AA which has been shown to be

associated with surface generation of free holes ⁽³²⁾. In view of the present results it may be suggested that the free hole generation may be due to interaction of the molecular excited states with the surface states.

It is possible that some impurities in sulphur are responsible for the observed emission. However, we are reasonably sure that this is an intrinsic property of the S_8 molecule since, specimens from different sources showed the same emission characteristics without any perceptible variation of intensity (section 7.2, p. 88).

The low emission efficiency may be due to some quenching processes such as internal and external quenching, and predissociation. The case of internal quenching has been discussed in section 7.1 where the excess energy of the molecule is converted into vibrational energy. It is favoured by the great flexibility of the molecule (i.e., by the existence of many low energy vibrational states) and is countered by rigidity. For this reason, fluorescence is likely to ^{be} observed in molecules which have rigid cyclic structures. The mechanism of external quenching consists of energy transfer to other molecules and is important in solutions.

In the process of predissociation the excited molecule is dissociated before emission occurs and returns to the ground state by a radiationless transition. This may be important in the case of sulphur as shown by the following consideration. Predissociation is almost certain to occur when some bonds in the molecule have a bond dissociation energy appreciably lower than the energy of the absorbed light.

Since a wavelength of 2000 \AA corresponding to almost 150 K cal/mole , this amount of energy is normally sufficient to break some bonds in most molecules, hence predissociation makes fluorescence highly improbable due to absorption in the ultraviolet. The bond dissociation energy of S_0 is not known but it should lie within an order of magnitude of the bond energy which is about 63 K cal/mole (65). For example, the bond energy and the dissociation energy of $-S=S-$ are 50 and 100 K cal/mole respectively (66).

Finally, a brief note is made regarding the nature of the excited state. It is difficult to specify the multiplicity of the excited state (the ground state of S_0 is a singlet) without the exact knowledge of the emission lifetime. The low emission efficiency has been assumed to be connected with a very short lifetime of the excited state which has been treated therefore as a singlet throughout the present chapter. This may be erroneous since, first, no experiment to measure the emission lifetime has been performed and second, it can be shown that in the presence of 'quenching centres' where the observed lifetime is very short the ^{radiative} lifetime of the excited state is different from the observed lifetime. For example, the ^{radiative} lifetime of the excited triplet state of benzene has been calculated to be about 0.1 sec whereas the observed lifetime is about 10^{-6} sec (67).

CHAPTER 8CONCLUSIONS

1. The negative charge transport in liquid ultrapure sulphur between 119°C and 160°C is an intermolecular hopping mechanism, as in the solid. The negative charges are electrons which have a hopping mobility at the melting point of $1.0 \times 10^{-4} \text{ cm}^2/\text{volt sec}$. The activation energy of $0.15 \pm 0.03 \text{ eV}$ corresponds to an approximate polaron binding energy of 0.48 eV equal to that in the solid. The drop in electron mobility by a factor of 30 at the melting point is thought to be due to a reduction in the intermolecular overlap energy. The lifetime of excess electrons in ultrapure sulphur with respect to negative ion formation is in excess of 50 milliseconds.
2. Similar conclusions may be drawn for the hole transport in the liquid. The mobility is, however, a factor of 2 smaller than that of electrons.
3. Above 160°C , the S_8 molecules break up and polymerise. This causes an increase of viscosity by four orders of magnitude and one would expect a corresponding decrease in ionic mobility. The fact that positive and negative mobilities were observed with little change up to 200°C is conclusive evidence of an electronic rather than ionic conduction mechanism. A sudden decrease of about $3 \times 10^{-5} \text{ cm}^2/\text{volt sec}$ in the hole mobility at about 160°C is associated with the disappearance of the ionic part of the drift mobility. The change in gradient of the

electron and hole mobility versus $1/T$ curves above 160°C is explained in terms of the increase in the average spacing between hopping sites as the S_8 rings polymerise.

4. The transport behaviour of charge carriers in the supercooled liquid is a normal extension of that in the liquid above the melting point.

5. After solidification the electron mobility in the solid is essentially unaffected by the destruction of the long range crystalline order.

But the holes, which in the crystalline solid move in a polaron band show a drop in mobility by a factor of 100. This is additional evidence for the fundamentally different transport mechanisms of electrons and holes in the solid.

6. Dark current measurements show that ultrapure and laboratory reagent samples behave differently. In ultrapure samples the steady current is ohmic at all applied fields. In relatively impure laboratory reagent samples the current voltage characteristic has an initial ohmic region, a sublinear and a superlinear region. This different behaviour of laboratory reagent samples has been attributed to impurities which ionise and form hetero - space - charge layers near the electrodes.

7. The dark conductivity does not show a sudden discontinuity on melting. The conductivity of the liquid is about $10^{-12} \text{ ohms}^{-1} \text{ cm}^{-1}$. The dark current increases with increasing temperature with the same activation energy as in the solid at room temperature. It continues to increase above 160°C after a slight drop due to the disappearance of the ionic component.

8. The transport of electrons and holes in laboratory reagent liquid sulphur shows a number of complicating features not observed with a fresh ultrapure sample. These arise from the ionisation of impurity molecules during the transit of the injected excess carriers. The electron lifetime with respect to this process is about 15 milliseconds. In thick specimens, having transit times appreciably longer than this value, the increase in the internal field due to the ionic space charge together with the decrease in the number of drifting carriers causes the maximum in the observed current signal.
9. The spectral response of photoconductivity (or generation efficiency) in liquid sulphur is essentially the same as in the solid. The peak of response occurs at 2600 Å. The corresponding generation efficiency is 10^{-2} at 33 K volt/cm. The product of quantum efficiency, η , and recombination lifetime, τ , of excess carriers is 10^{-8} sec. Assuming a likely value of η to be 10^{-1} , τ is 10^{-7} sec.
10. From the observed visible emission of sulphur under x - ray irradiation, the first excited state of an S_8 molecule has been tentatively fixed at 2.7 eV. The three emission peaks at 4900, 5300 and 5700 Å correspond to vibrational 'de - activation' by molecular modes of 0.15 eV energy. The emission efficiency is extremely low, between 10^{-4} and 10^{-6} .

TABLE 2.1

Charge Carrier Mobilities in Liquid Hexane at 20°C

Author	Range of Applied Field (KV/cm)	Specimen Thickness (cm)	Mode of Excitation	Scatter of Results (%)	Negative Carrier Mobility (10^3) $\text{cm}^2/\text{V}\cdot\text{sec}$	Positive Carrier Mobility (10^3) $\text{cm}^2/\text{V}\cdot\text{sec}$
LeBlanc (Ref. 7)	0 - 2	1.5	u. v. radiation	10	1.23	-
Gzowski & Terlecki (Ref. 8)	1	0 - 1.5	x - ray	5	1.3	0.41
Chong & Inuishi (Ref. 9)	0 - 500	0.01 - 0.05	u. v. radiation	20	1.0	-
Allen & Hummel (Ref. 10)	0 - 4	0.5 - 0.3	x - ray	5	0.76	0.38
Secker & Lewis (Ref. 11)	1.34	0.9 - 6	x - ray	200	2.0	1.0

TABLE 3.1

Experimentally Obtained Values for the Electron HoppingParameters in Solid Sulphur

γ	$E_b(\text{ev})$	$\hbar\omega_0(\text{ev})$	$1/\lambda (\text{cm}^{-1})$	Vibrational mode
15	0.49	0.0330		
17	0.49	0.0291	236	b ₂ fundamental
18	0.48	0.0265	214.5	a ₁ fundamental
20	0.475	0.0238	193	e ₁ fundamental
25	0.47	0.0186	151	e ₂ fundamental
35	0.455	0.013		
45	0.44	0.0094		

APPENDIX IAnalysis of starting materialsAnalysis of CS₂ used as solventAnalar Reagent, BDH

Specific gravity, (20°C)	1.262 to 1.265
Distillation range	95 % distills between 46° and 47°C
Acidity, (as SO ₂)	0.001 % max
Non - volatile matter	0.003 % max
Hydrogen sulphide, (H ₂ S)	0.00015 % max
Sulphur dioxide, (SO ₂)	0.00025 %

Analysis of sulphur used as starting materialBDH, Laboratory Reagent

Ca	0.6 ppm
Na	0.8 ppm
K	0.5 ppm
Cl	7 ppm

Koch - light Laboratories Ltd, 99.9999 % purityUltrapure Sulphur

Ca	0.2 ppm	Na	0.1 ppm
Cu	0.1 ppm	Non -	0.001 %
Mg	0.05 ppm	Volatiles	
Si	0.02 ppm	(Traces of CS ₂	
Ag	0.01 ppm	dissolved in S)	

REFERENCES

- (1) Adamczewski, I., Brit. J. Appl. Phys. 16, 759 (1965)
- (2) Walden, P., and Ulich, H., Z. Physik Chem. Leipzig 107, 219 (1923)
- (3) Eyring, H., J. Chem. Phys. 4, 283 (1936)
- (4) See e.g., Landau, L. D., and Lifshitz, E., "Fluid Mechanics" p.63
(Pergamon Press, 1963)
- (5) Caravajal, C., Toelle, K. J., and Szwarc, M., J. Am. Chem. Soc.
87, 5548 (1965)
- (6) deGroot, K., Gary, L. P., and Jarnagin, R. C., J. Chem. Phys. 47,
3084 (1967)
- (7) LeBlanc, O. H., J. Chem. Phys. 30,(6), 1443 (1959)
- (8) Gzowski, O., and Terlecki, J., Acta. Phys. Polon. 18, 191 (1959)
- (9) Chong, P., and Inuishi, Y., Tech. Repts. Osaka. Univ. 10, 545 (1960)
- (10) Allen, A. O., and Hummel, A., Disc. Far. Soc. 36, 95 (1963)
- (11) Secker, P., and Lewis, T. J., Brit. J. Appl. Phys. 16, 1649 (1965)
- (12) Crowe, R. W., J. Appl. Phys. 27, 156 (1956)
- (13) Lewis, T. J., and Ward, B. W., Proc. Roy. Soc. A, 269, 233 (1962)
- (14) Gary, E., and Lewis, T. J., Brit. J. Appl. Phys., 16, 1049 (1965)
- (15) LeBlanc, O. H., J. Chem. Phys. 37, 916 (1962)
- (16) Bepler, W., Zeit. Phys. 185, 507 (1965)
- (17) Morant, M. J., Brit. J. Appl. Phys. 14, 469 (1963)
- (18) Forster, E. O., J. Chem. Phys. 37, 1021 (1962)
- (19) Forster, E. O., J. Chem. Phys. 40, 86 (1964)
- (20) Forster, E. O., J. Chem. Phys. 40, 91 (1964)
- (21) Silver, M., J. Chem. Phys. 42, 1011 (1965)
- (22) Thomson, J. J., and Thomson, G. P., "Cond. Elec. Thro' Gases" (Cam-
bridge Univ. Press, 1928), 3rd edition, Vol. 1, p. 193.

- (23) Wilson, H. A., Phys. Rev. Suppl. (1930), see also "Modern Physics", 306 - 311 (Blackie, 1937)
- (24) Davis, H. T., Rice, S. A., and Meyer, L., J. Chem. Phys. 37, 947 (1962) and J. Chem. Phys. 37, 1521 (1962)
- (25) Davis, H. T., Rice, S. A., and Meyer, L., J. Chem. Phys. 37, 2470 (1962)
- (26) Rice, S. A., and Allnatt, A. R., J. Chem. Phys. 34, 2144 (1961)
- (27) Barker, J. A., J. Chem. Phys. 5, 1061 (1962)
- (28) Spear, W. E., Miller, L. S., and Howe, S. H., To be published in Physical Review, 1968.
- (29) Fowler, J. F., Proc. Roy. Soc., Lond., A 236, 464 (1956)
- (30) Terlecki, J., Nature, Lond., 194, 172 (1962)
- (31) Adams, A. R., and Spear, W. E., J. Phys. Chem. Solids, 25, 1113 (1964)
- (32) Spear, W. E., and Adams, A. R., J. Phys. Chem. Solids, 27, 281 (1966)
- (33) Adams, A. R., Gibbons, D. J., and Spear, W. E., Solid St. Comm. 2, 387 (1964)
- (34) Gibbons, D. J., and Spear, W. E., J. Phys. Chem. Solids, 27, 1917 (1966)
- (35) Holstein, T., Ann. Physik, 8, 343 (1959)
- (36) Yamashita, J., and Kurosawa, T., J. Phys. Chem. Solids, 5, 34 (1958)
- (37) Fröhlich, H., and Sewell, G. L., Proc. Phys. Soc. Lond. 74 643 (1959)
- (38) Joffe, A. F., Can. J. Phys. 34 1393 (1956)
- (39) Glarum, S. E., J. Phys. Chem. Solids, 24, 1577 (1963)
- (40) Scott, D. W., et. al., J. Molec. Spectrosc. 13, 313 (1964)
- (41) Gibbons, D. J., To be published
- (42) Bacon, R. F., and Fanelli, R., J. Am. Chem. Soc. 65, 639 (1943)
- (43) Fanelli, R., J. Am. Chem. Soc. 67, 1832 (1945)
- (44) Poulis, J. A., and Massen, C. H., "Elemental Sulphur" (Ed., B. Meyer)

- pp. 109, Interscience (1966)
- (45) Powell, R., and Eyring, H., J. Am. Chem. Soc. 65, 648 (1943)
- (46) Gee, G., Trans. Far. Soc. 48, 515 (1952)
- (47) Tobolsky, A. V., J. Polymer Sci. 25, 220 (1957) and J. Polymer Sci. 31, 126 (1958)
- (48) Tobolsky, A. V., and Eisenberg, A., J. Am. Chem. Soc. 82, 289 (1959) and J. Am. Chem. Soc. 81, 780 (1959). See also MacKnight, W. J., and Tobolsky, A. V., "Elemental Sulphur" (Ed., B. Meyer), pp.95 Interscience (1966)
- (49) Spear, W. E., Proc. Phys. Soc., Lond. B70, 669 (1957)
- (50) Spear, W. E., Proc. Phys. Soc., Lond. 76, 826 (1960)
- (51) Spear, W. E., J. Phys. Chem. Solids 21, 110 (1961)
- (52) Spear, W. E., and Mort, J., Proc. Phys. Soc., Lond. 81, 130 (1963)
- (53) LeComber, P. G., Spear, W. E., and Weinmann, A., Brit. J. Appl. Phys. 17, 467 (1966)
- (54) Shockley, W., J. Appl. Phys. 9, 635 (1938)
- (55) Hecht, K., Z. Phys. 77, 235 (1932)
- (56) Adams, A. R., Thesis (Leicester University, 1964)
- (57) Spear, W. E., Adams, A. R., and Henderson, G. A., J. Sci. Instr. 40, 332 (1963)
- (58) Heilmeyer, G. H., and Heyman, P. M., Phys. Rev. Letters 18, 583 (1967)
- (59) Zaky, A. A., Tropper, H., and House, H., Brit. J. Appl. Phys. 14, 651 (1963)
- (60) "International Critical Tables", (McGraw - Hill, 1926 - 1930)
- (61) Curtis, J. H., J. Chem. Phys. 1, 160 (1930)
- (62) Rose, A., "Concepts in Photoconductivity and Allied Problems" (Interscience, J. Wiley, 1963), p. 129

- (63) See for example, Garlick, G. F. J., "Luminescent Materials"
(Oxford Press, 1949)
- (64) Ware, W. R., and Baldwin, B. A., J. Chem. Phys., 43, 1194 (1965)
- (65) Berkowitz, J., "Elemental Sulphur" (Beat Meyer) p. 125
- (66) Barrow, R. F., and du Parcq, R. P., "Elemental Sulphur" (Beat Meyer)
p. 251
- (67) Parmenter, C., and Ring, B. L., J. Chem. Phys. 46, 1998 (1967)

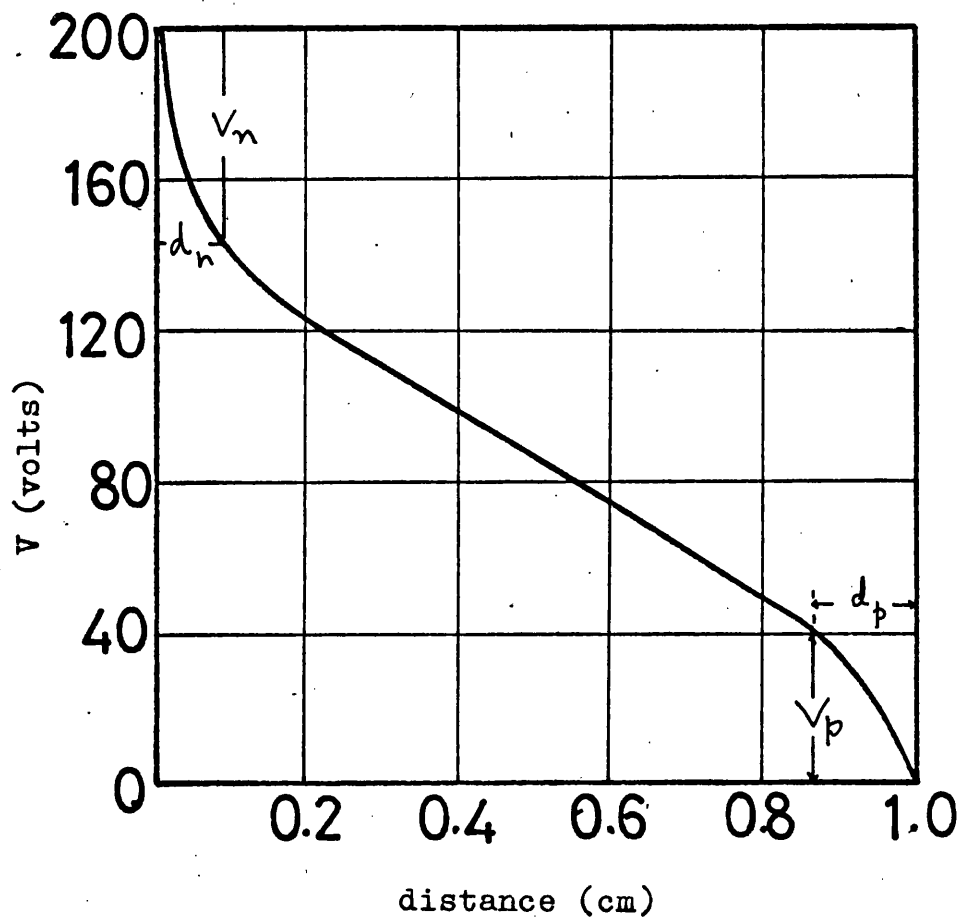


Fig. 2.1 : The form of potential distribution as obtained in benzene by Forster (Ref. 18). This type of potential distribution is also the basis of Thomson's model of conduction in gases as applied to liquids by Silver (Ref. 21).

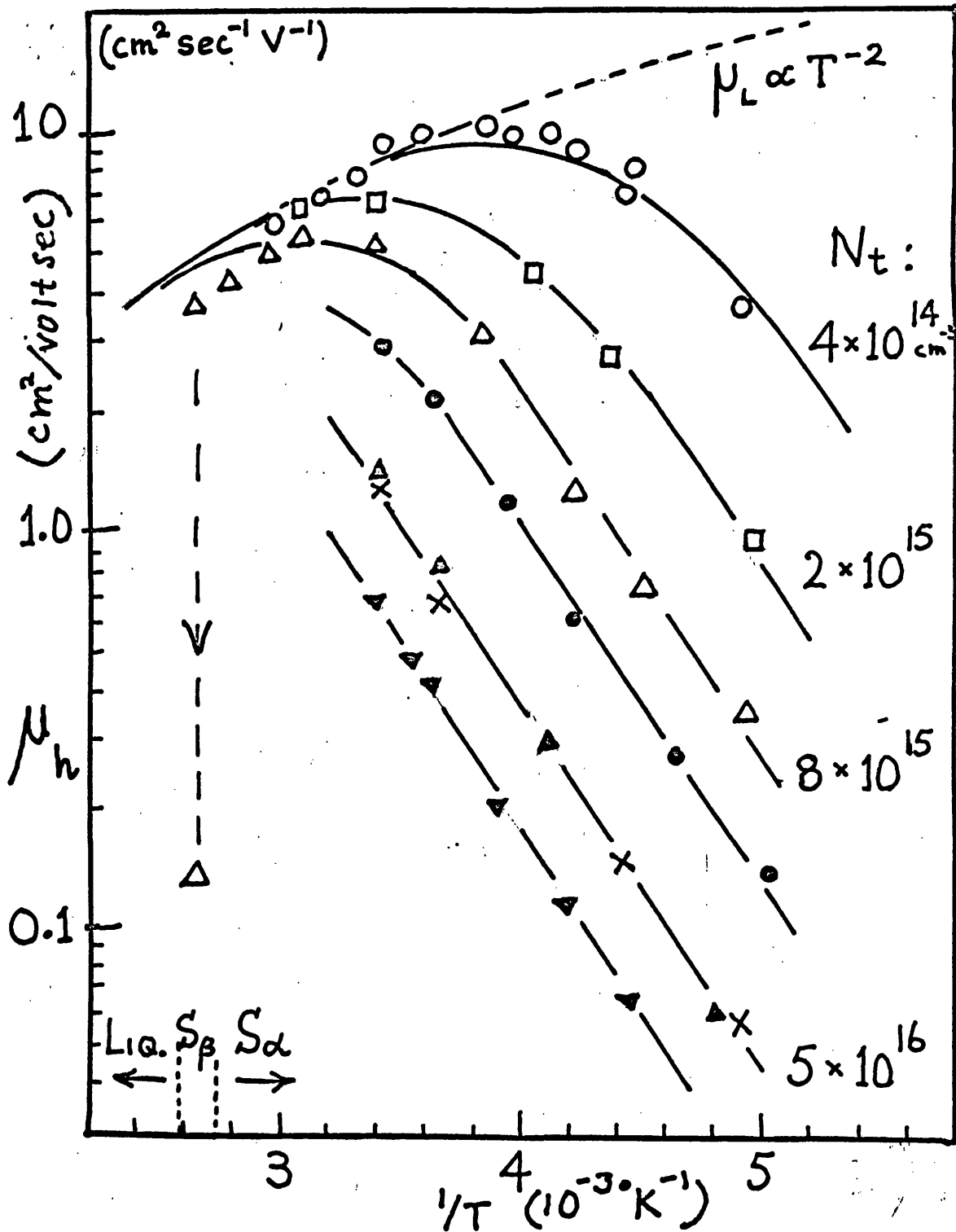


Fig. 3.1 : Temperature dependence of the hole mobility in crystalline sulphur. μ_L is the lattice mobility curve; the solid curves have been calculated using the values of N_t indicated (Ref. 31).

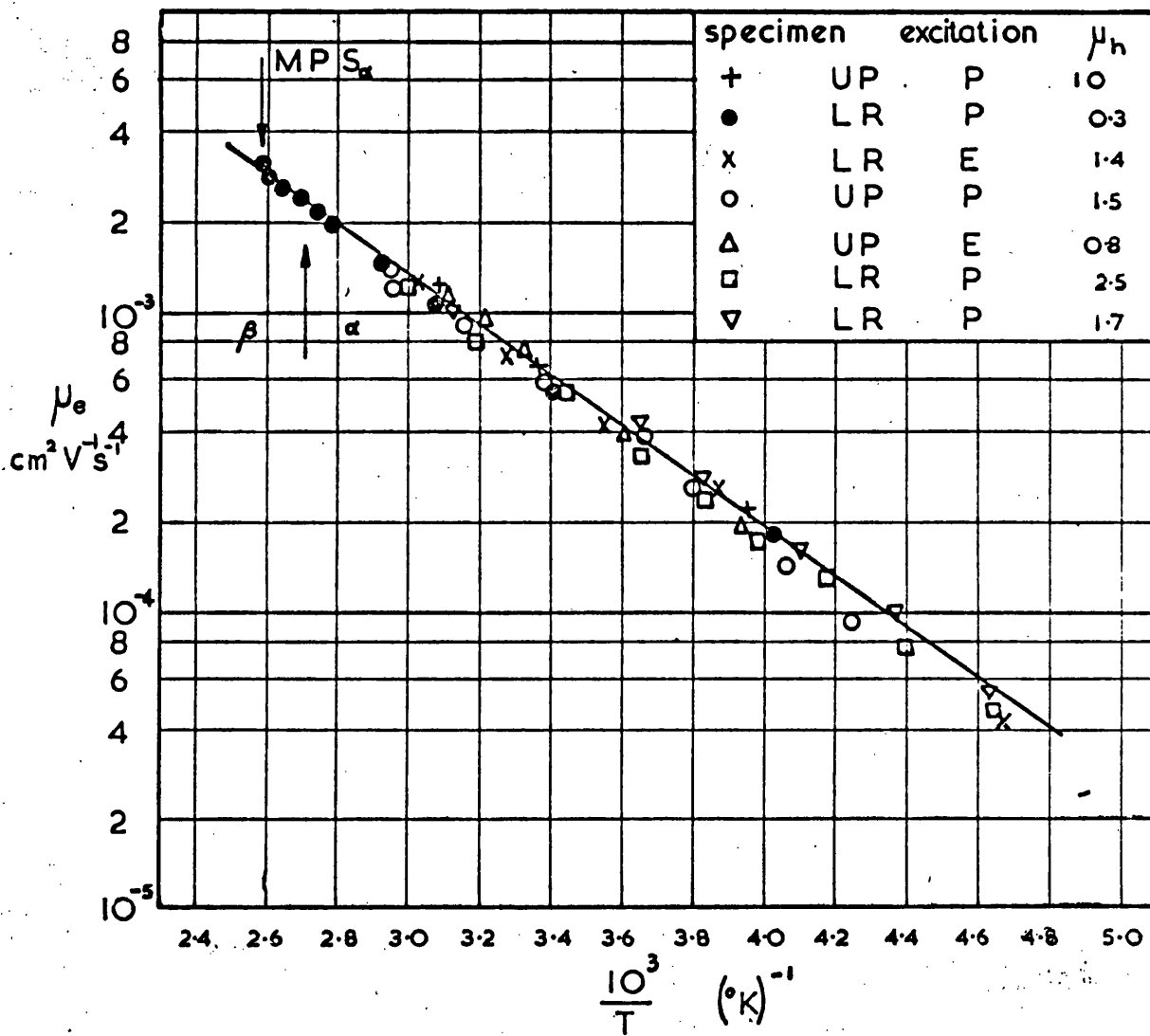


Fig. 3.2 : Temperature dependence of the electron drift mobility in crystalline sulphur in the [111] direction. LR - crystal grown from laboratory reagents; UP - crystal grown from ultrapure reagents; E - electron beam excitation; P - Photon excitation; μ_h - room temperature hole drift mobility in $\text{cm}^2/\text{volt sec}$ (Ref. 34)

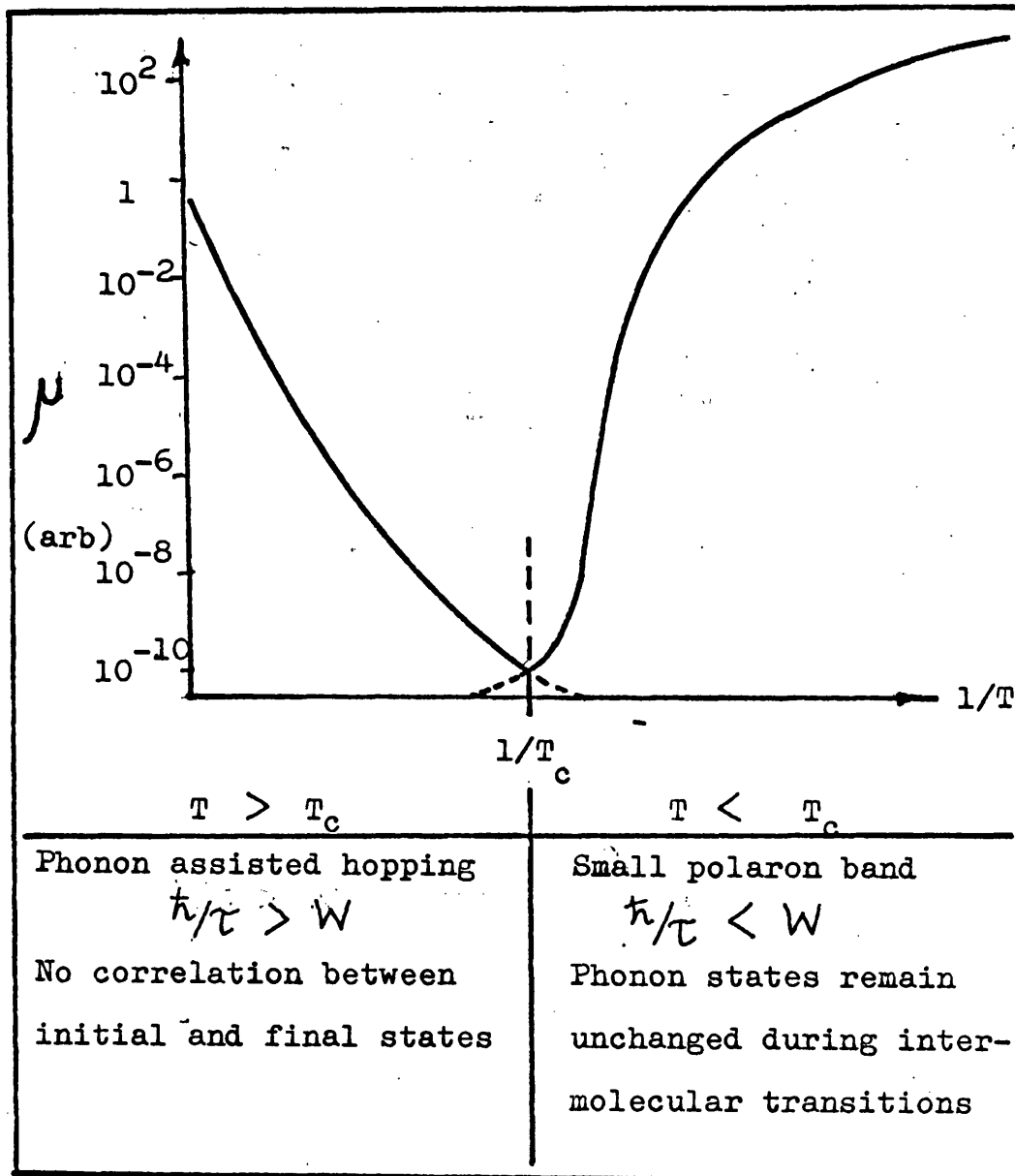


Fig. 3.3 : Theoretical temperature dependence of electron mobility in the phonon assisted hopping and polaron band motion range. T_c is the temperature which marks the transition between the two ranges.

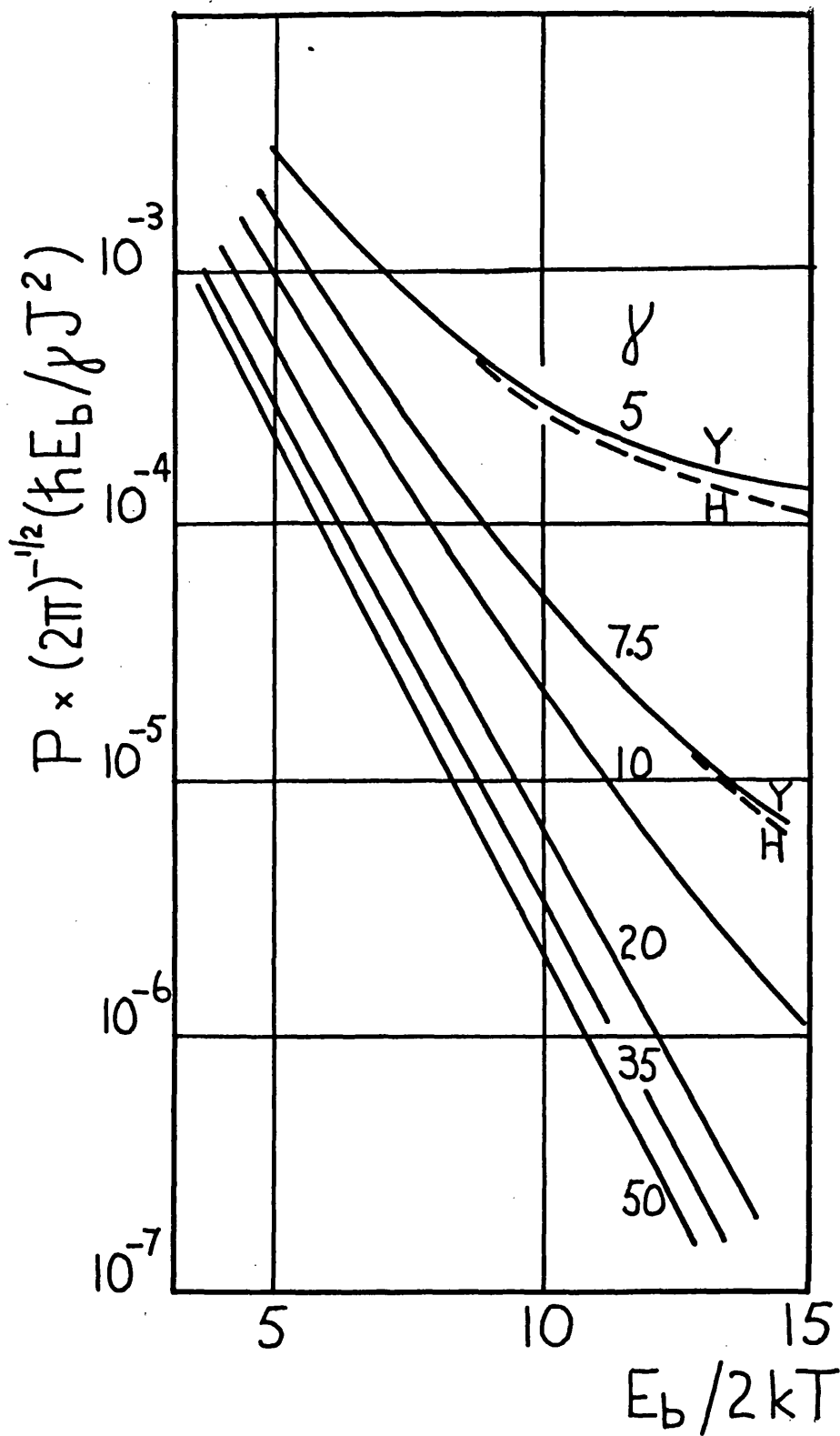


Fig. 3.4 : Plot of Eq. (3.4) (marked Y) and Eq. (3.6) (marked H) for different values of the interaction parameter γ (Ref. 34).

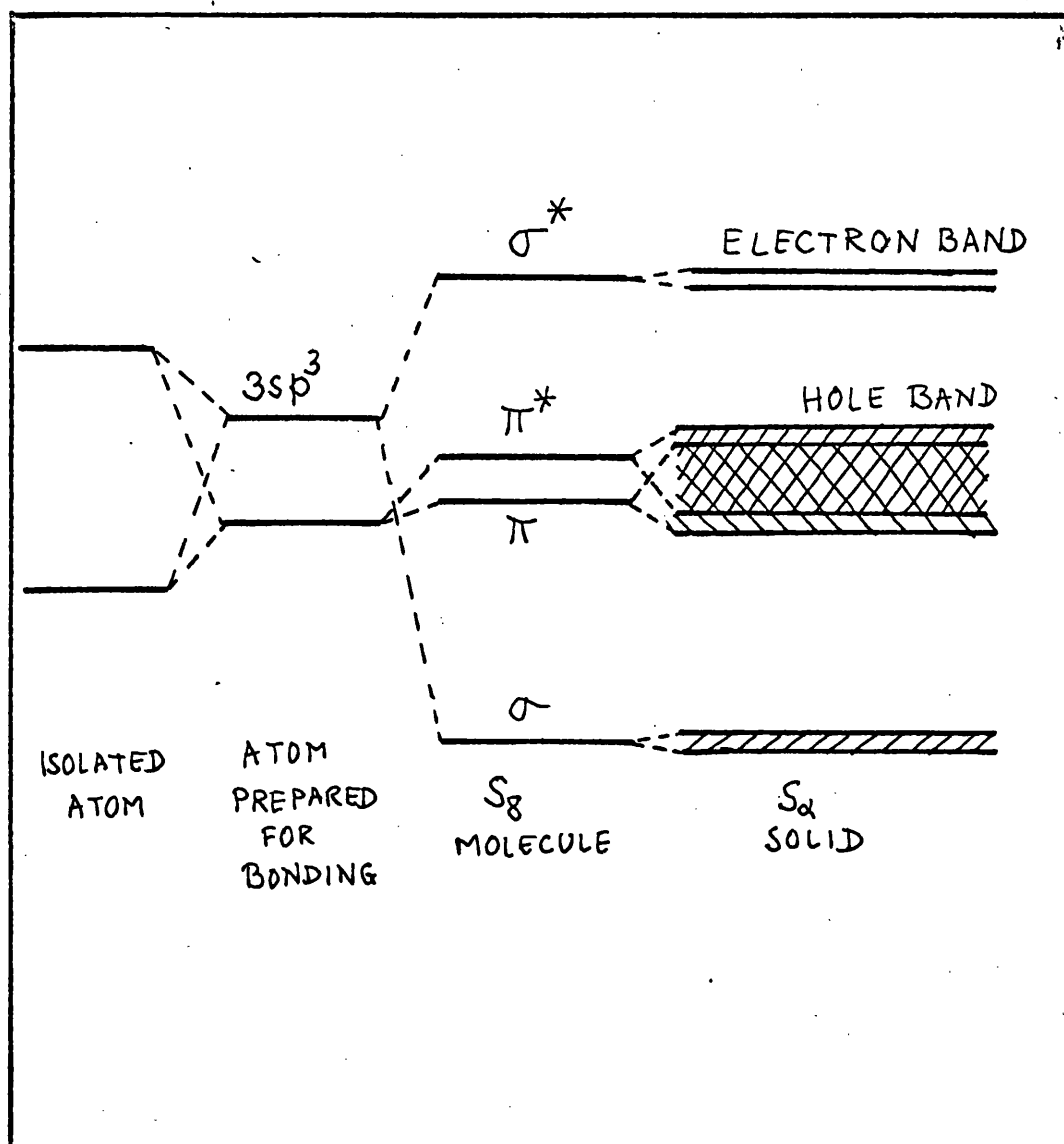


Fig. 3.5 : Energy level scheme showing how the band structure in S_{α} is derived from the levels of an isolated S atom (qualitative only).

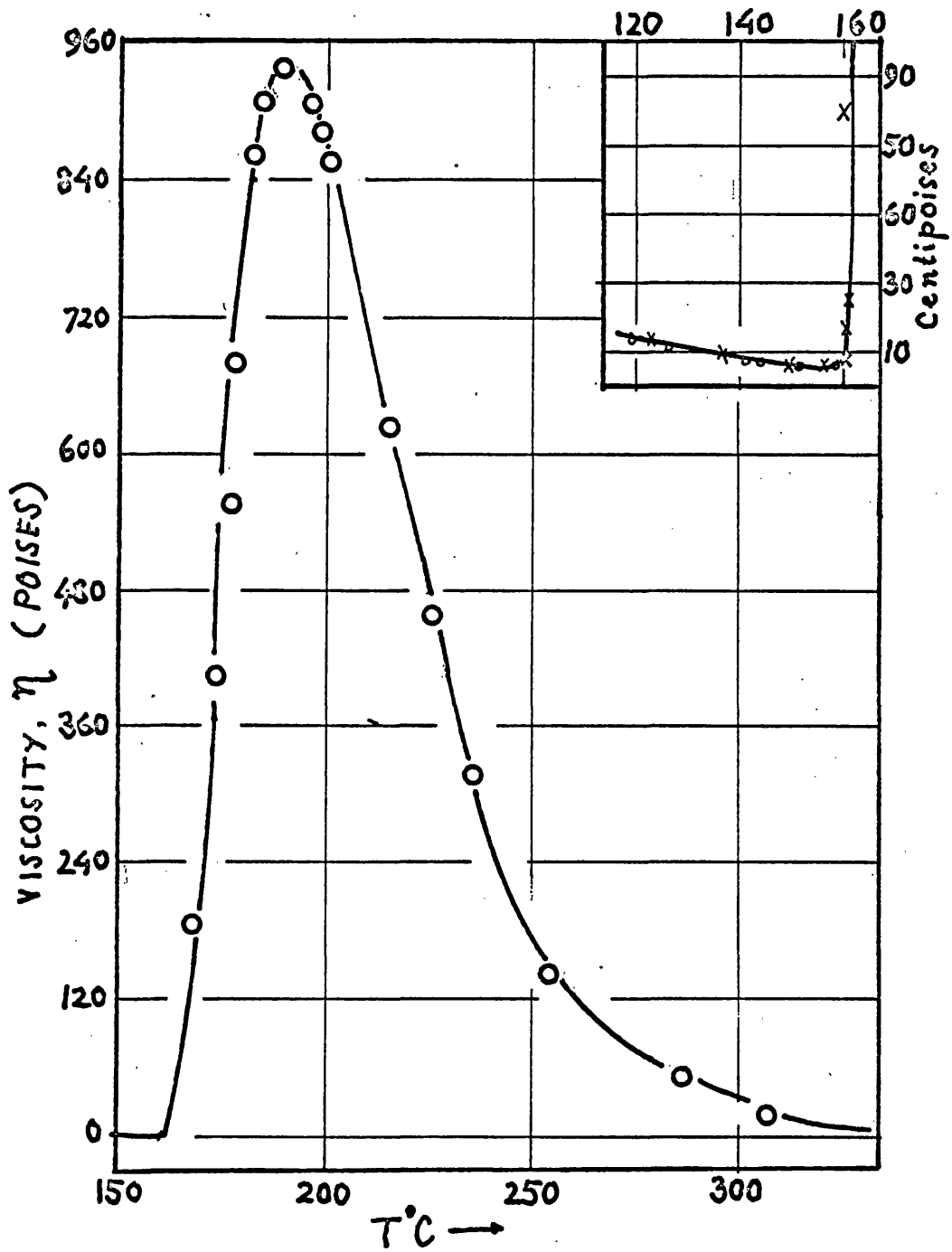


Fig. 3.6 : Temperature dependence of the viscosity of liquid sulphur over the complete range. The inset curve corresponds to the range between the melting point (119°C) and 160°C (Ref. 42).

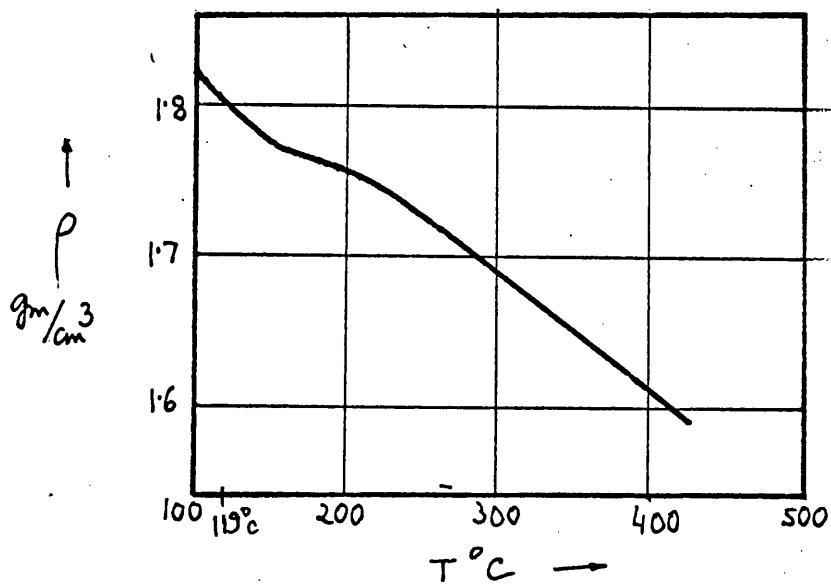


Fig. 3.7 : Temperature variation of the density of sulphur below and above the melting point of 119°C (Ref. 44).

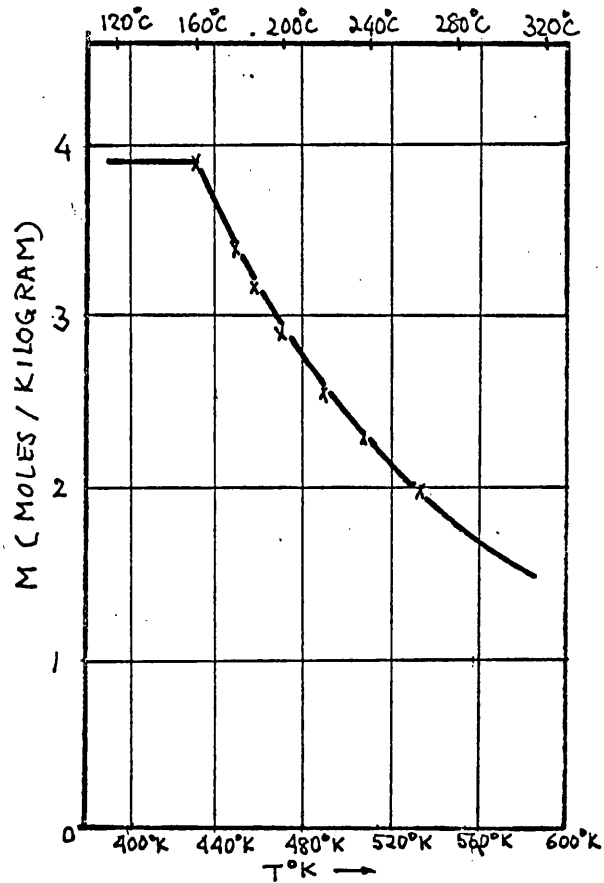


Fig. 3.8 : Temperature dependence of the concentration of S_8 rings in equilibrium with polymeric sulphur.

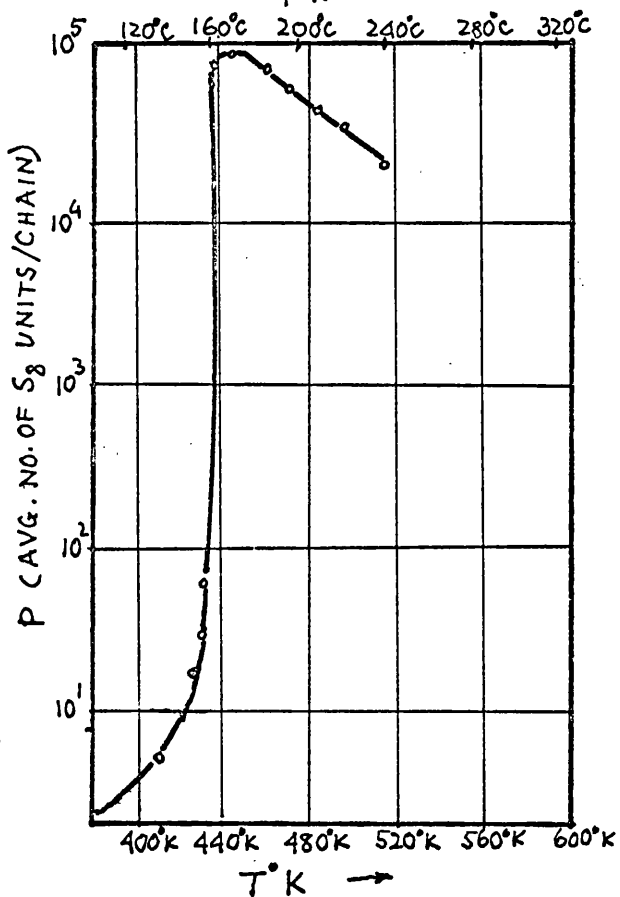


Fig. 3.9 : Temperature dependence of the average number of S_8 units per chain of polymeric sulphur or the number - average degree of polymerisation.

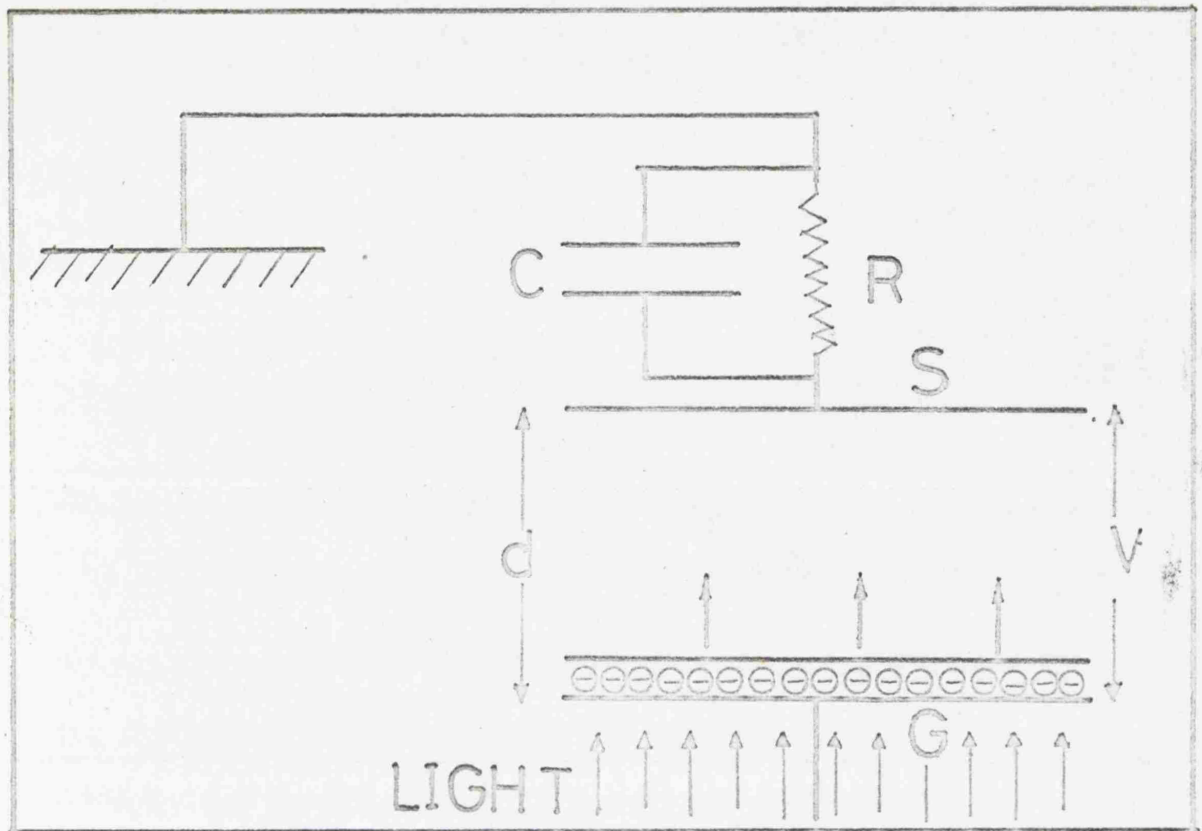


Fig. 4.1 : Schematic diagram illustrating the principles of drift mobility measurements. R - load resistor across which the signal develops; C - specimen capacity; G - generation electrode; S - signal or collecting electrode.

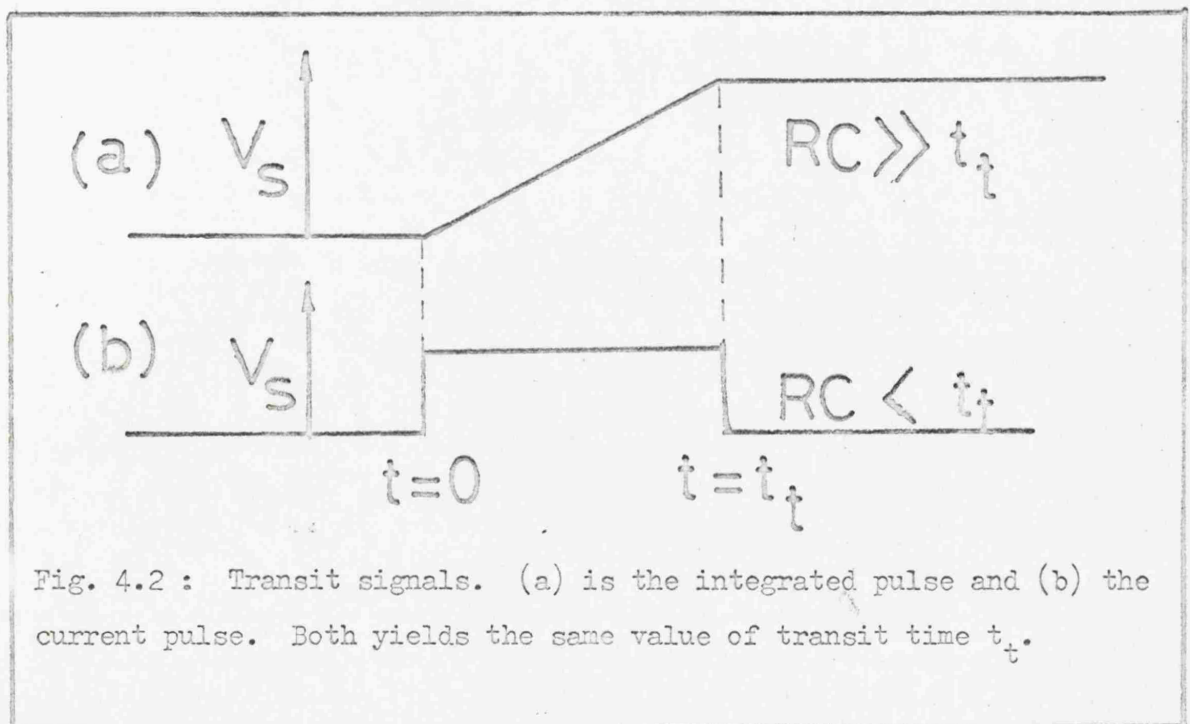


Fig. 4.2 : Transit signals. (a) is the integrated pulse and (b) the current pulse. Both yields the same value of transit time t_t .

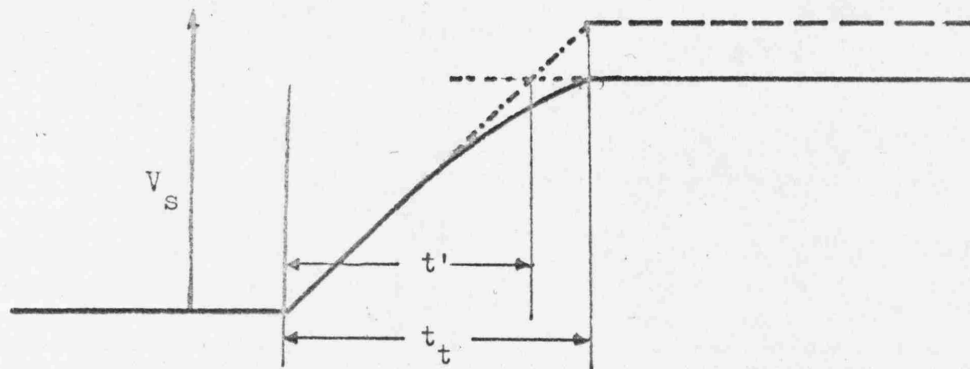


Fig. 4.3 : Effect of deep - trapping ($\tau \sim t_t$) on integrated pulse.

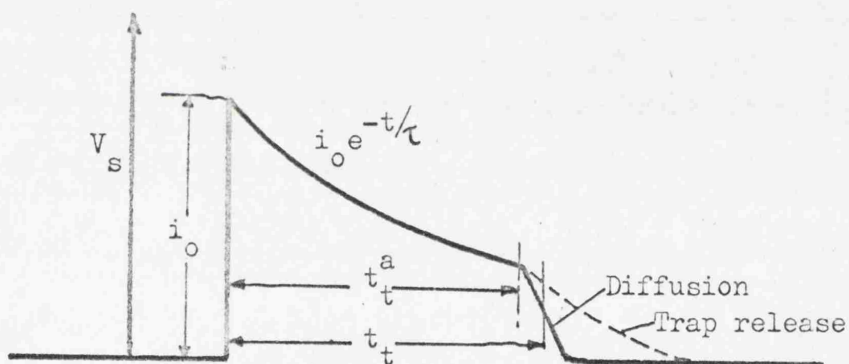


Fig. 4.4 : Effect of deep - trapping ($\tau \sim t_t$) on current pulse. The broadening of the tail due to diffusion and trap release is also shown.



Fig. 4.5 : Effect of deep - trapping for the case $\tau < t_t$. (a) is the integrated pulse; the rising edge is extremely non - linear. (b) is the current pulse; no discontinuity at t_t appears.

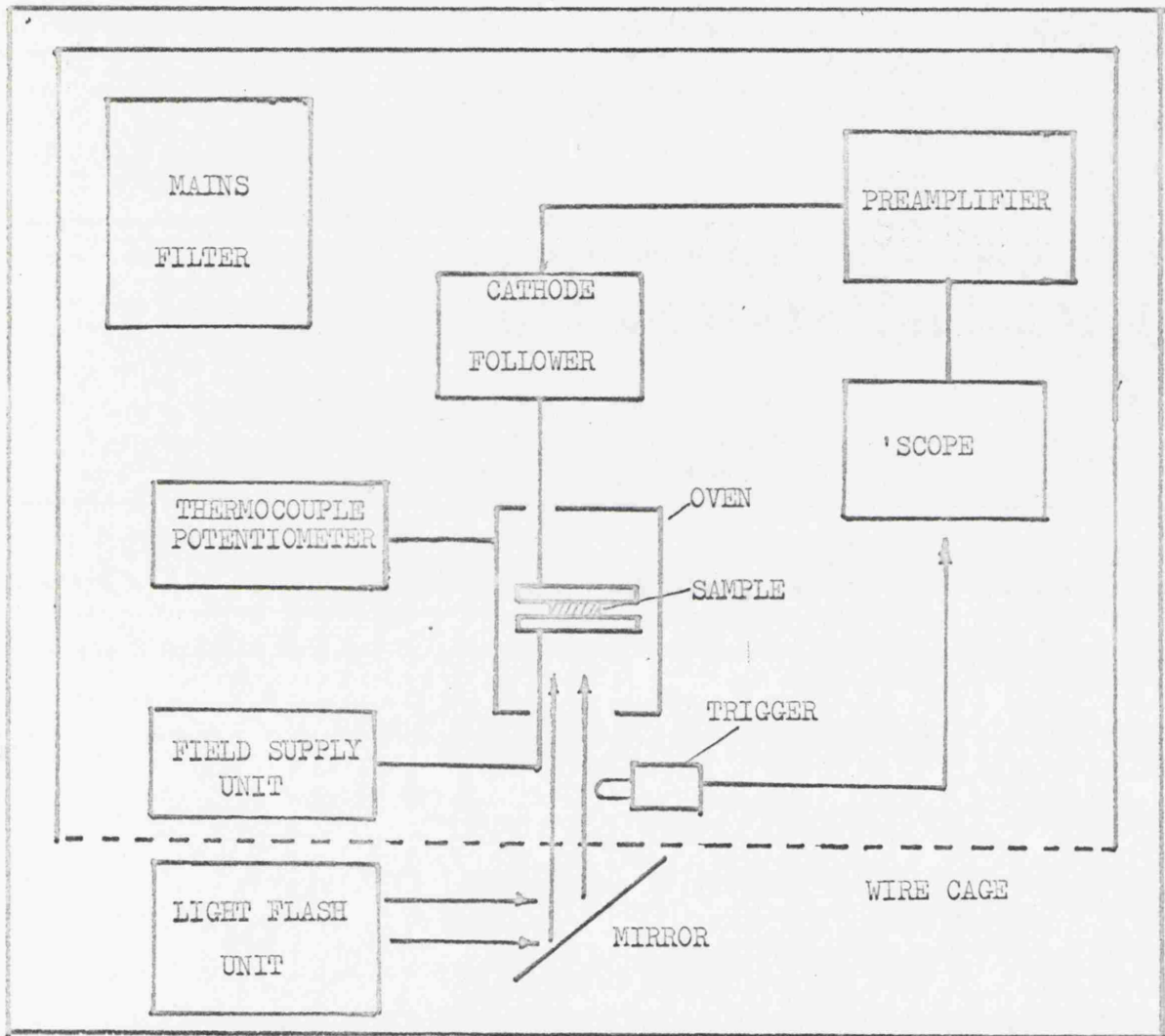


Fig. 4.6 : Block diagram of the arrangement for measuring the drift mobility of charges in liquid sulphur.

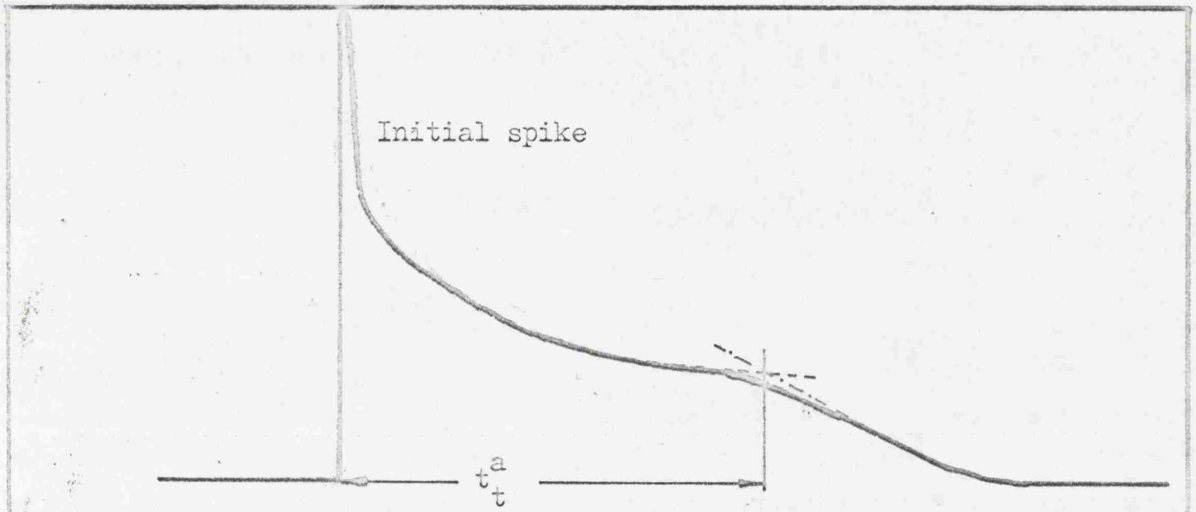


Fig. 4.7 : Transit signal showing the initial spike due to carriers of opposite polarity moving backwards.

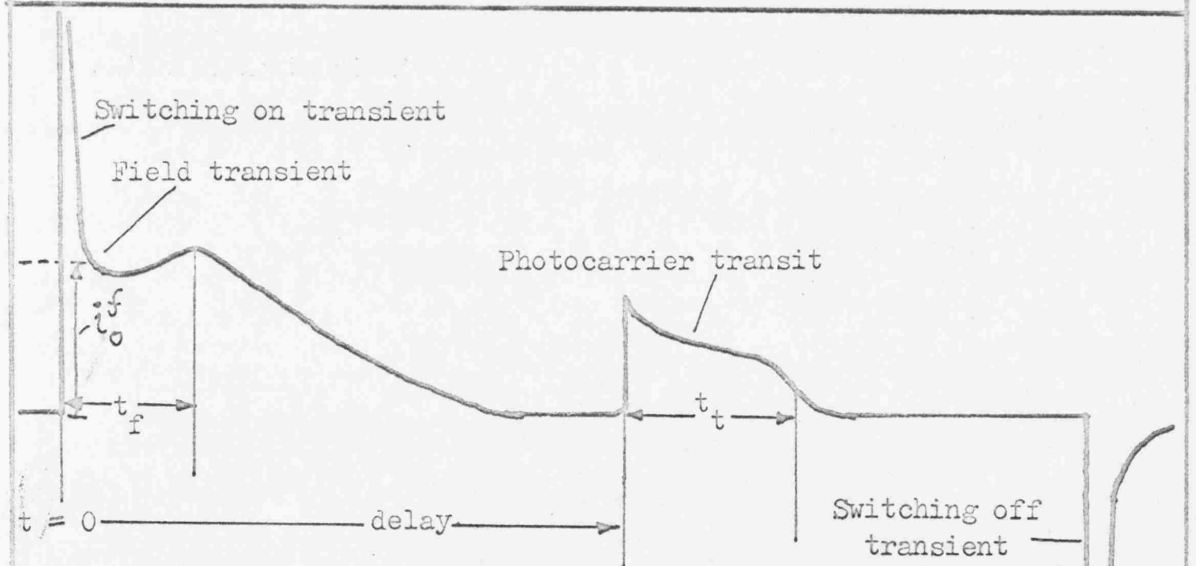


Fig. 4.8 : Switching transients, Field transient and photocarrier transit. i_0^f is the initial height of the field transient signal and t_f is the 'transit time' of carriers giving rise to the field transient.

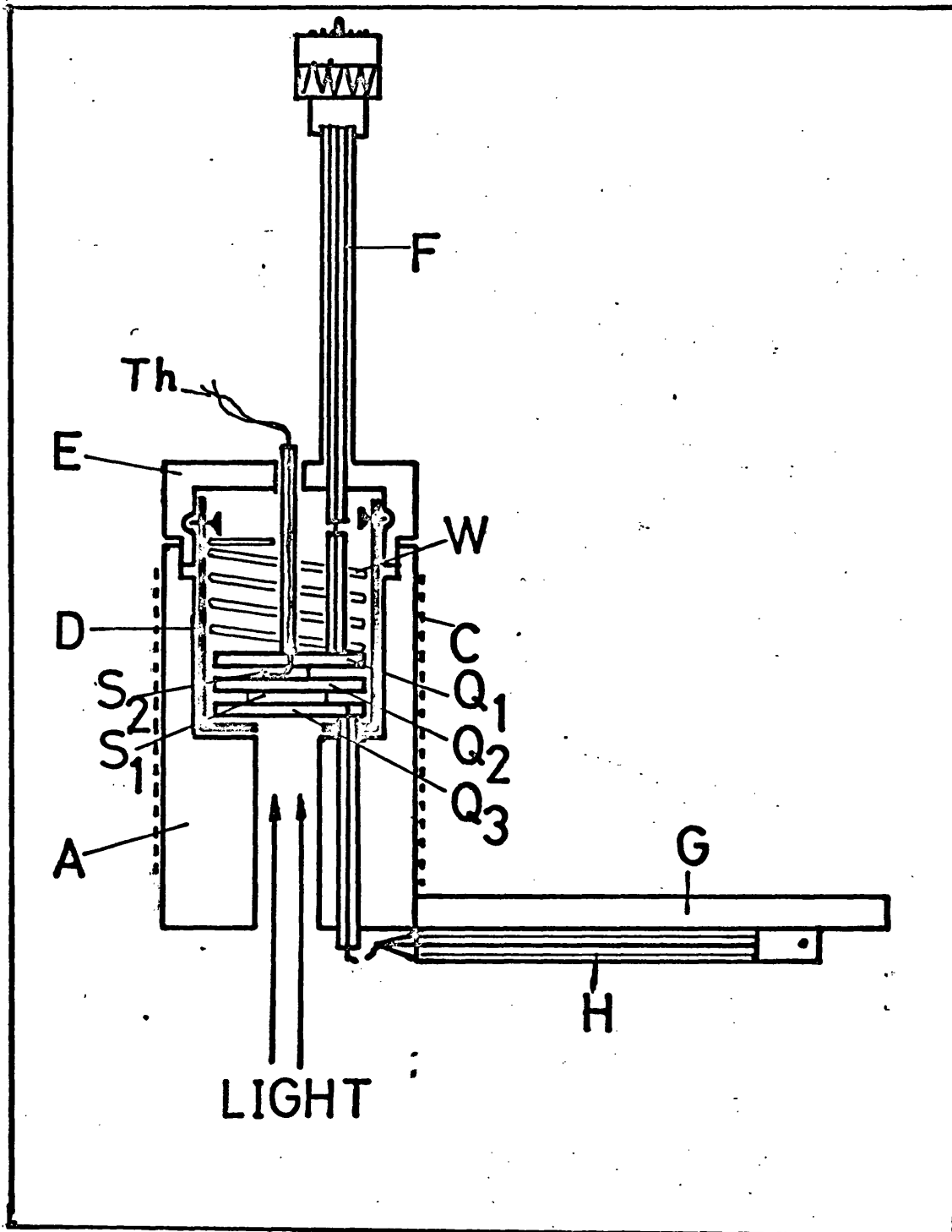
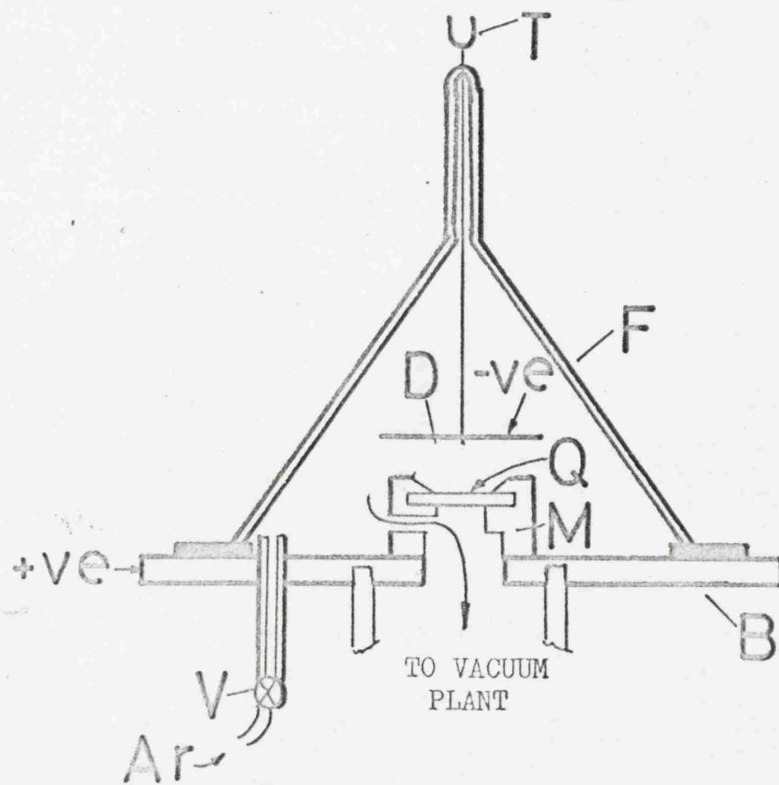
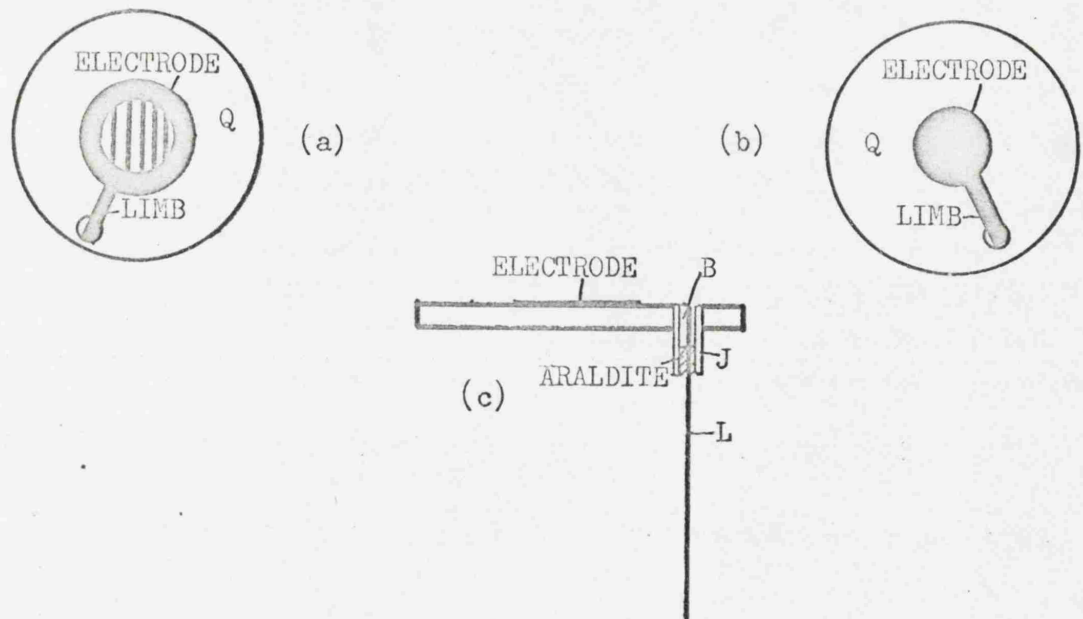


Fig. 4.9: The specimen chamber. Q_1 , Q_2 and Q_3 are the quartz discs which enclose the liquid specimens S_1 and S_2 . Specimen S_2 is for temperature measurement.



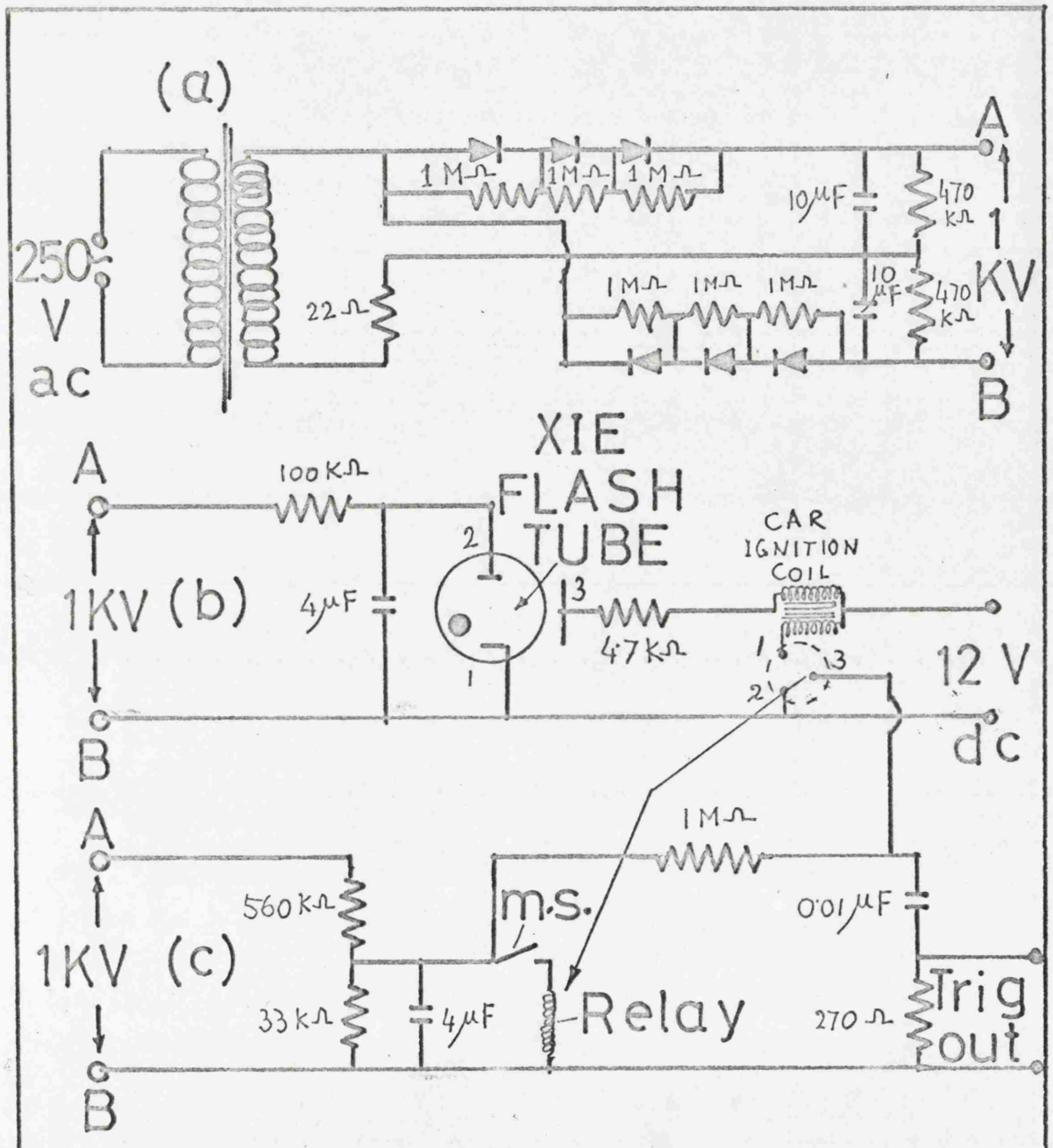


Fig. 4.12 : Circuit diagram of the flash unit using XIE - type xenon - mercury flash tube.

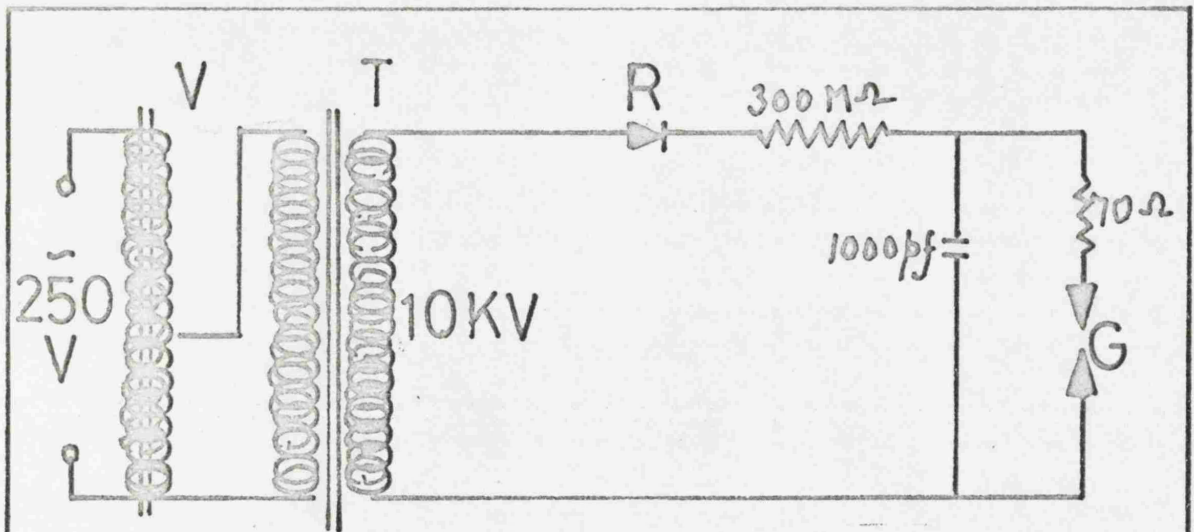


Fig. 4.13 : Spark gap circuit. V - Variac; T - transformer; R - copper oxide rectifier; G - the gap across which spark occurs.

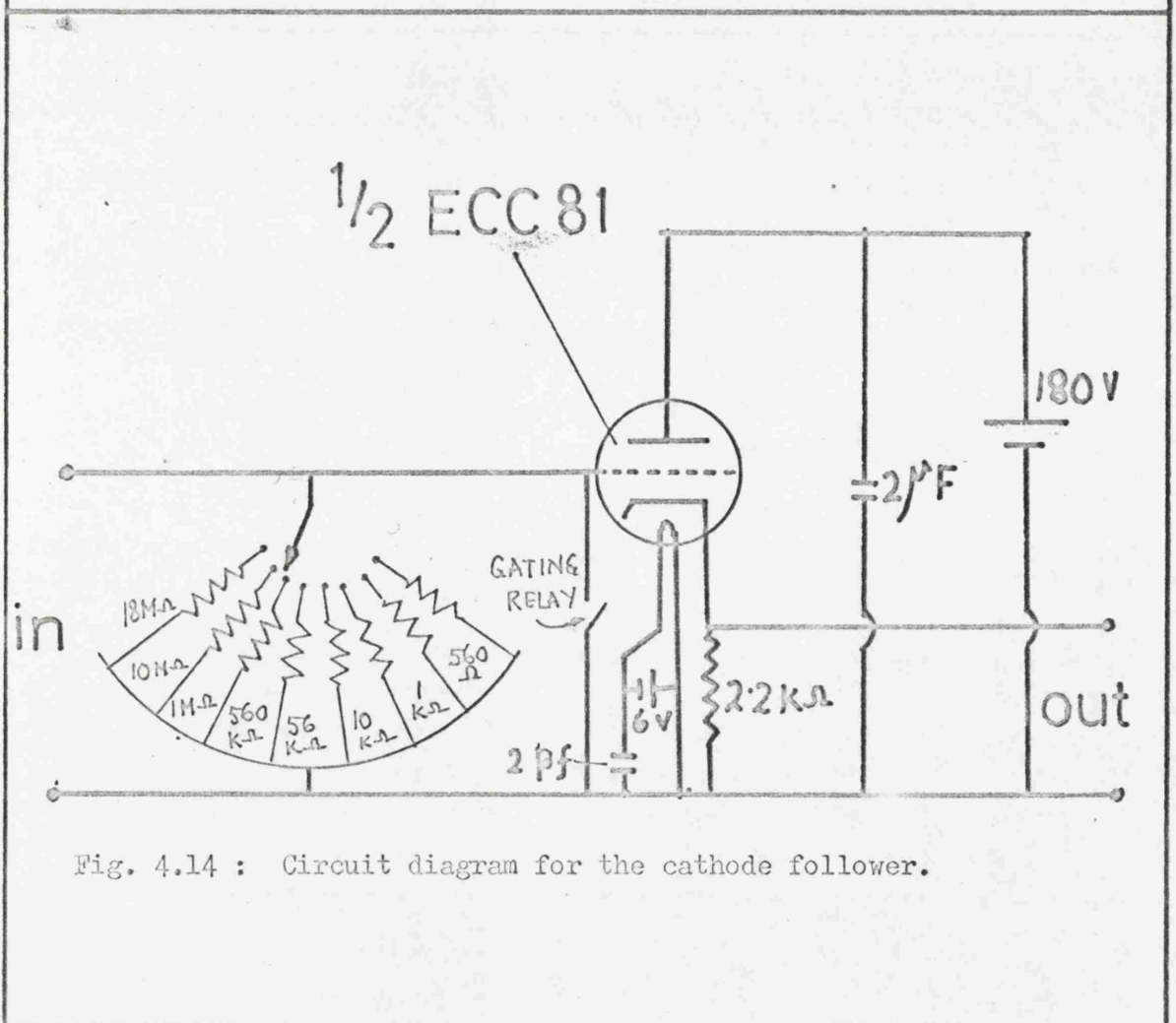


Fig. 4.14 : Circuit diagram for the cathode follower.

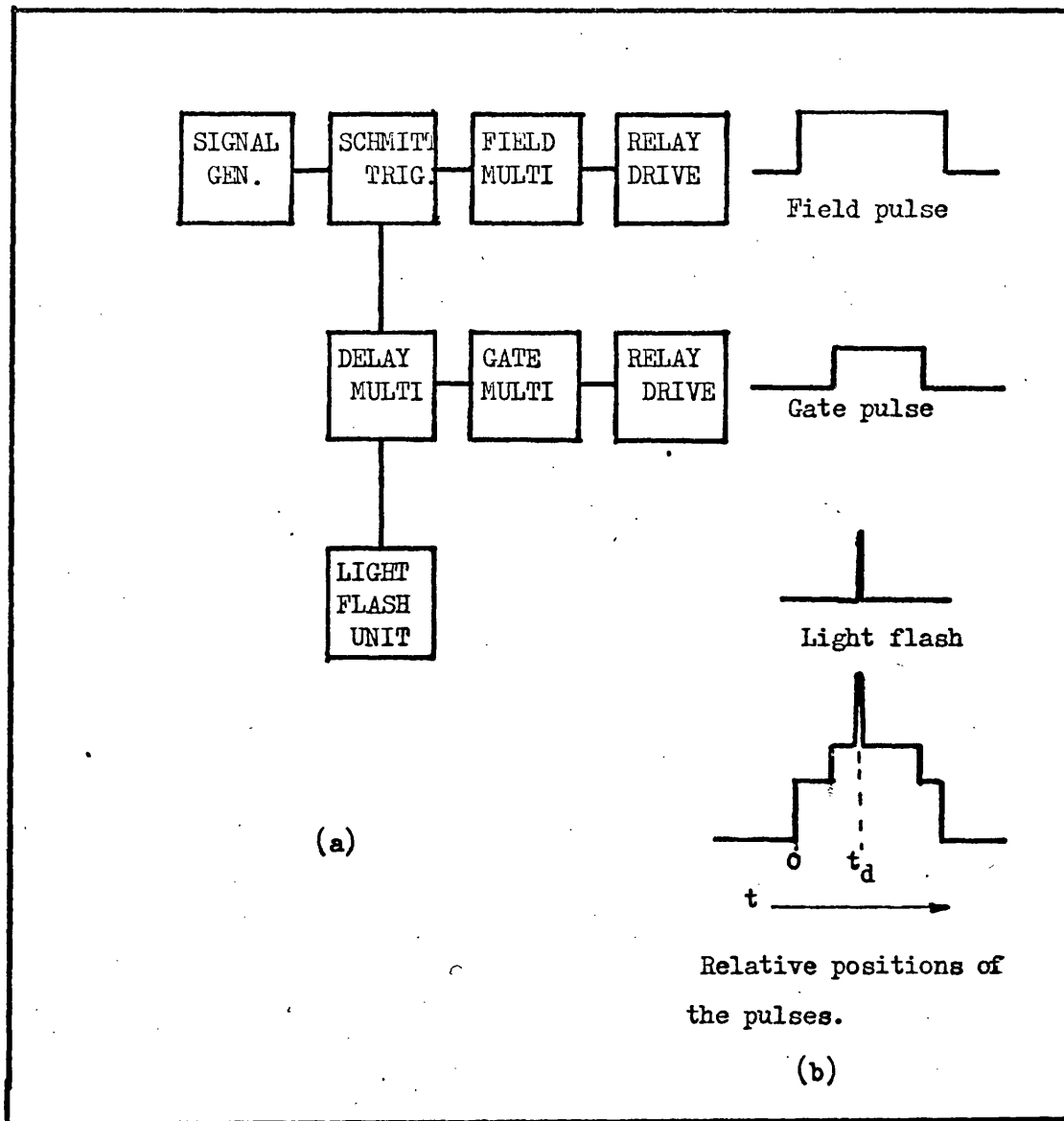


Fig. 4.15 : Field pulse unit. (a) shows the block diagram of the unit. (b) shows the pulses and their relative positions.

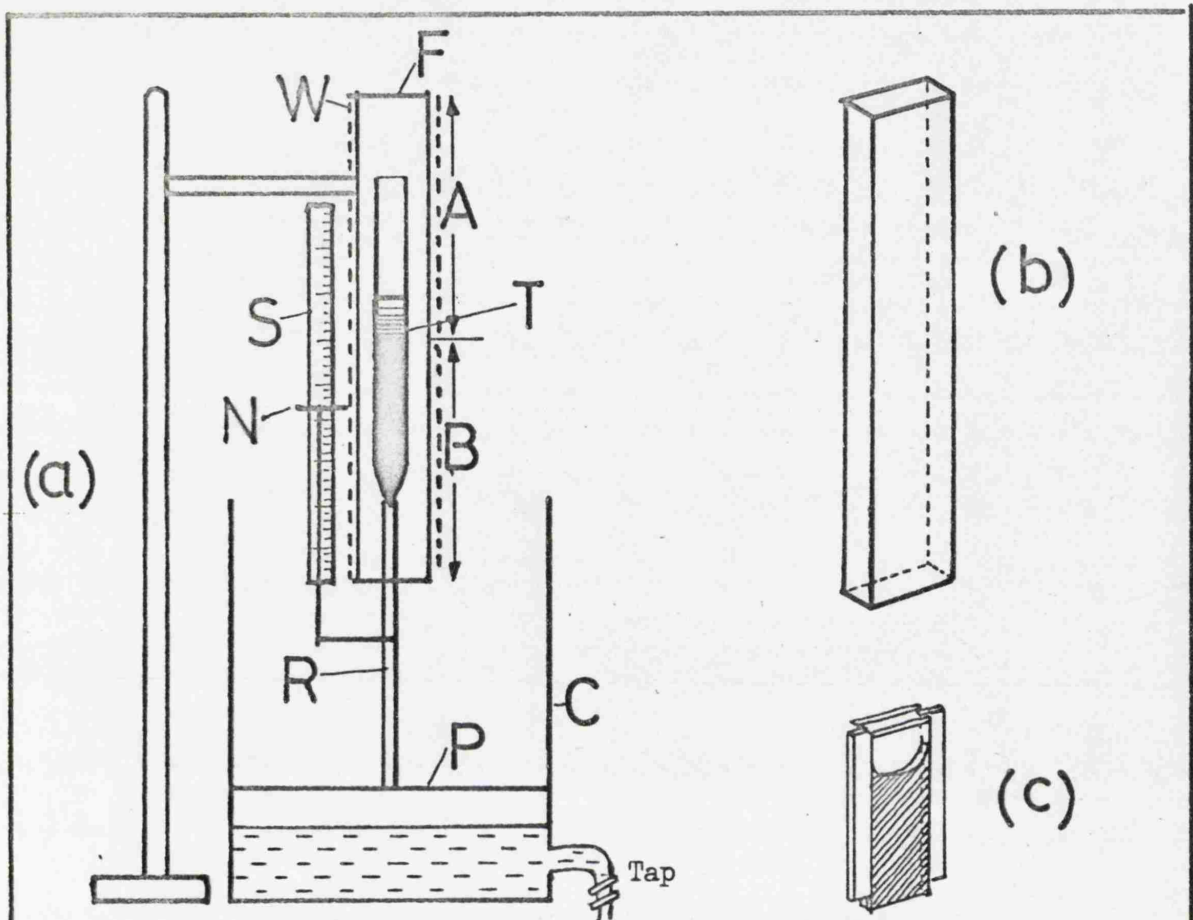


Fig. 4.16 : Bridgeman's method for growth of sulphur from the melt. T is the tube containing the specimen. (b) shows the rectangular furnace and, (c) the rectangular cell.

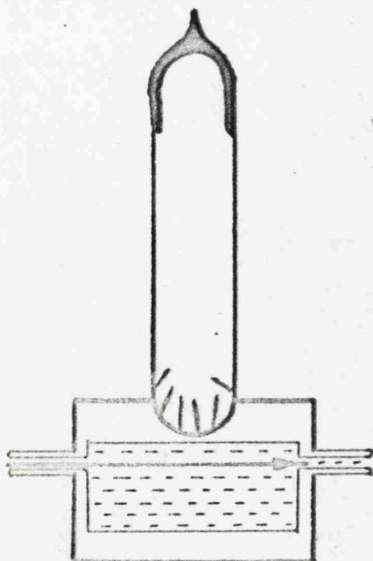


Fig. 4.17 : Arrangement for growing sulphur from vapour phase.

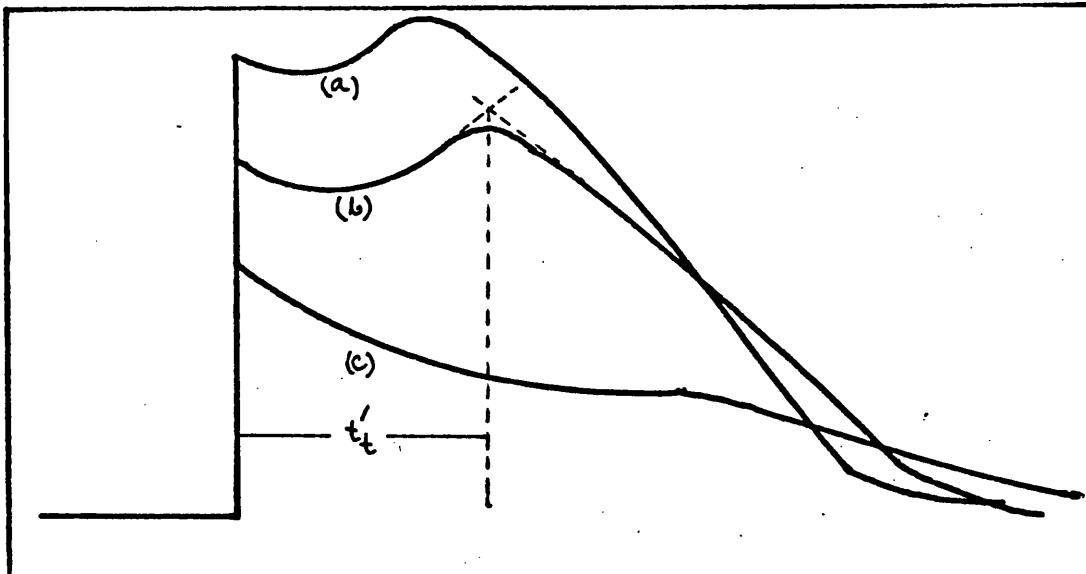


Fig. 5.1 : Positive photosignals in laboratory reagent liquid sulphur. (a), (b) and (c) are observed with decreasing applied field. Similar positive signals were also observed with ultrapure liquid specimens.

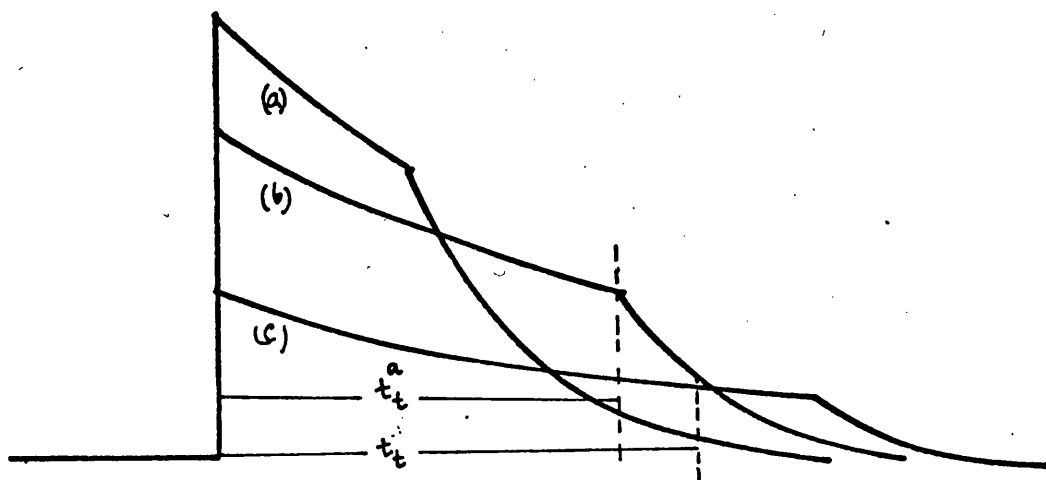


Fig. 5.2 : Negative photosignals in ultrapure liquid sulphur. (a), (b) and (c) are observed with decreasing applied field.

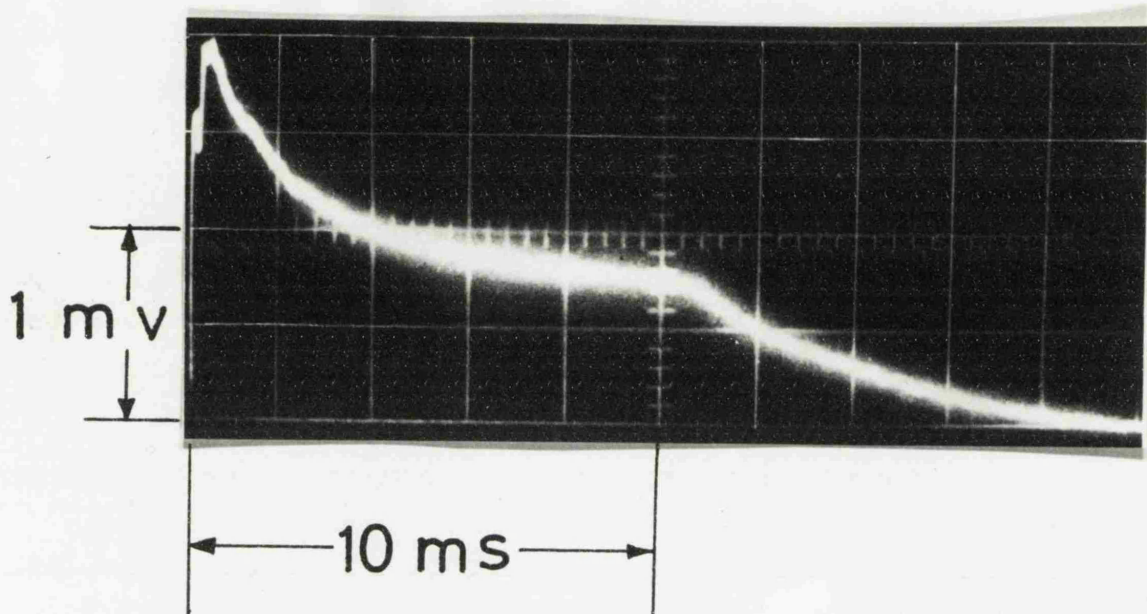


Fig. 5.3 : Negative charge transit in liquid ultrapure sulphur near the melting point, showing the lengthening of the tail due to heating. The initial decay is not truly exponential and is thought to be due to electronics and loss of carriers by recombination in the generation region.

C. F. input resistance - 10^7 ohms

Specimen thickness - 210 microns

Applied potential - 400 volts

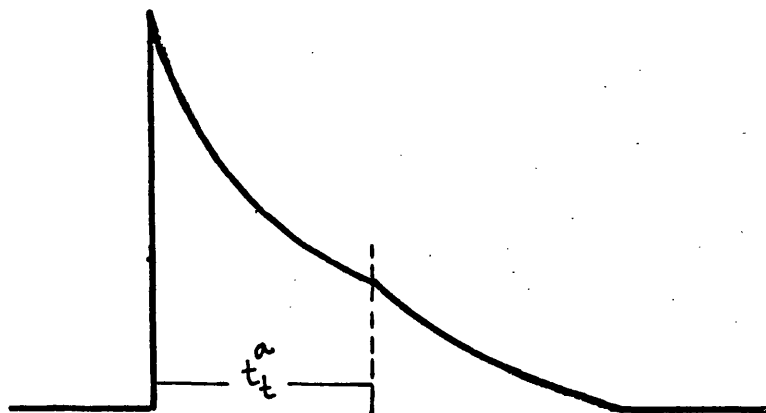


Fig. 5.4 : Negative photosignals in ultrapure liquid sulphur above 160°C.

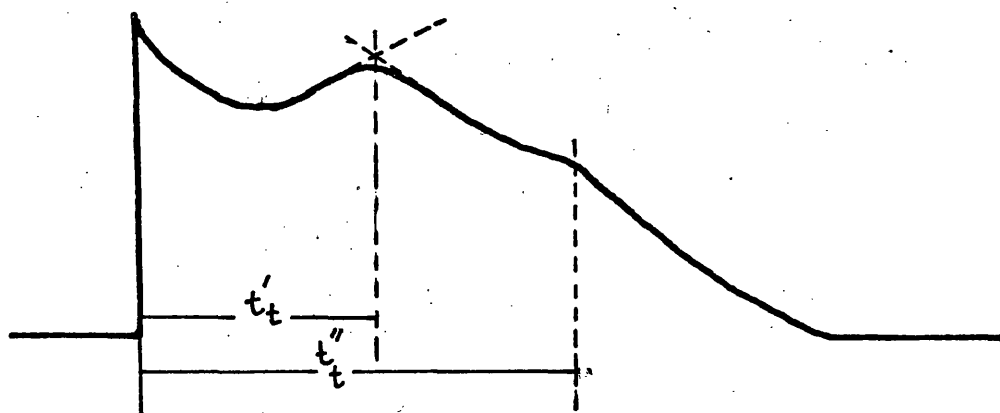


Fig. 5.5 : Positive signal at the same applied field as Fig. 5.1 (b) but at lower light intensity where two - component structure is observed.

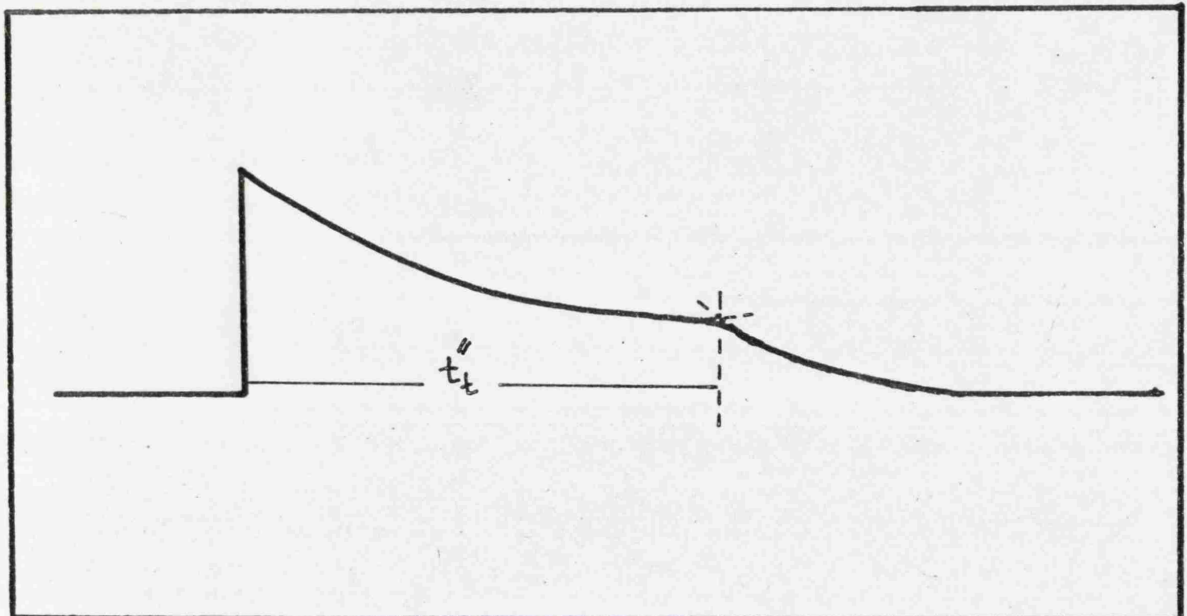


Fig. 5.6 : Positive signal at the same applied field as Fig. 5.1 (b) and Fig. 5.5 but at very low light intensity when the slow component t_t^n only can be seen.

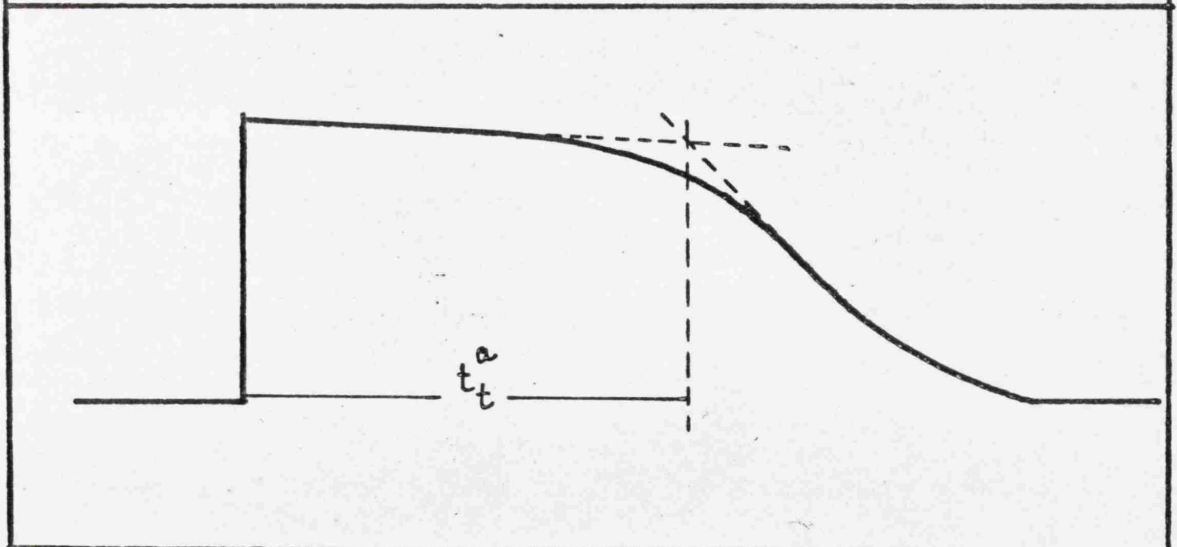


Fig. 5.7 : Positive photosignal in ultrapure liquid sulphur above 160°C .

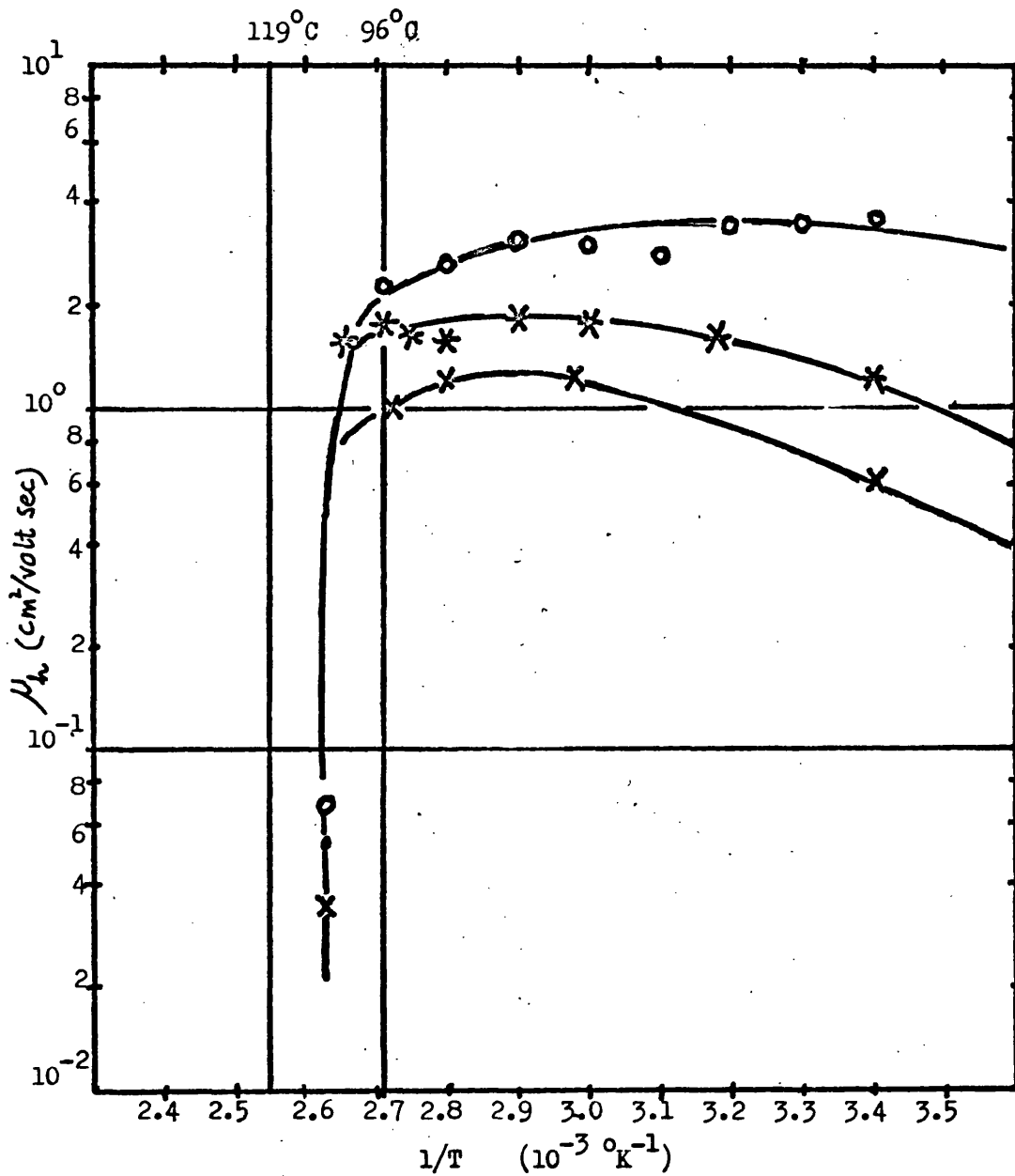


Fig. 5.8 : Hole mobility in crystalline sulphur plotted against $1/T$. Monoclinic range from 96° to the melting point at 119°C is indicated.

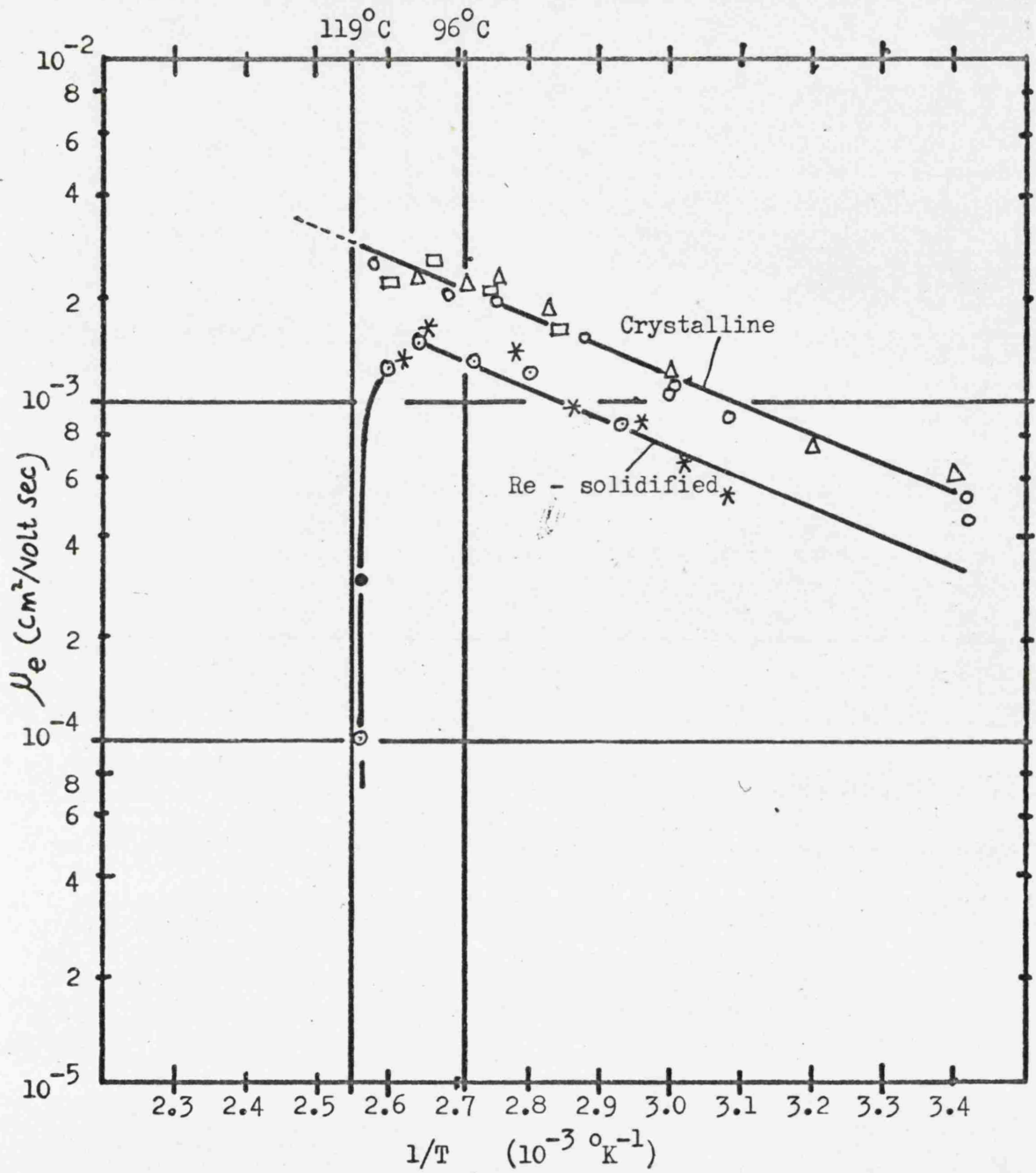


Fig. 5.9 : Electron mobility in crystalline and re - solidified sulphur plotted against $1/T$. The monoclinic range is from 96° to 119°C .

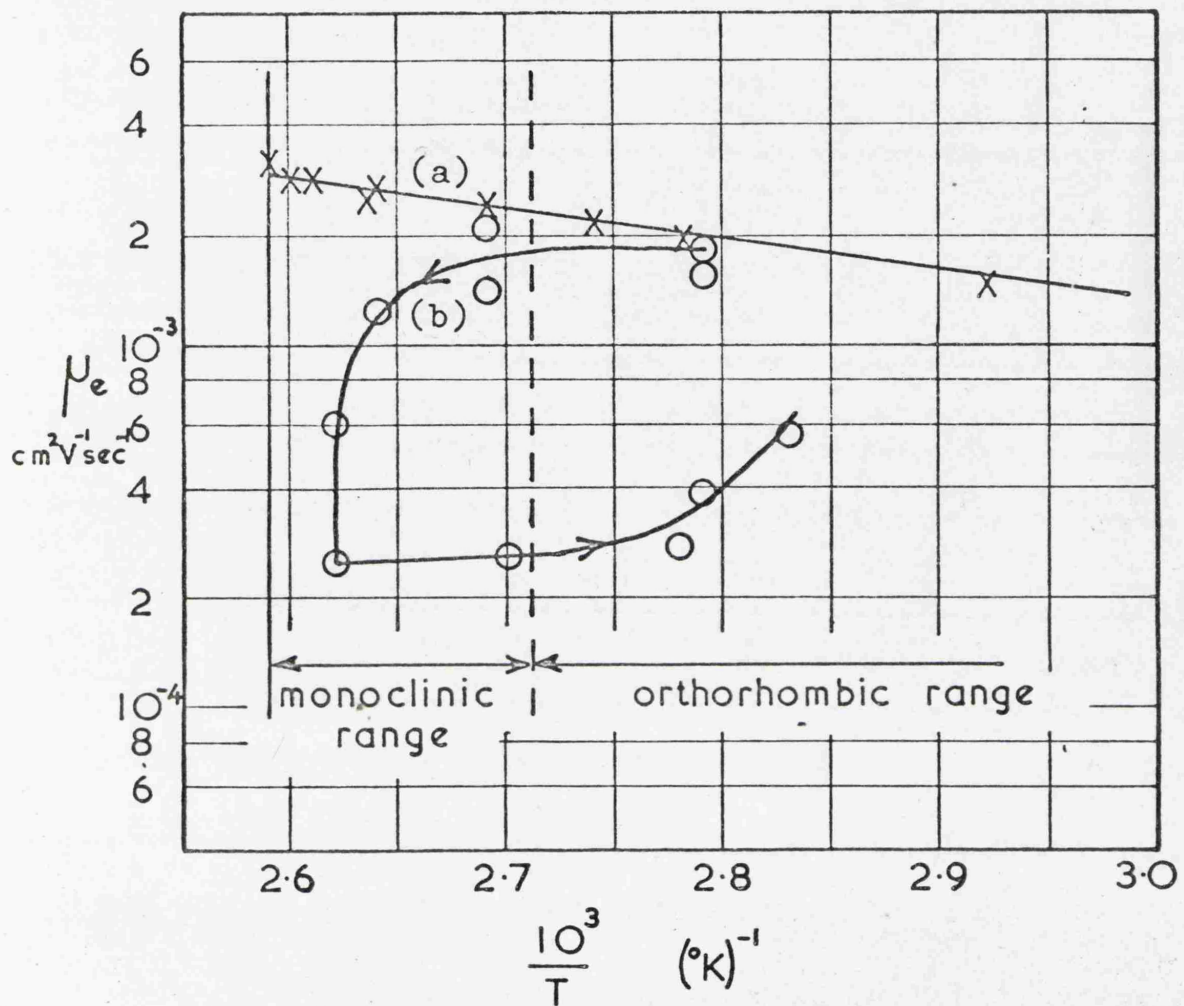


Fig. 5.10 : Temperature dependence of electron mobility in sulphur crystal in the monoclinic range up to 113°C (Ref. 34). (a) shows the points obtained in a quick run. (b) was obtained in a slower run and shows a drop in mobility before the melting point of orthorhombic sulphur is reached. (b) also shows a hysteresis effect.

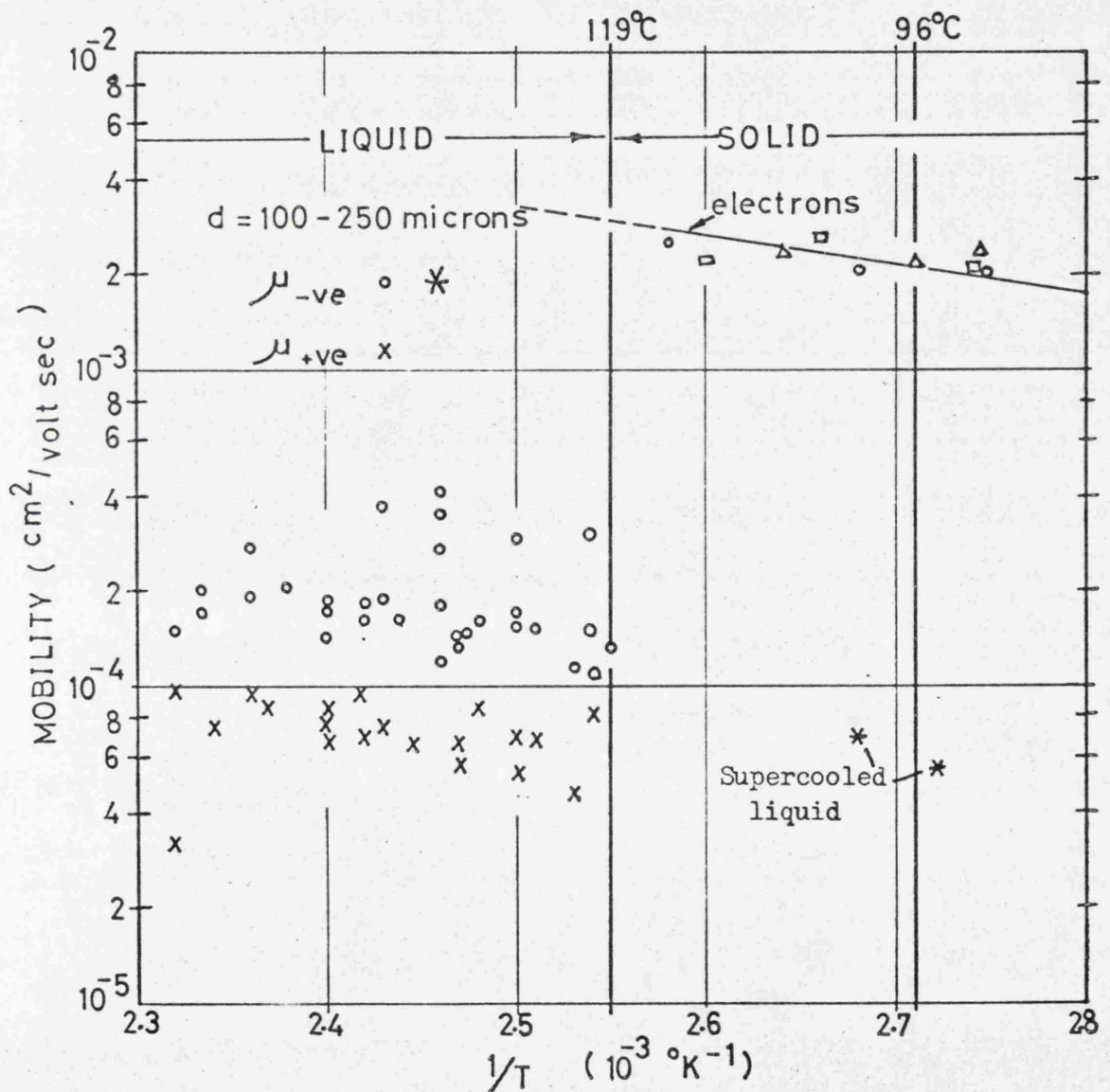


Fig. 5.11 : Negative and positive carrier mobilities in liquid laboratory reagent sulphur obtained with gold electrodes are plotted against $1/T$. The results in the solid are included to show the drop in mobility. The hole mobility drops by a factor of 10^4 . The results for the supercooled liquid are shown by the asterisks (*).

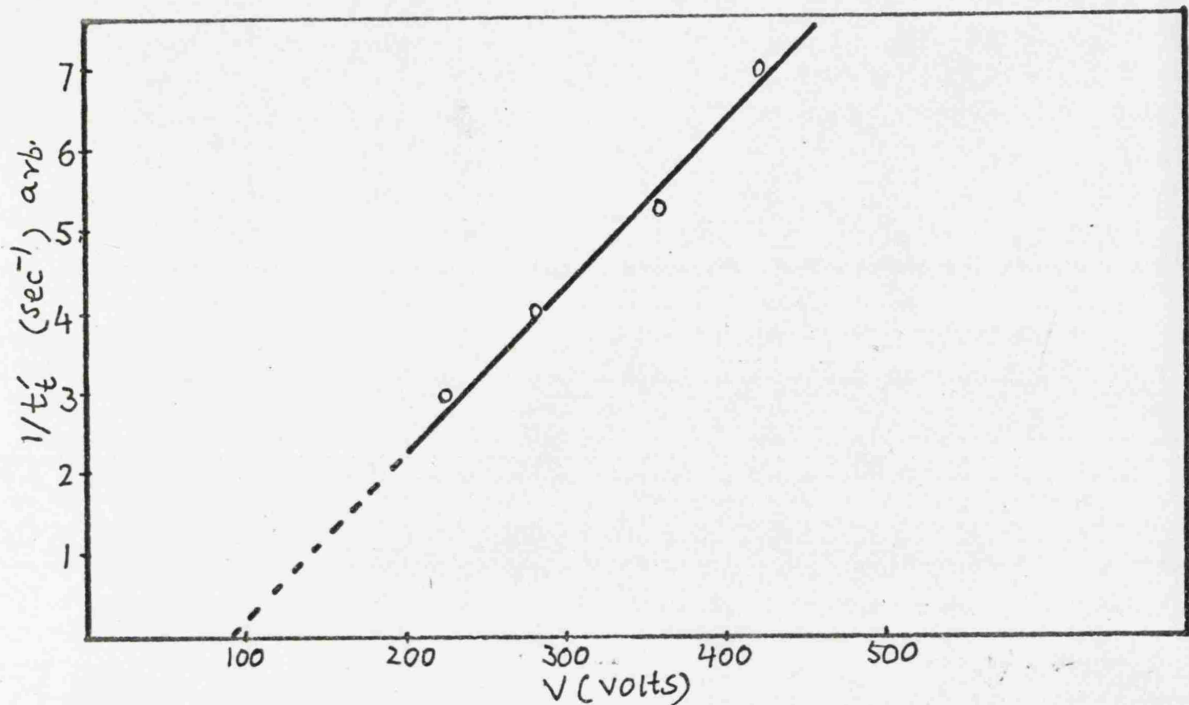


Fig. 5.12 : Field dependence of $1/t_t'$ in laboratory reagent liquid sulphur. $1/t_t'$ plotted against V.

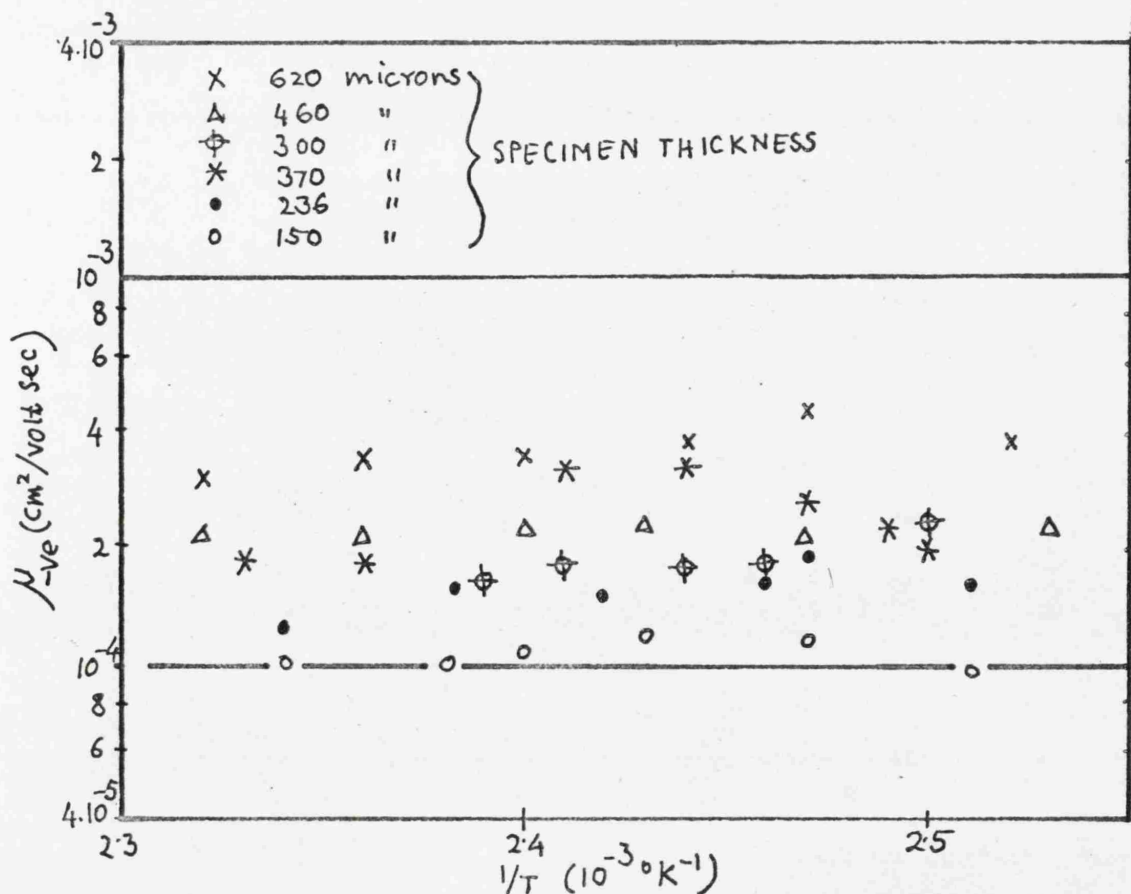


Fig. 5.13 : Negative carrier mobility in laboratory reagent liquid sulphur obtained with Nesa electrodes are plotted against $1/T$.

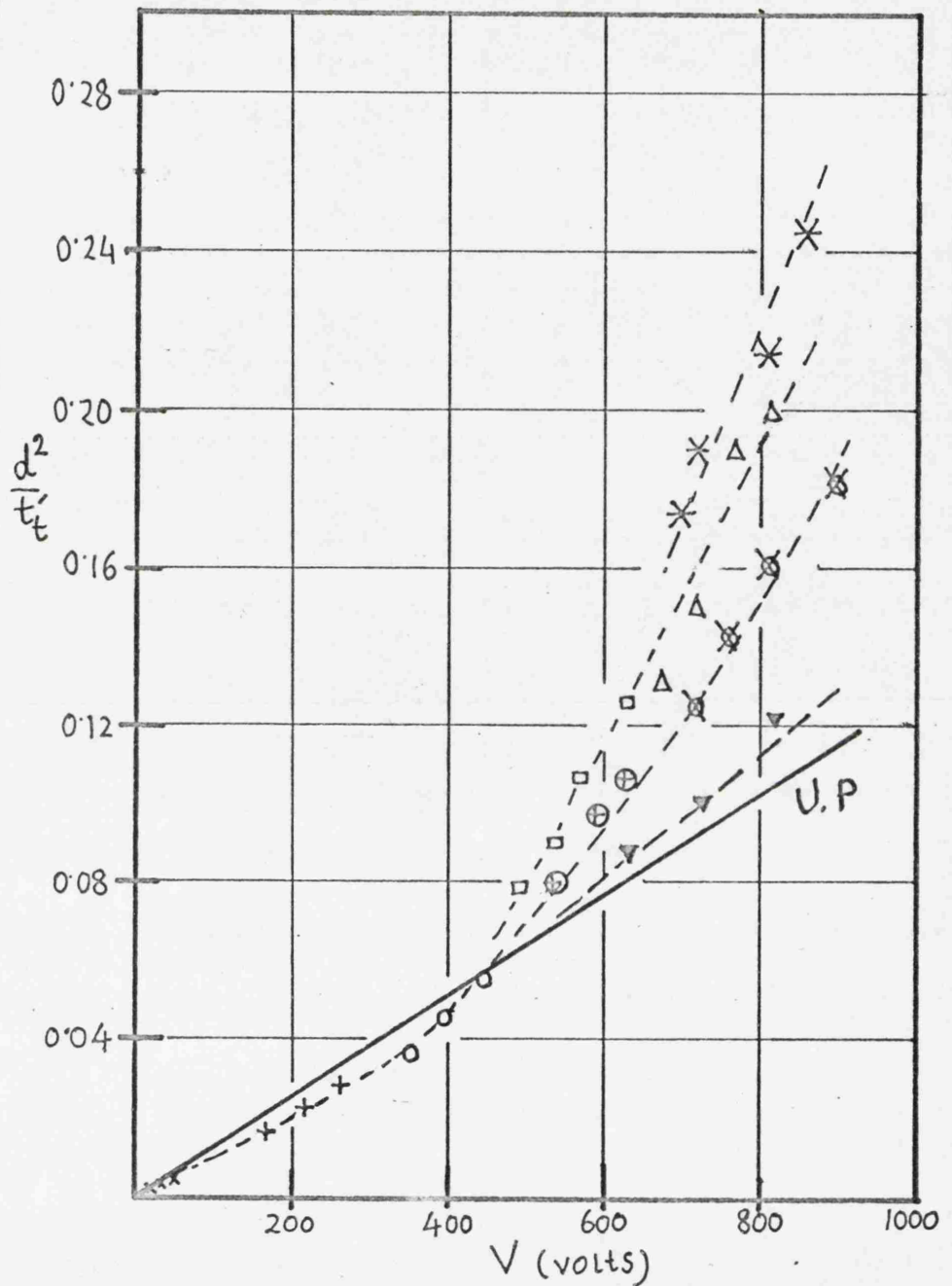


Fig. 5.14 : $d^2/t_t'^2$ plotted against V for a number of specimen thicknesses. Results correspond to negative signals in the laboratory reagent liquid used with nesa electrodes. x - 50 microns; + - 180 microns; o - 236 microns; ⊕ - 400 microns; ▼ - 370 microns; ◻ - 480 microns; ⊗ - 605 microns; Δ - 620 microns; * - 680 microns. The solid line represents the results obtained with the ultrapure liquid; t_t^a , the true transit time, is plotted.

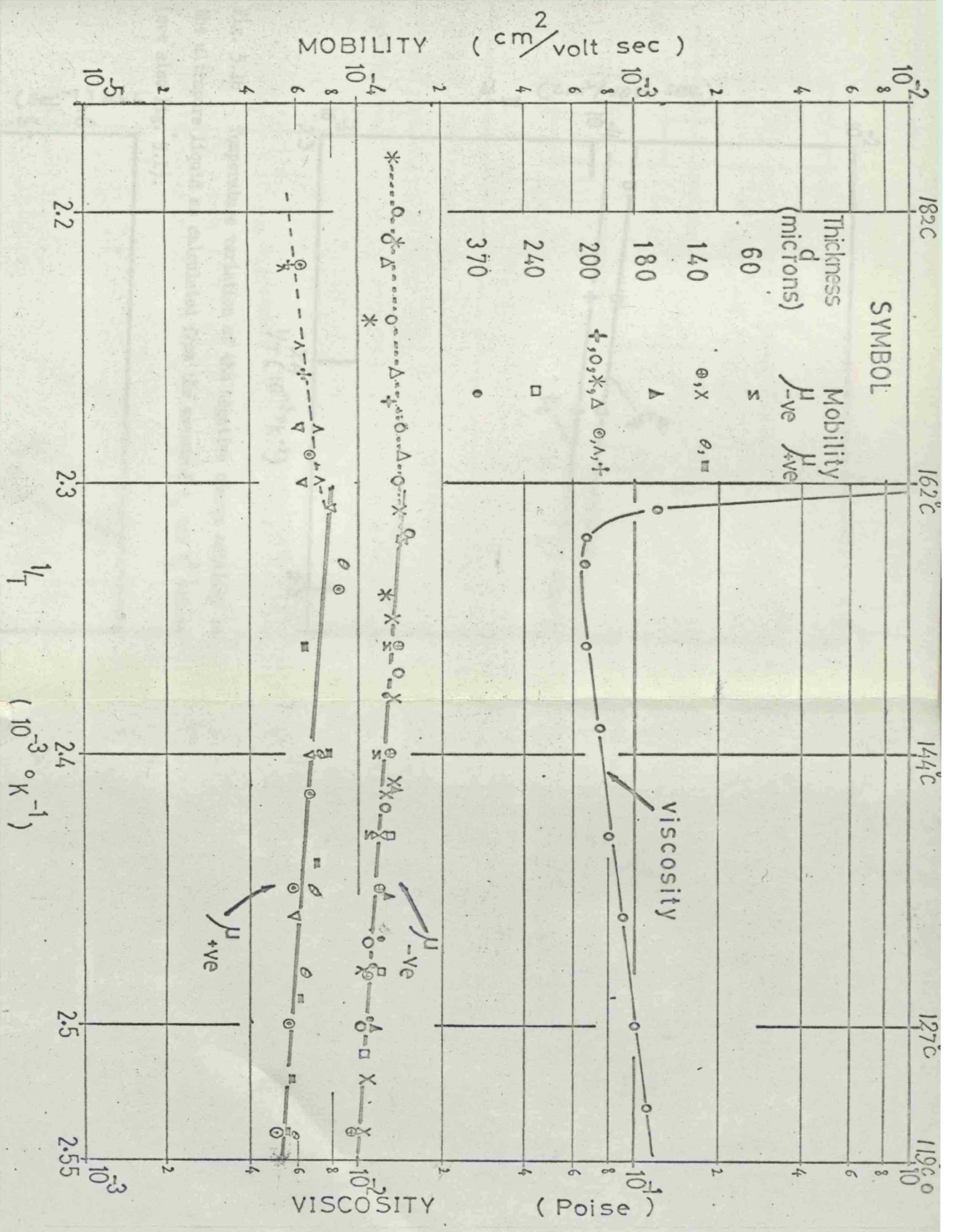


Fig. 5.15 : Temperature dependence of negative and positive charge carrier mobilities in ultrapure liquid sulphur. Viscosity is also plotted to indicate the viscosity activation of the normal liquid and the temperature ($\sim 160^\circ\text{C}$) where polymerisation of liquid sulphur starts.

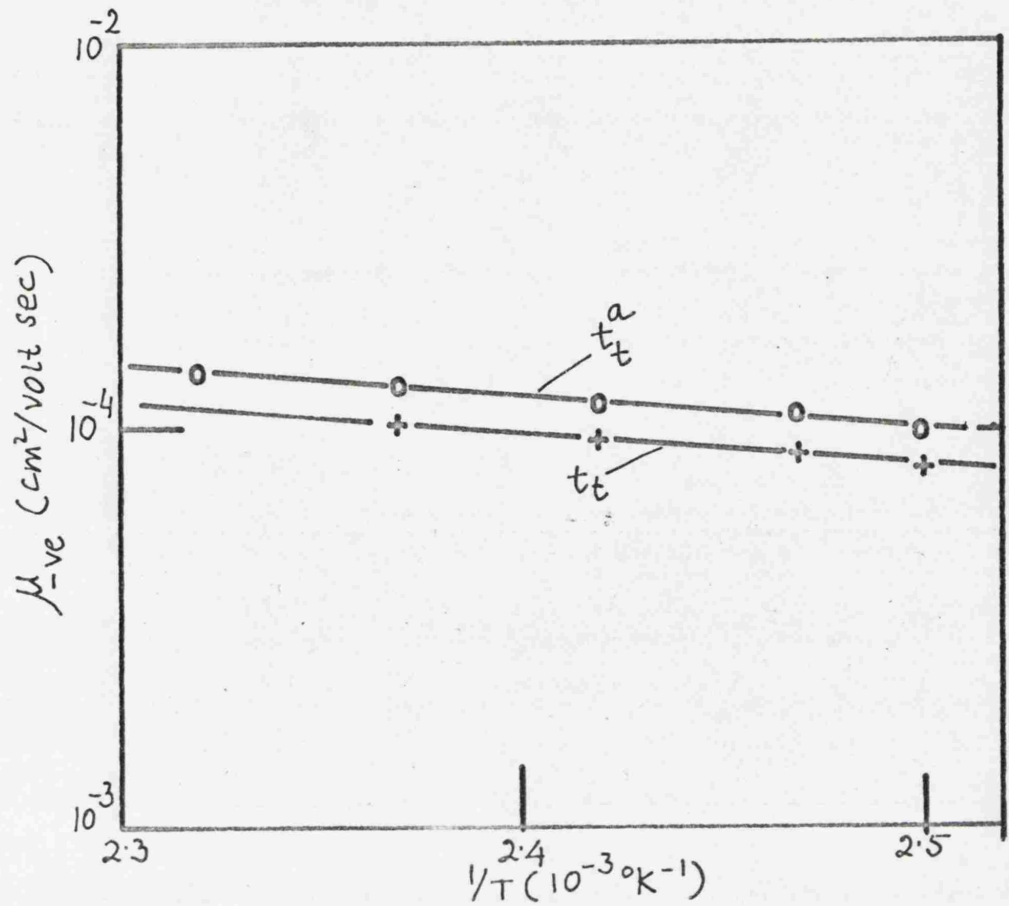


Fig. 5.16 : Temperature variation of the negative charge mobility in the ultrapure liquid as calculated from the measured t_t and t_t^a values (see also Fig. 5.1).

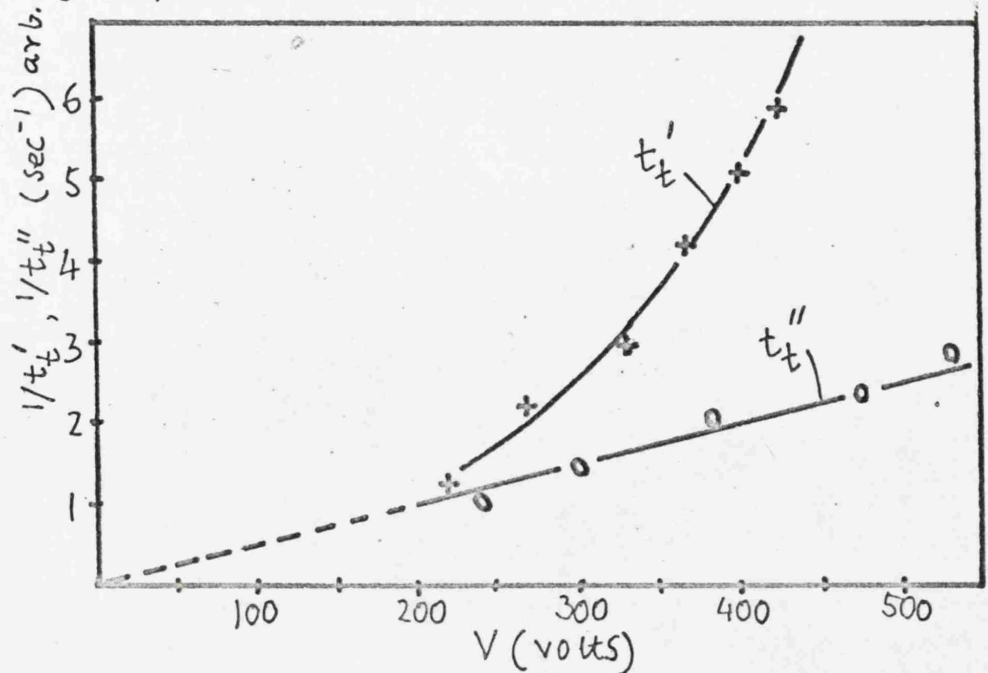


Fig. 5.17 : Field dependence of t_t' and t_t'' (see also Figs. 5.5 and 5.6).

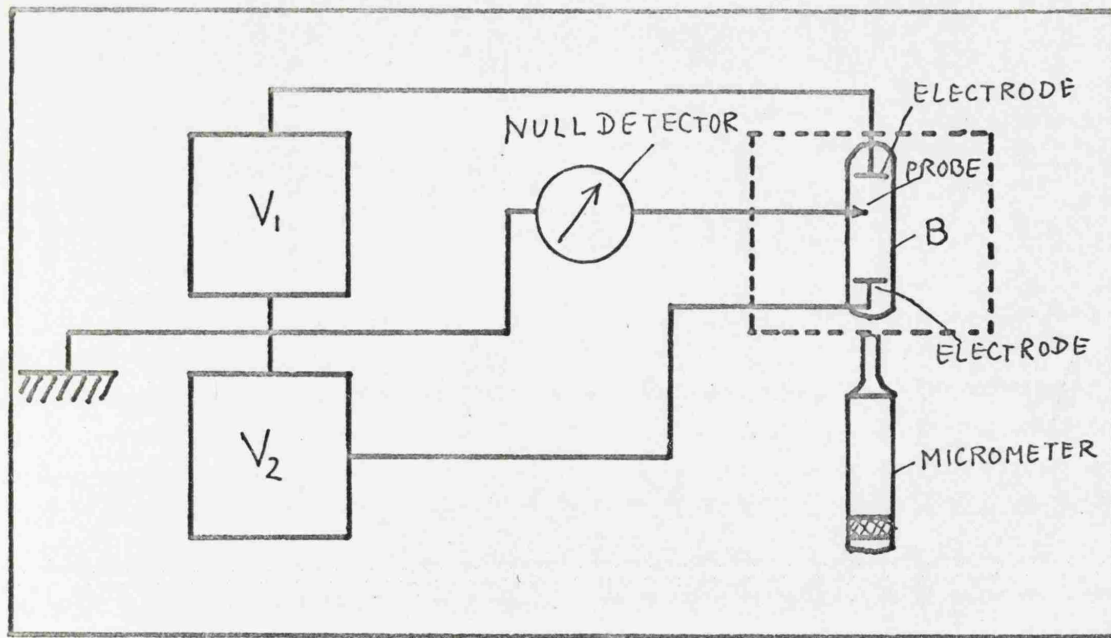


Fig. 5.18 : Experimental arrangement for probe measurements of the potential distribution in liquid sulphur. B is the boat containing the liquid specimen.

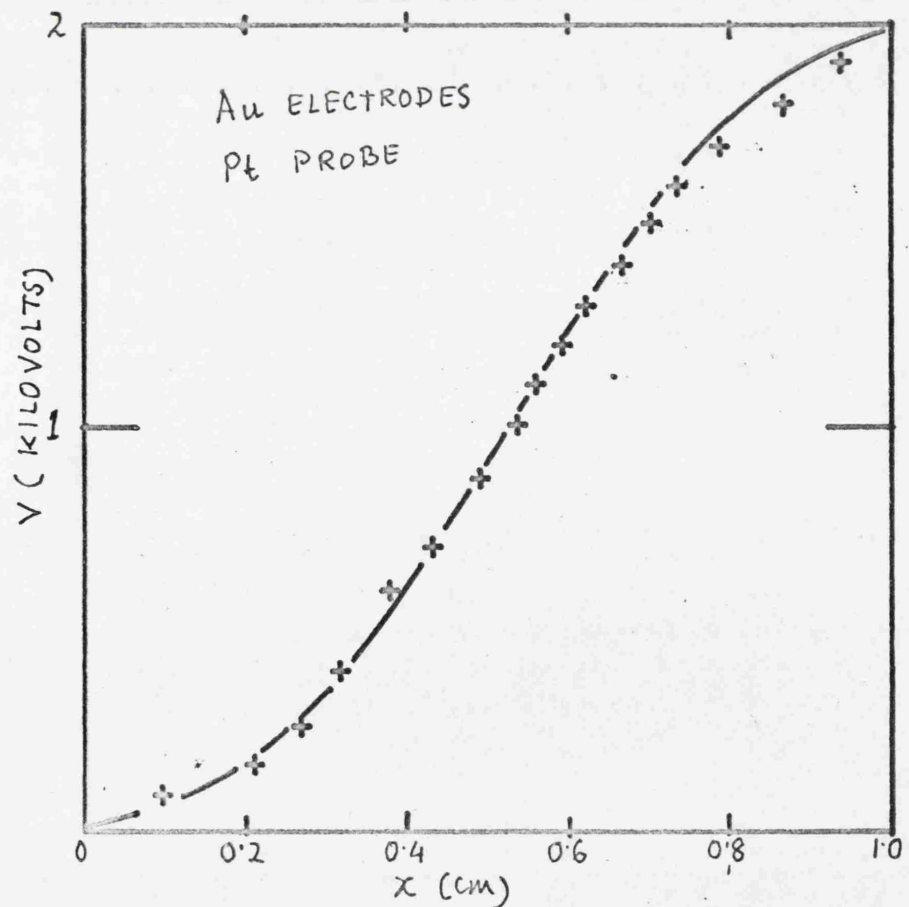


Fig. 5.19 : The potential distribution in liquid sulphur with gold electrodes and platinum probe.

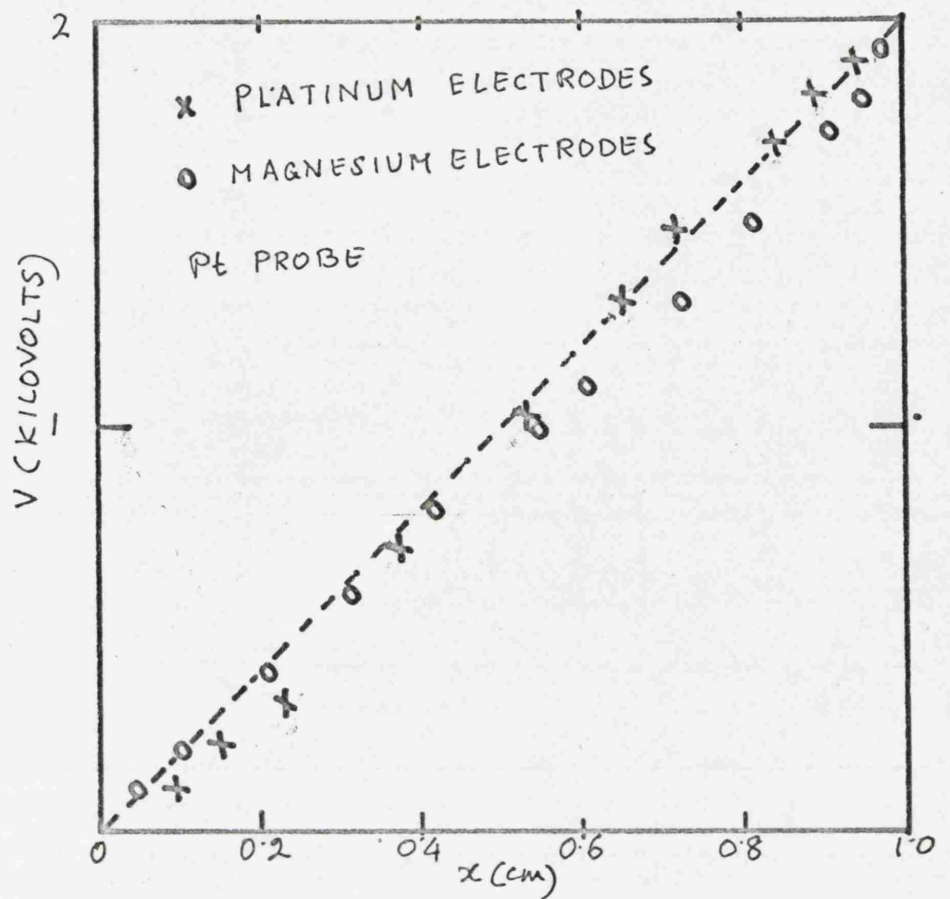


Fig. 5.20 : The potential distribution in liquid sulphur with platinum and magnesium electrodes and platinum probe. The results shown correspond to the ultrapure liquid.

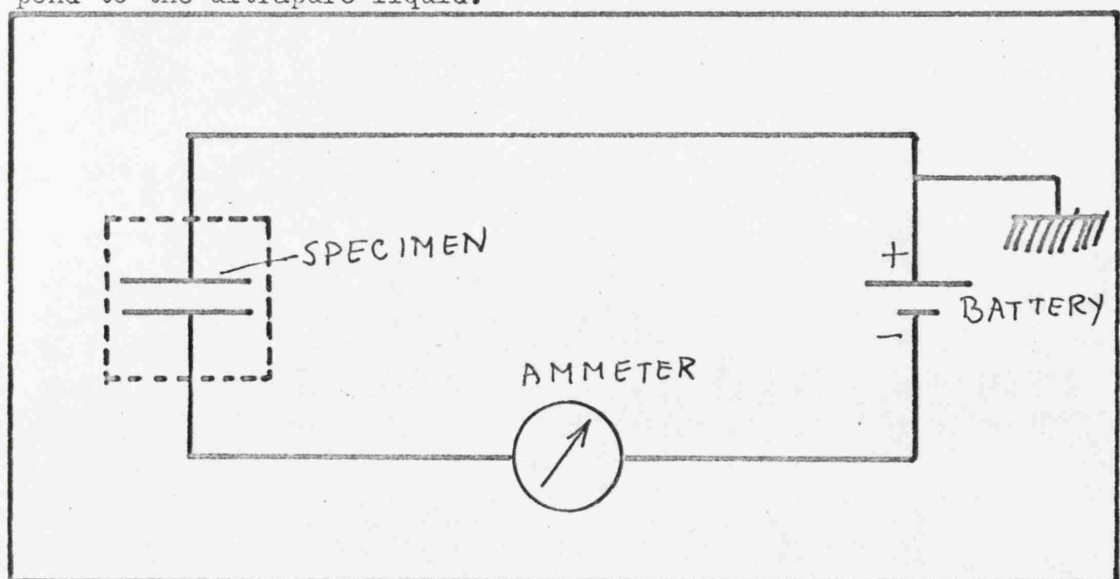


Fig. 5.21 : Experimental arrangement for dark current measurements on liquid sulphur.

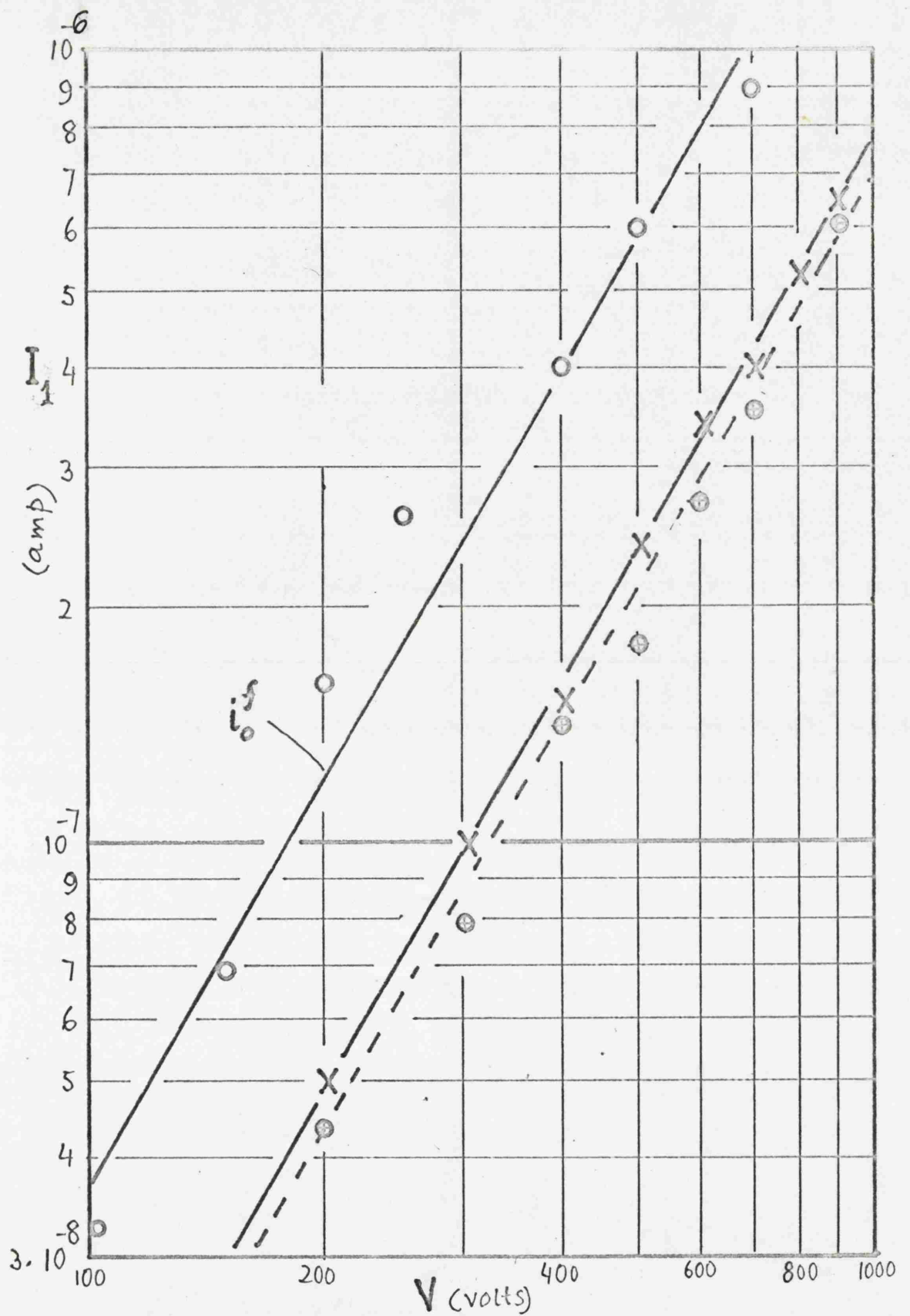


Fig. 5.22 : Variation of the field transient and 'peak current' I_1 in liquid sulphur with the applied potential. Specimen thickness 150 microns
 ○ - Field transient current in the ultrapure liquid, X - I_1 in the ultrapure liquid and ⊕ I_1 in the laboratory reagent liquid.

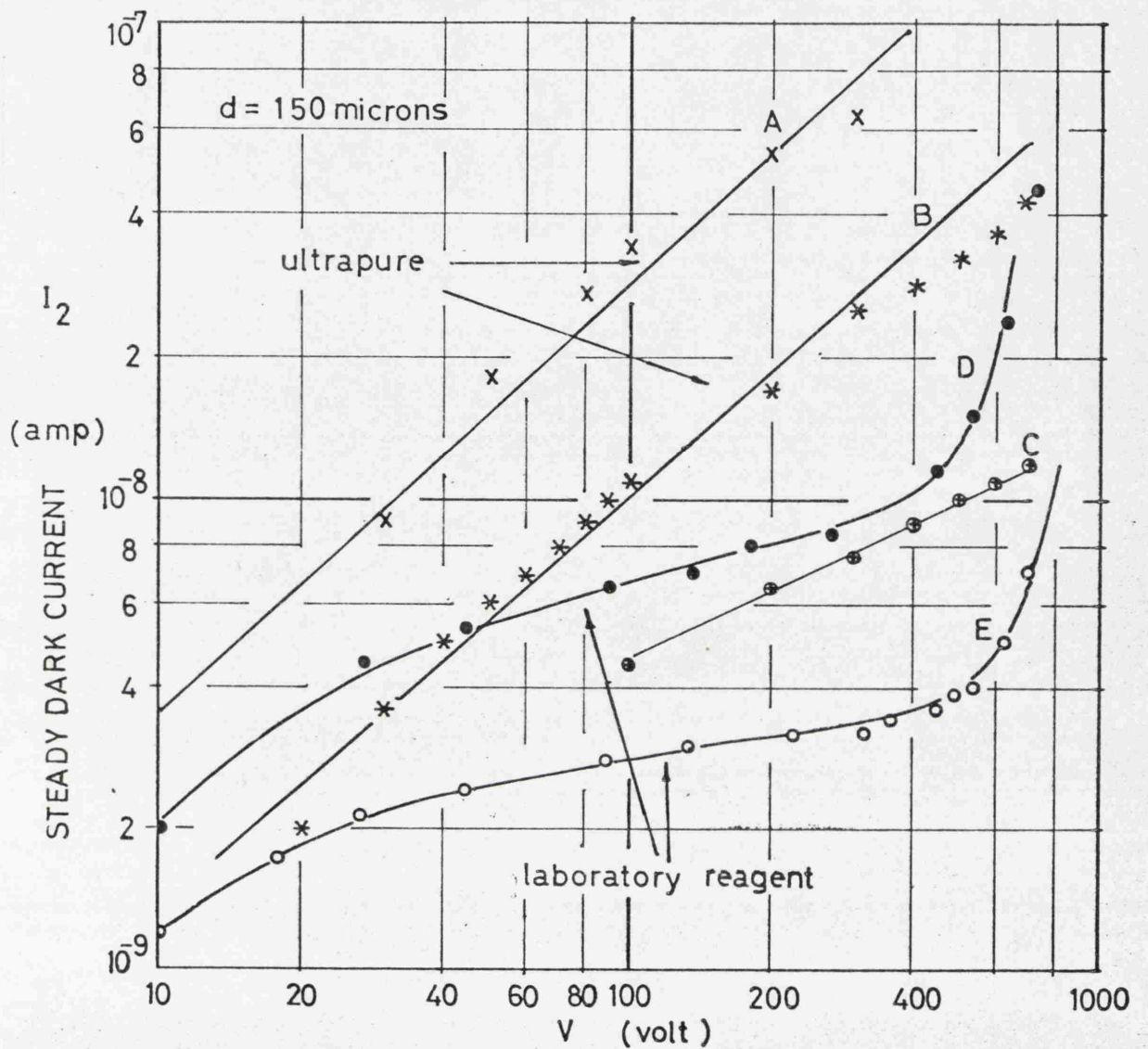


Fig. 5.23 : Variation of the steady dark current I_2 with the applied potential. Specimen thickness 150 microns. Curves A and B belong to fresh ultrapure samples, C to an ultrapure liquid sample after half - hour of heating at a temperature of 140°C . Curves D and E correspond to the laboratory reagent liquid.

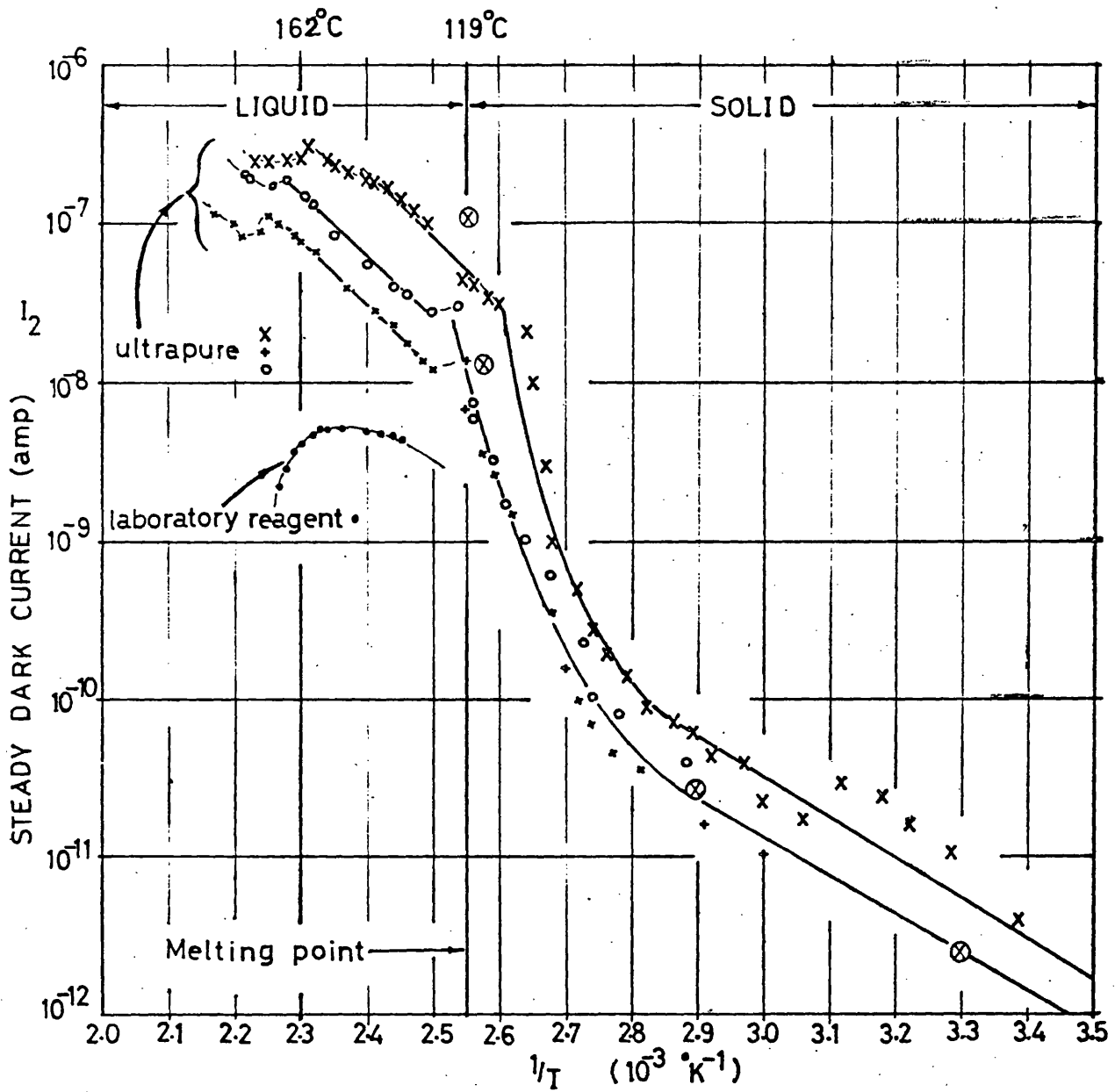


Fig. 5.24 : The temperature dependence of the ohmic dark current in sulphur in the solid, solid to liquid transition region and the liquid.
 ⊗ corresponds to the value obtained from I. C. T. (60)

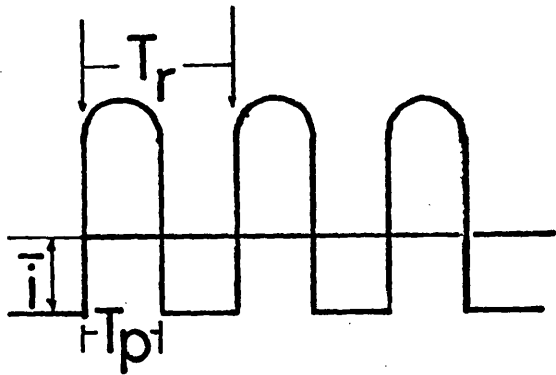


Fig. 5.25 : Averaging of fast pulses. T_r is the pulse rate. T_p is the pulse width. \bar{i} is the average value given by a slow detector.

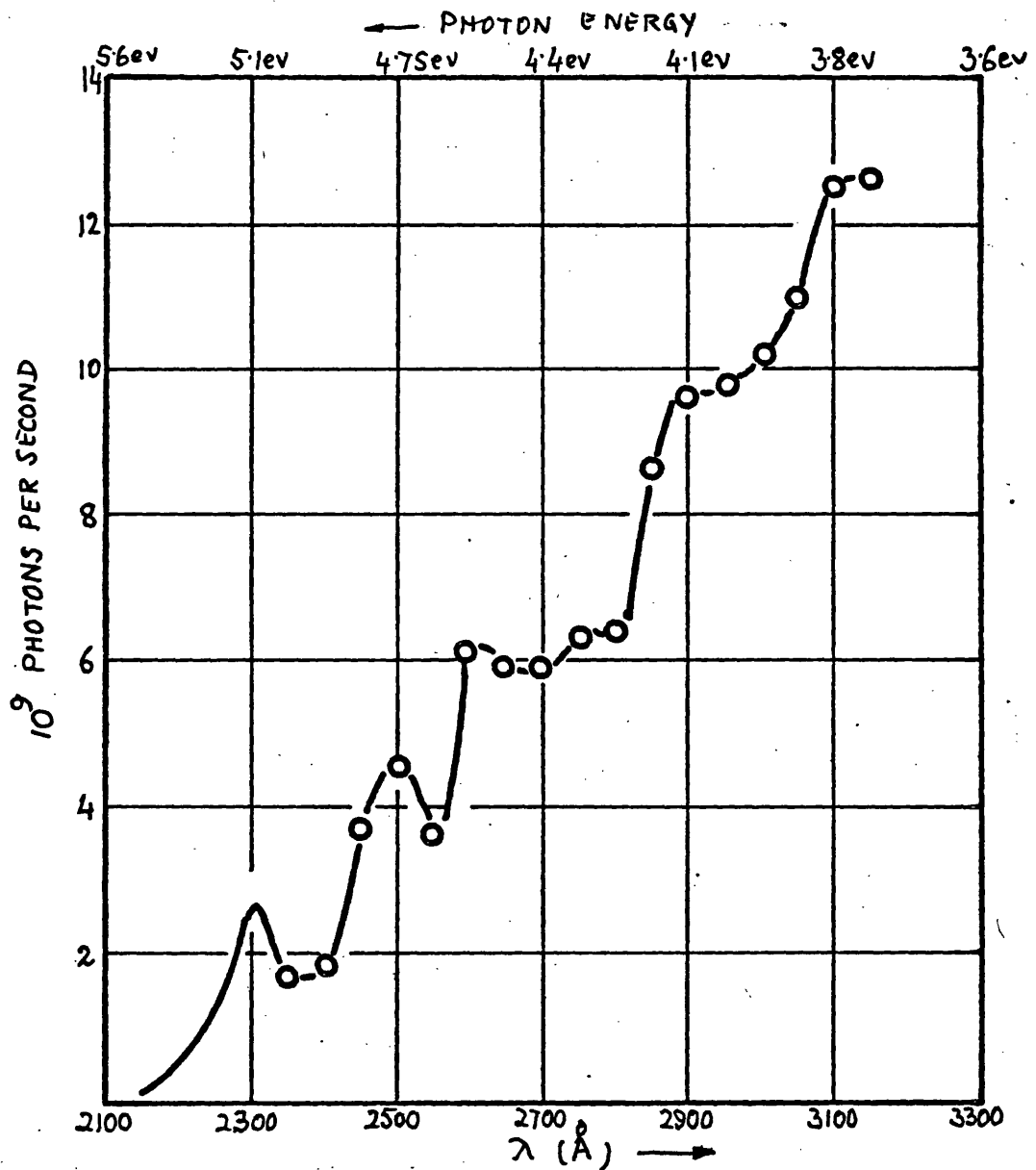


Fig. 5.26 : The spectral distribution of photons per sec of a xenon - mercury flash tube.

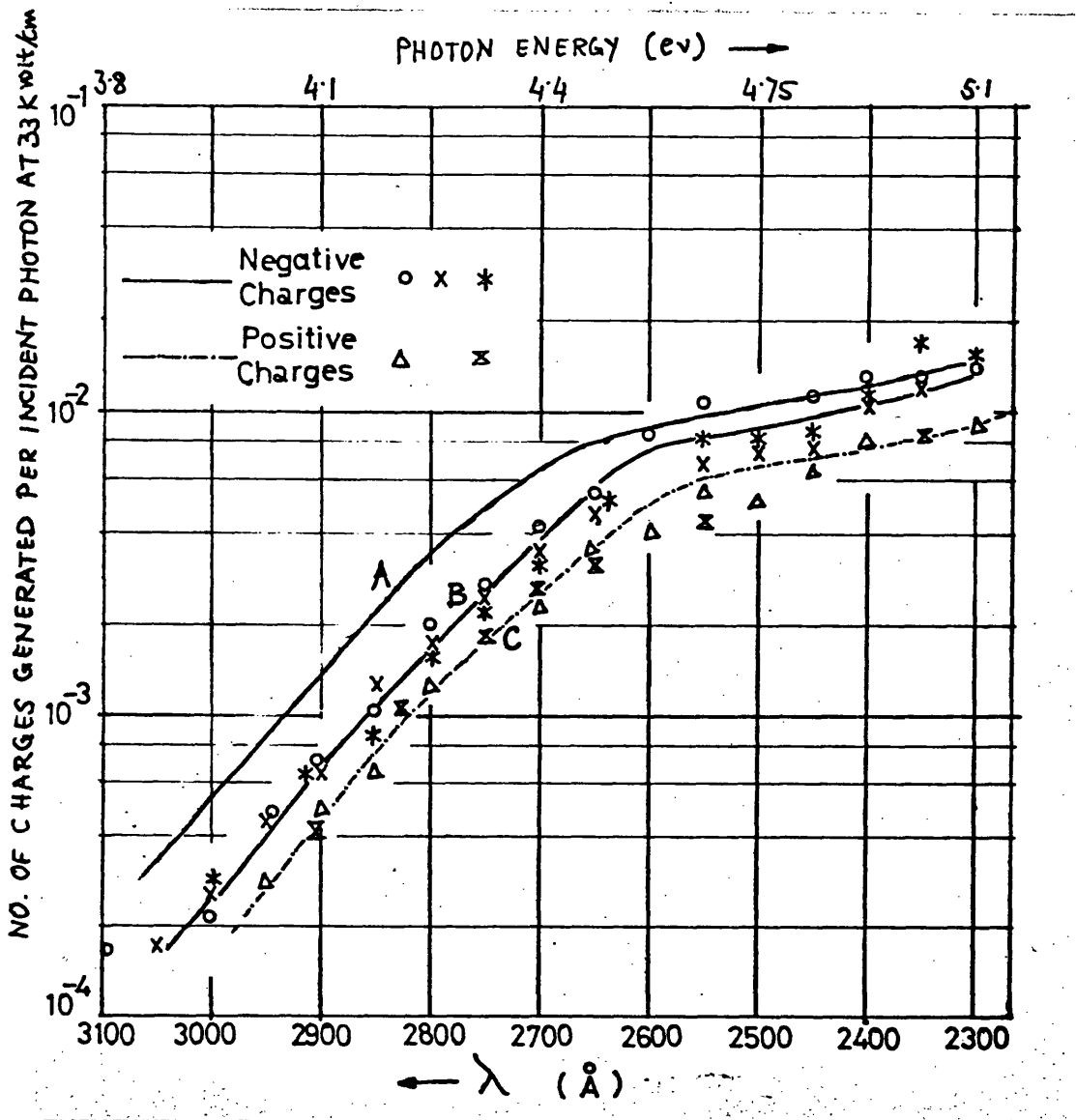


Fig. 5.27 : The generation efficiency of charge carriers in liquid sulphur versus the wavelength of exciting radiation at an applied field of 33 K volt/cm. Curve A corresponds to the solid (the efficiency reduced by a factor of 100). B and C are the curves for the negative and positive charges in the liquid.

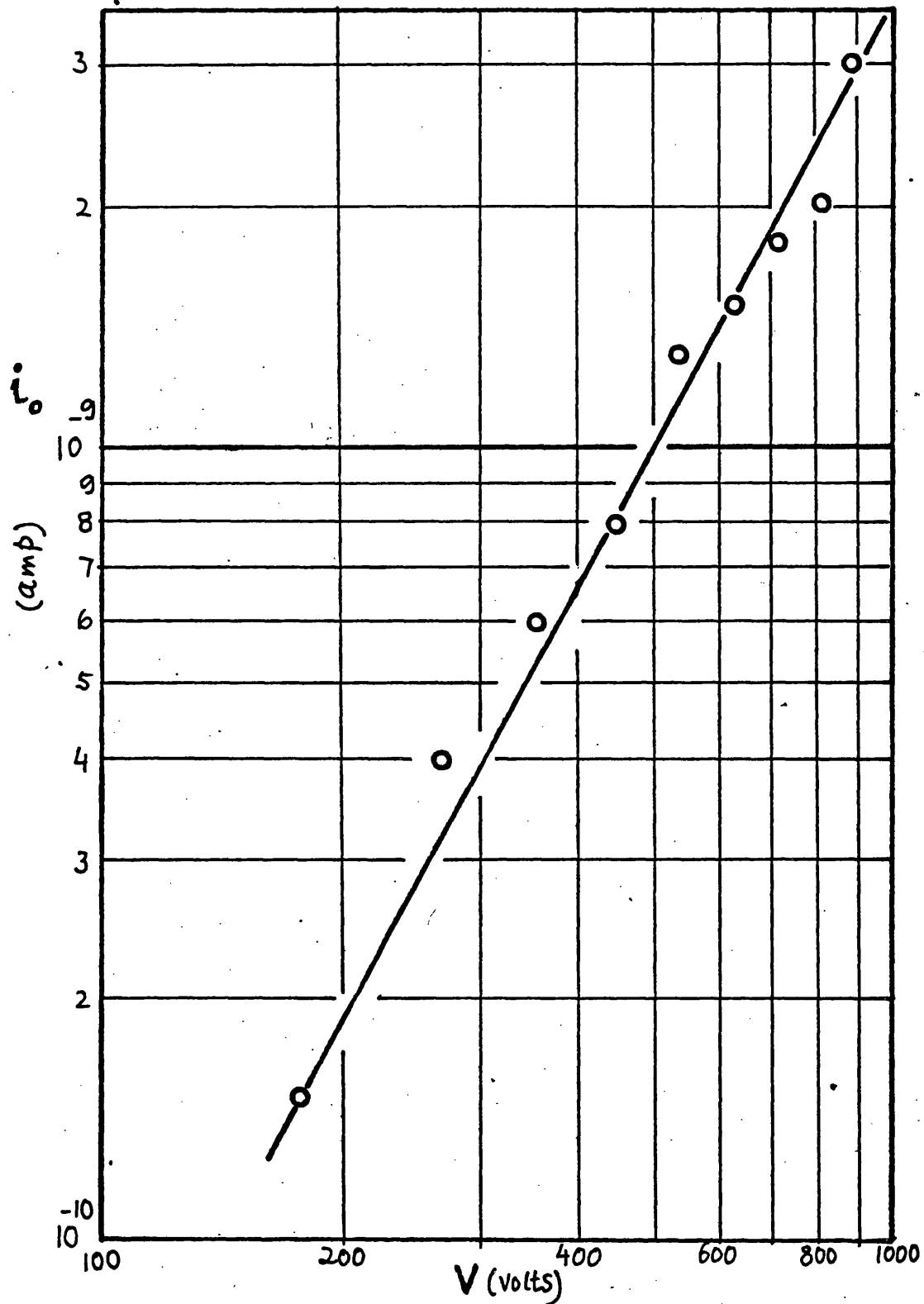


Fig. 5.28 : The dependence of the negative photocurrent on the applied potential. Specimen thickness is 150 microns.

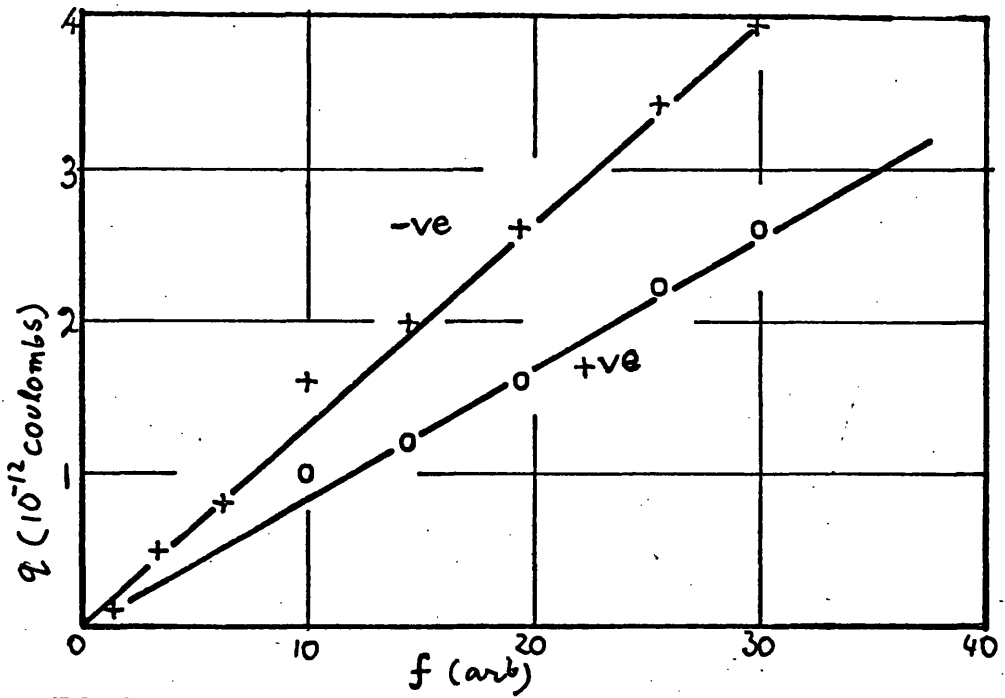


Fig. 5.29: Charge generated per pulse of monochromatic radiation (2500 Å) in liquid sulphur plotted against intensity. Intensity was varied by varying the slitwidth. Specimen thickness 150 microns and applied potential 360 volts.

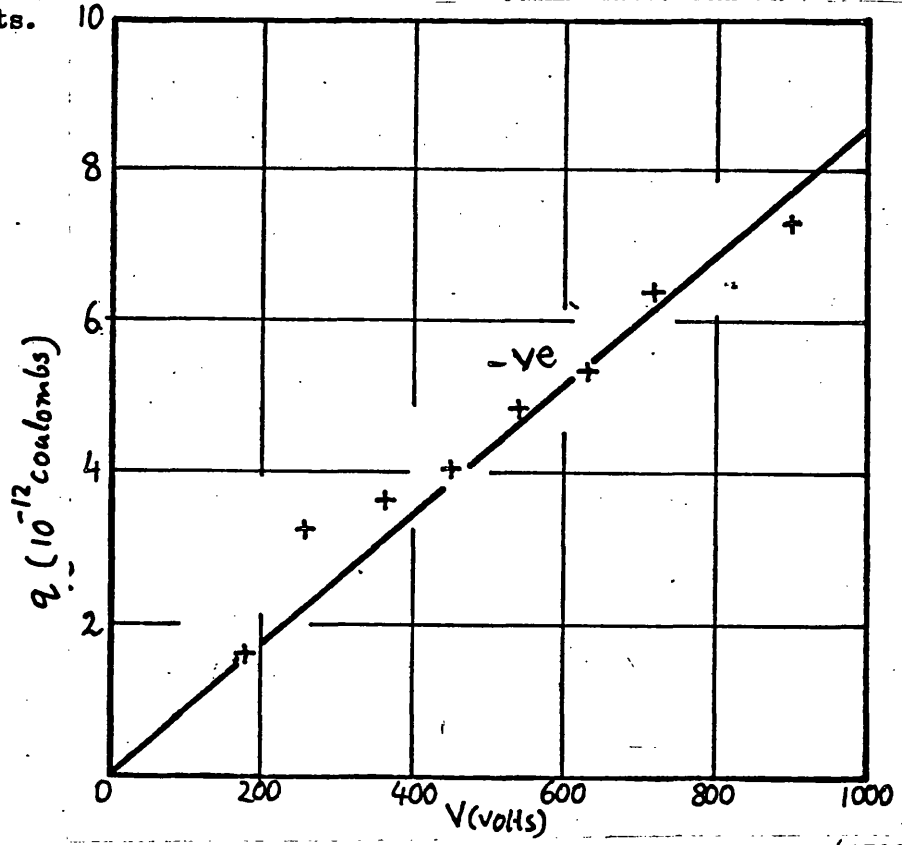


Fig. 5.30 : Charge generated per pulse of monochromatic radiation (2500 Å) in liquid sulphur plotted against the applied potential. Specimen thickness 150 microns.

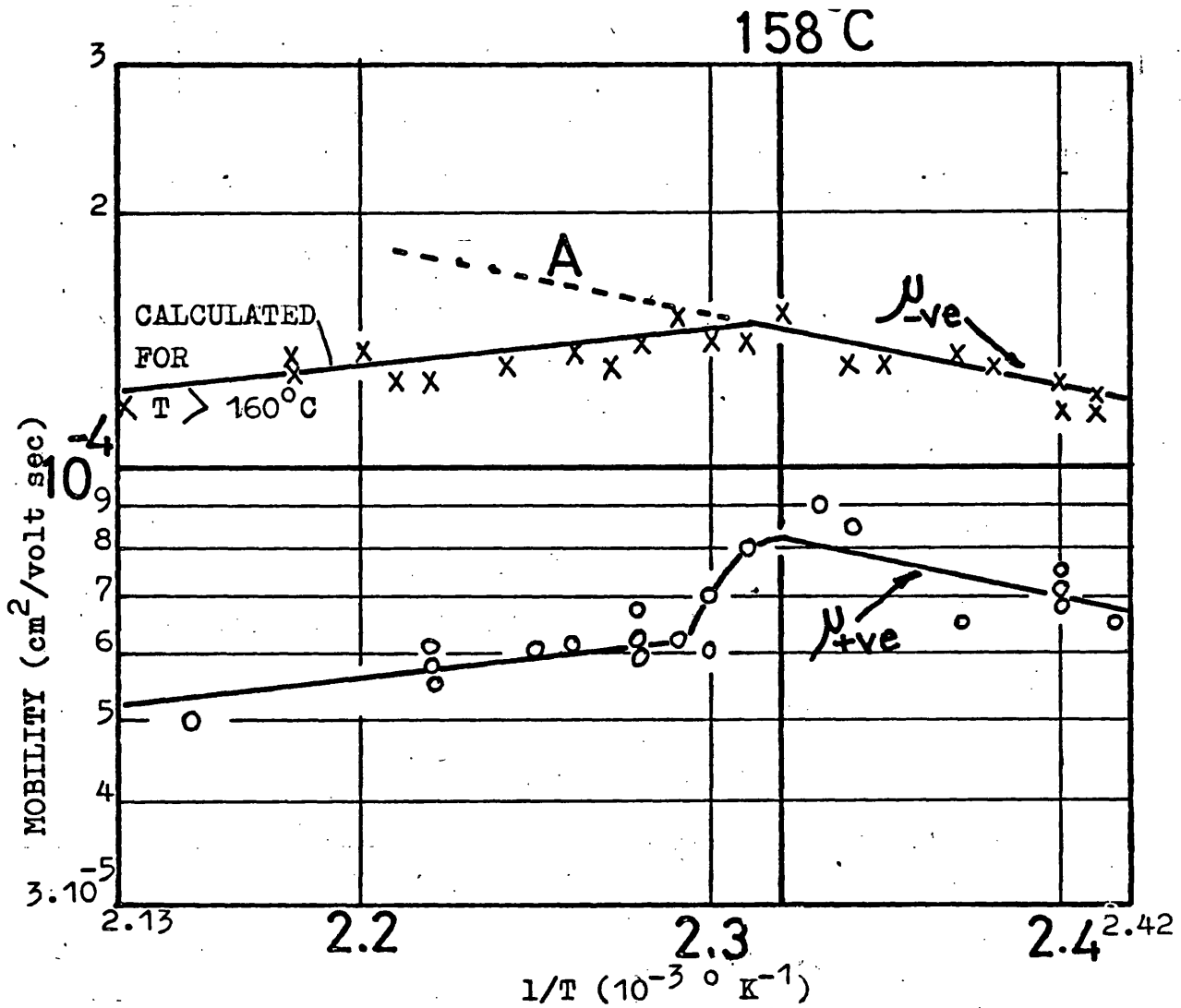


Fig. 6.1 : Re-plotted version of Fig. 5.15 in the temperature range between 141° and 197°C showing the drop in the positive charge mobility in the liquid at 160°C .

The experimental points above 160°C for electrons have been fitted to the theory. The solid line represents the theoretical curve. Curve A is extrapolated from the results below 160°C .

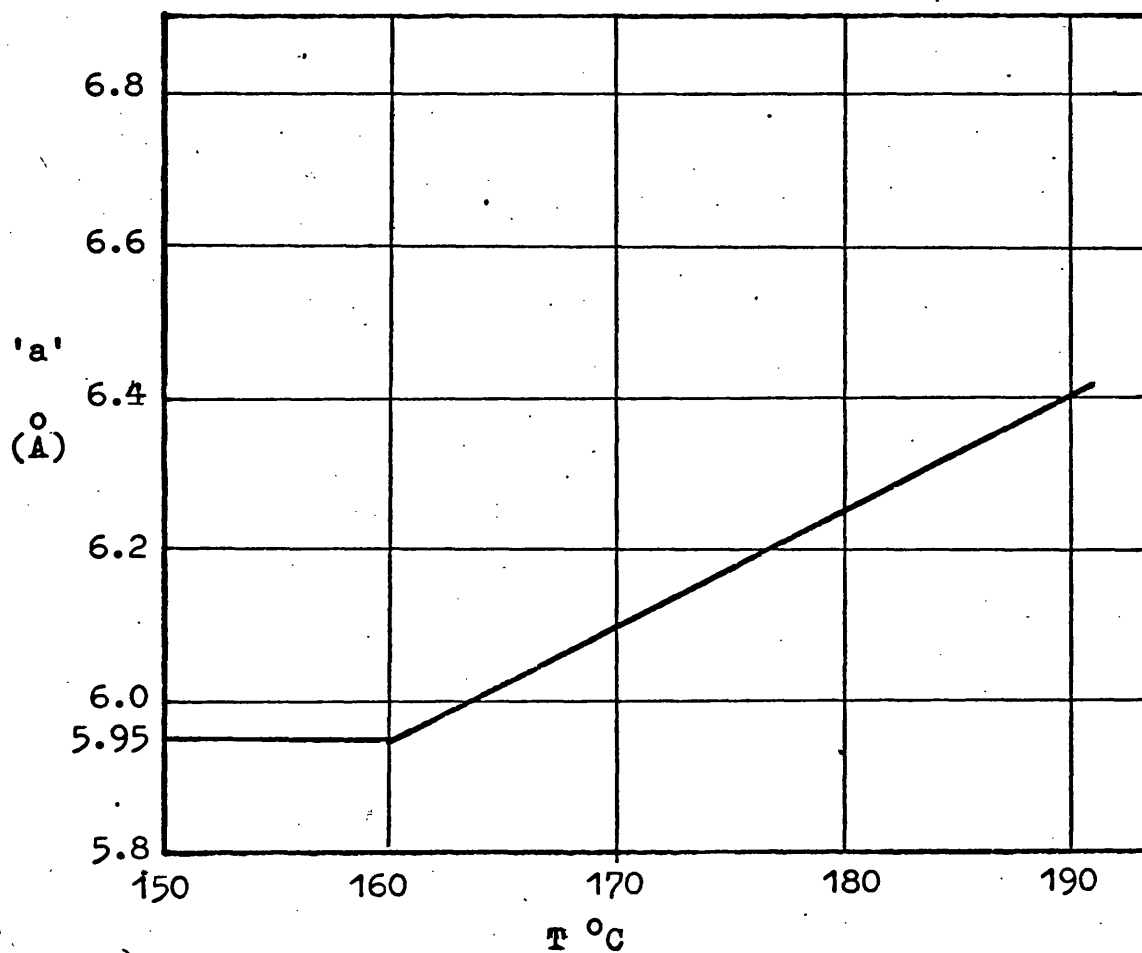


Fig. 6.2 : 'a', the distance between neighbouring S_8 ring molecules, is plotted against temperature with the data calculated from the temperature dependence of the number of S_8 rings in liquid sulphur in equilibrium with polymeric sulphur (Fig. 3.8).

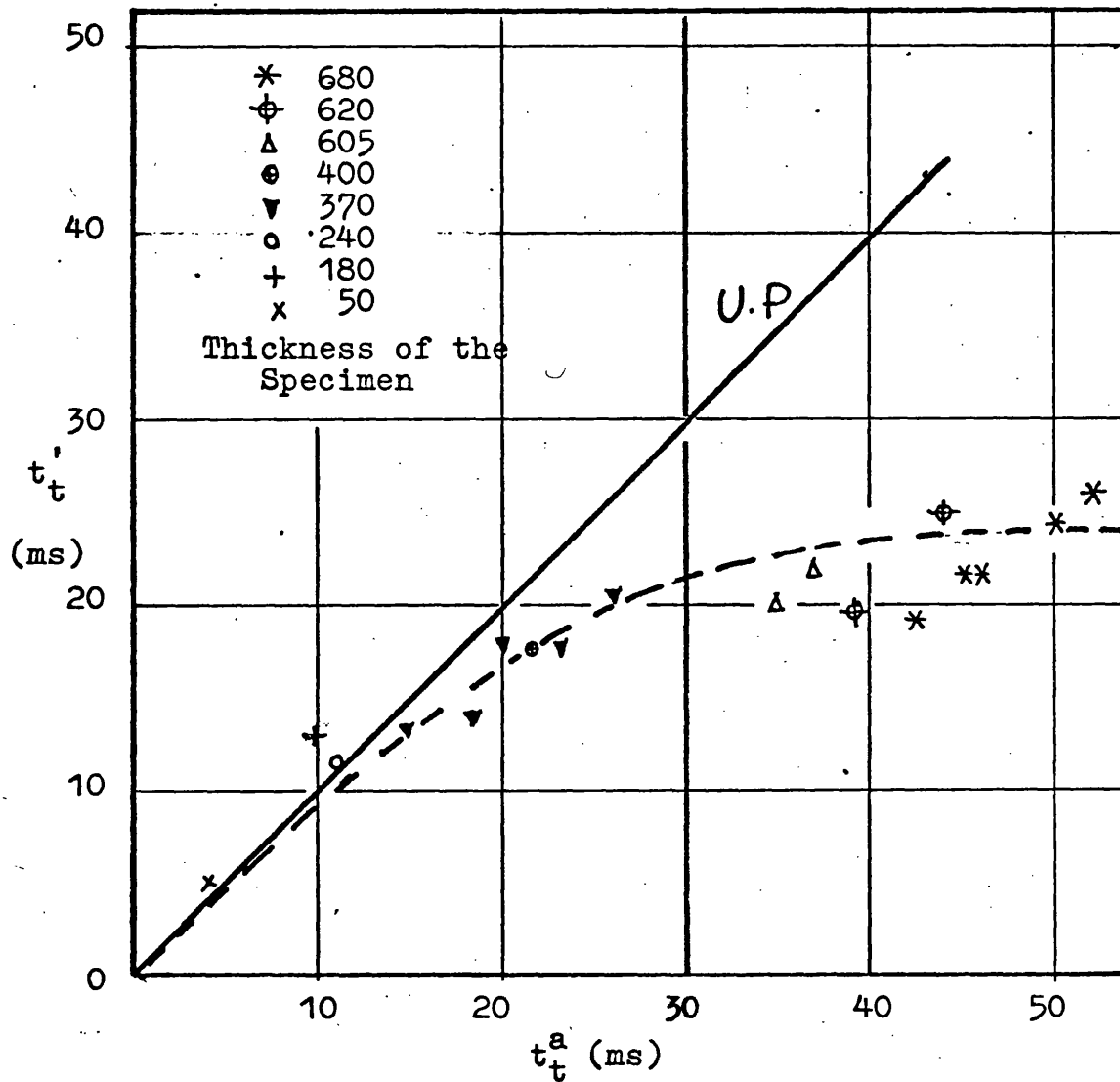


Fig. 6.3 : The true transit time t_t^a in ultrapure liquid sulphur is plotted against t_t in the laboratory reagent liquid obtained from Fig. 5.14 for specimens of widely different thicknesses.

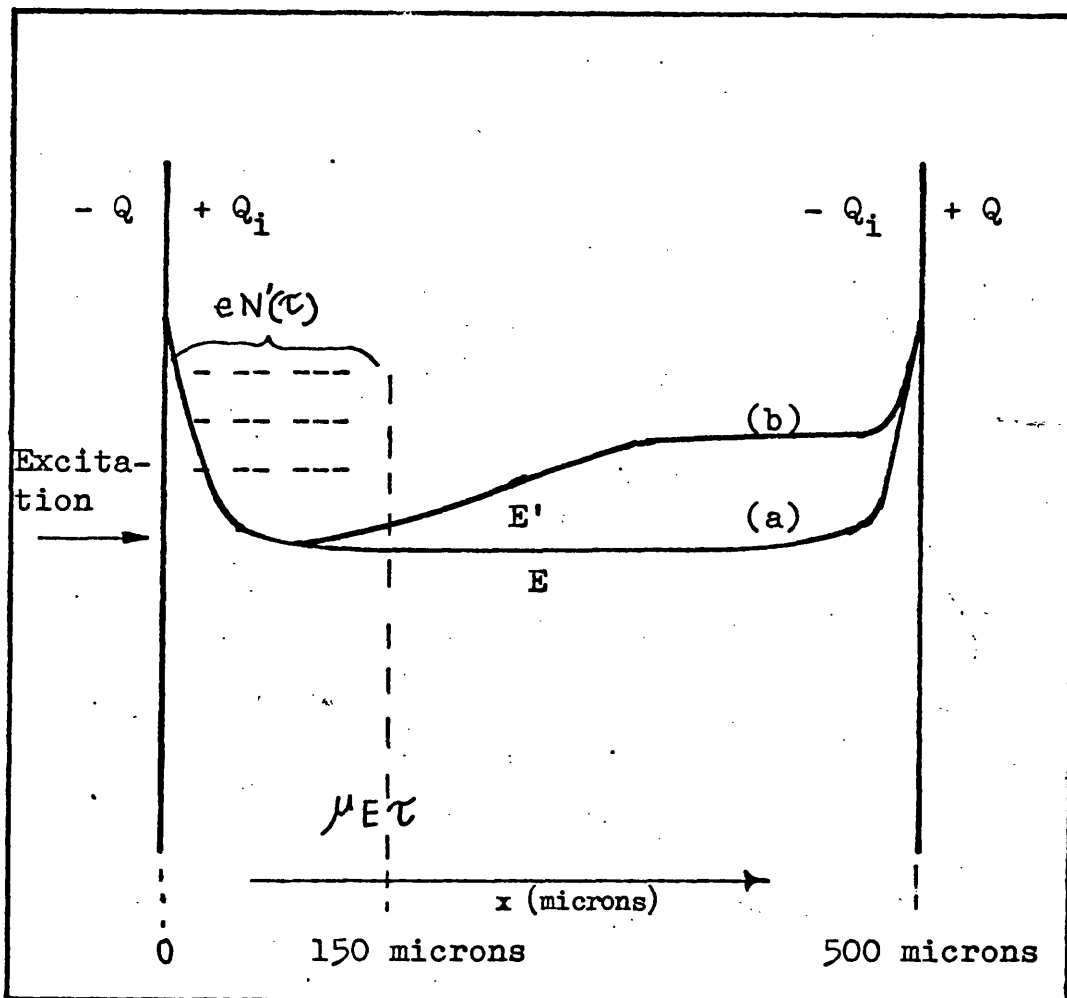


Fig. 6.4 : Field distribution in laboratory reagent liquid sulphur. (a) is the field distribution $E(x)$ that would be expected in a laboratory reagent specimen in the absence of excitation. When excess charge carriers are generated, the ions formed by carrier trapping will modify the field distribution to (b). Q - surface charge; Q_i - polarisation charge in the dark; $eN'(\tau)$ is the total number of ions up to time τ formed by trapping carriers (electrons) generated by optical excitation.

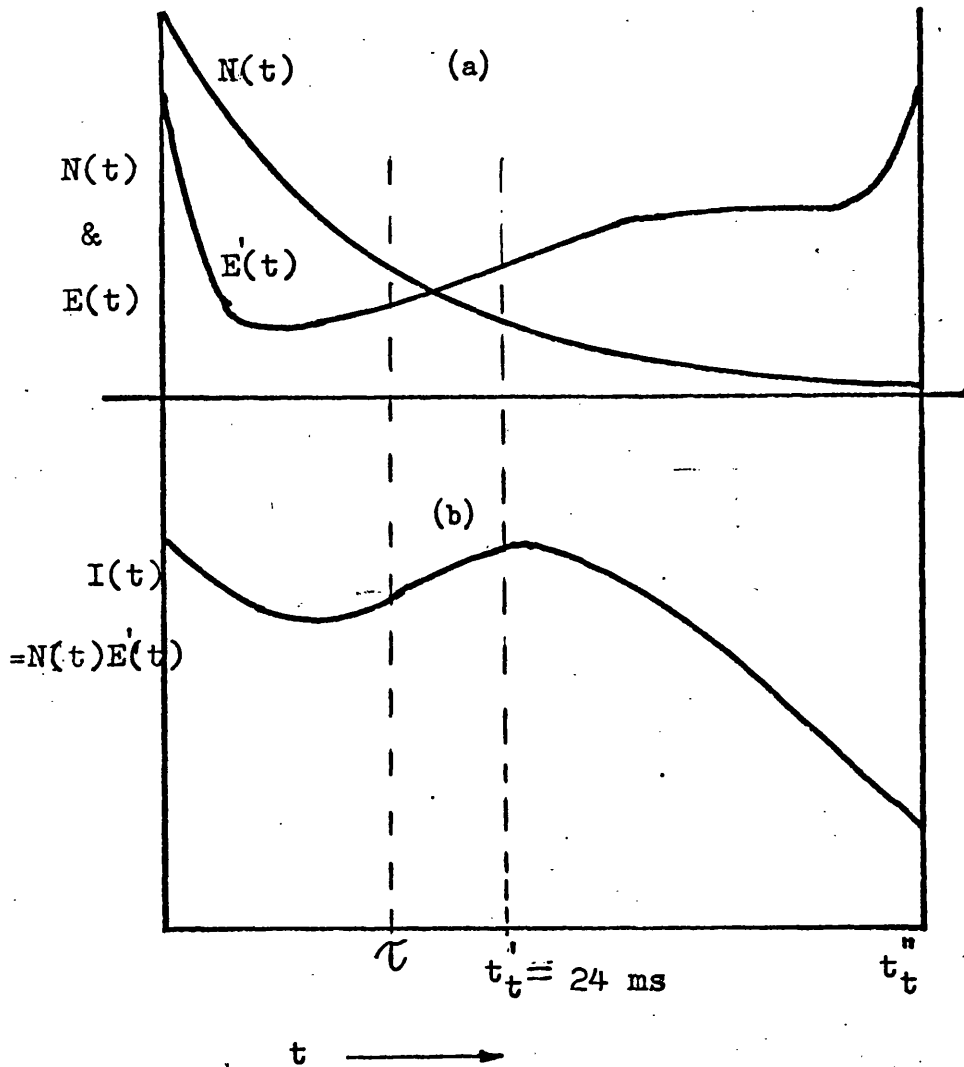


Fig. 6.5 : The number of excess fast carriers (electrons), $N(t)$ and the field distribution $E'(t)$ due to ionic space charge are plotted against time in the laboratory reagent liquid sulphur in (a). (b) shows the resulting current $I(t)$ due to the fast carriers. $I(t)$ is a function of the product $N(t) E'(t)$.

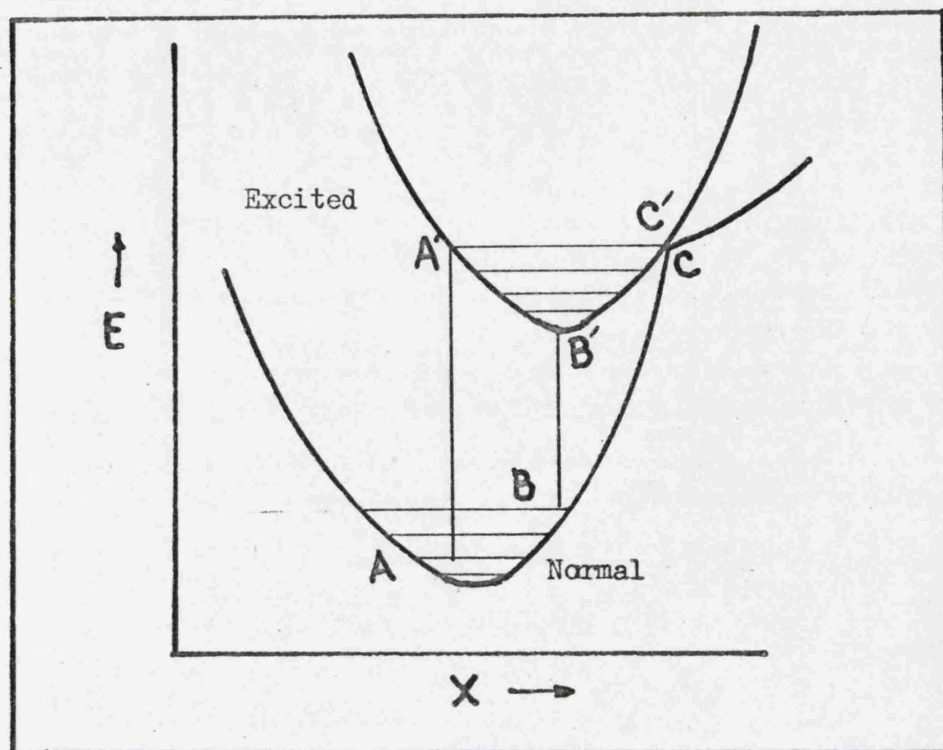


Fig. 7.1 : Potential energy configuration of a diatomic molecule in its normal and excited states.

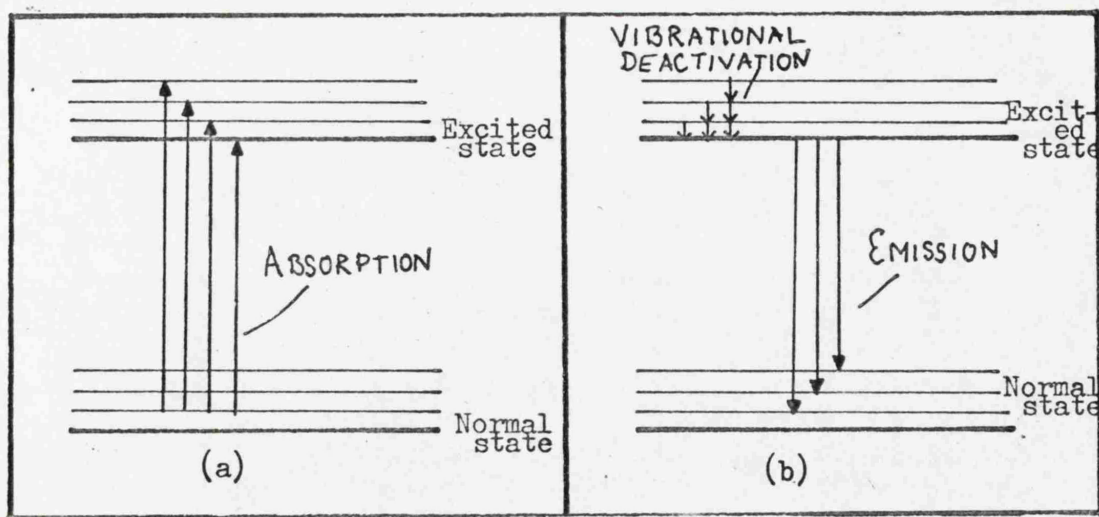


Fig. 7.2 : Schematic diagram of the energy state of the same molecule as above. (a) shows the transitions leading to absorption of light. (b) shows the transitions leading to emission.

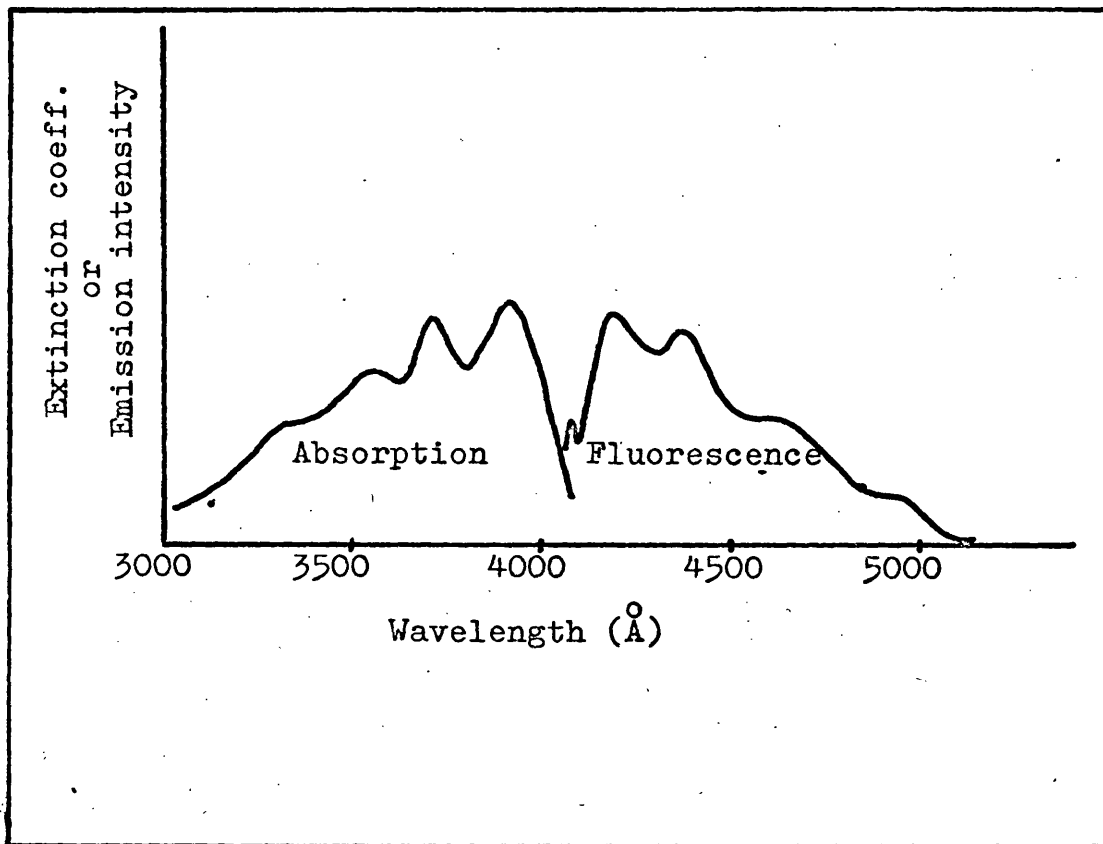


Fig. 7.3 : Absorption and emission spectra of solid anthracene (Ref. 63)

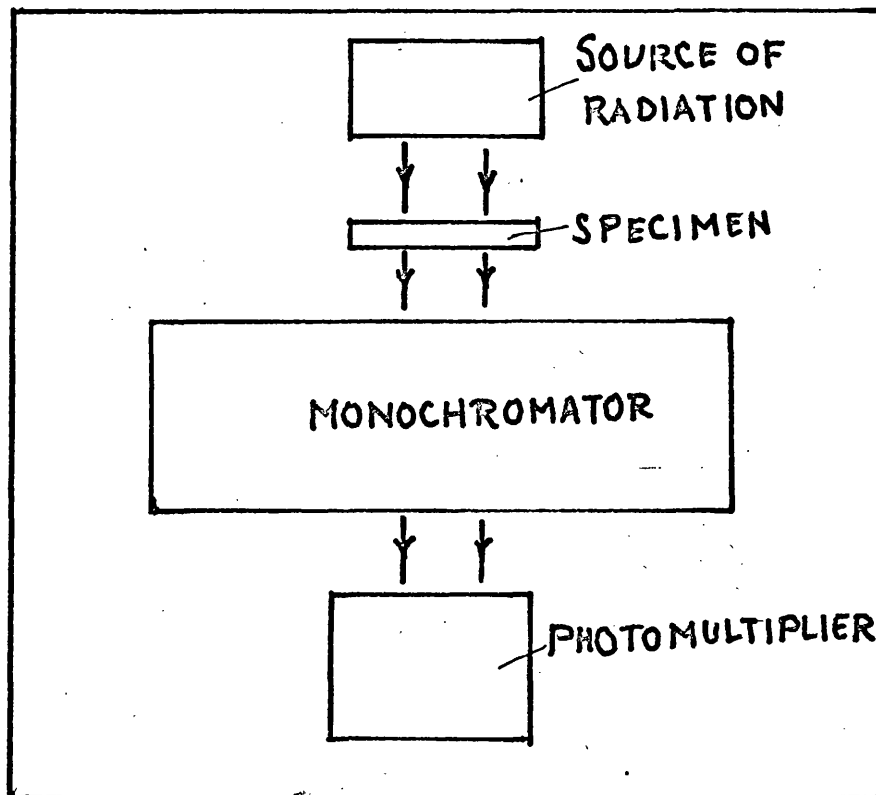


Fig. 7.4 : Block diagram of the experimental arrangement for the detection of sulphur emission.

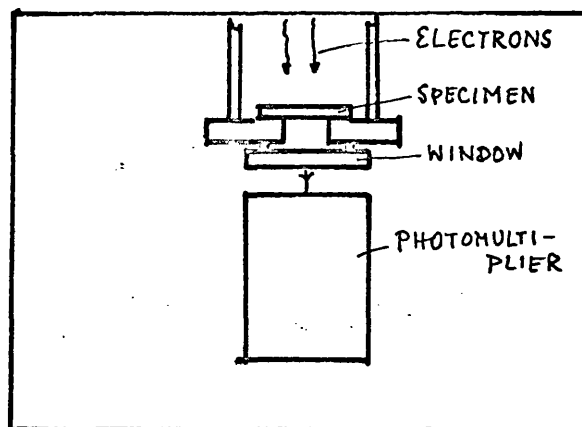


Fig. 7.5 : Arrangement for the excitation of sulphur by high energy electrons.

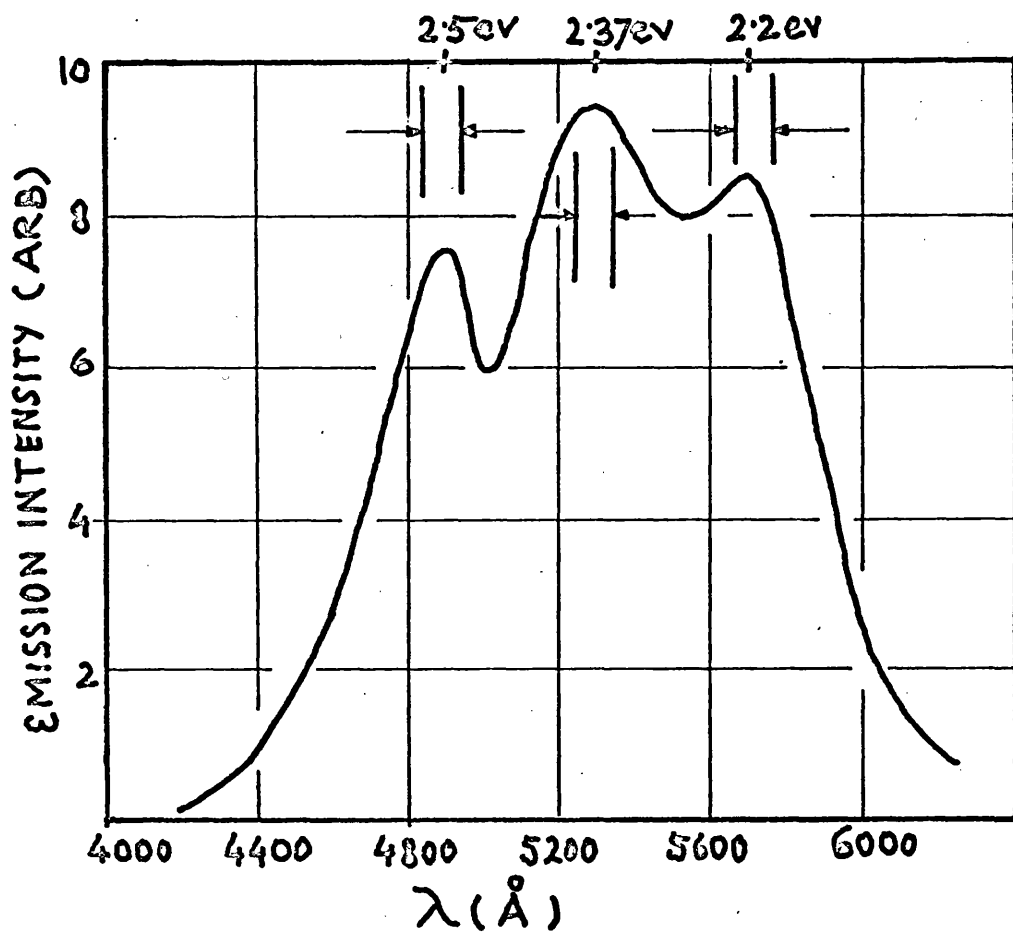


Fig. 7.6 : Emission spectrum of solid sulphur obtained experimentally by x - ray excitation. The spectral window of the dense flint prism monochromator (100 Å) is indicated.

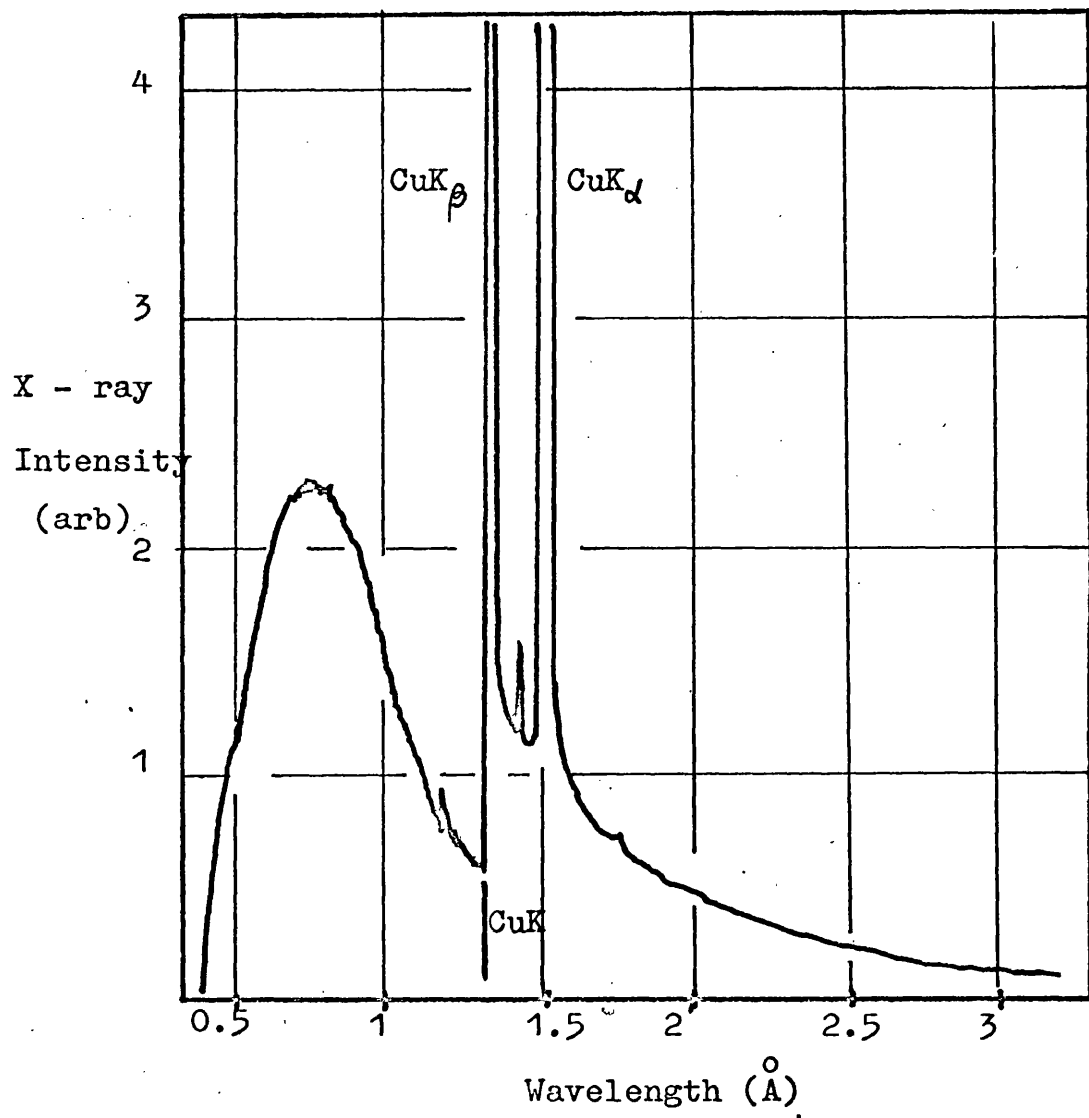


Fig. 7.7 : Spectrum of Cu target x - ray tube.

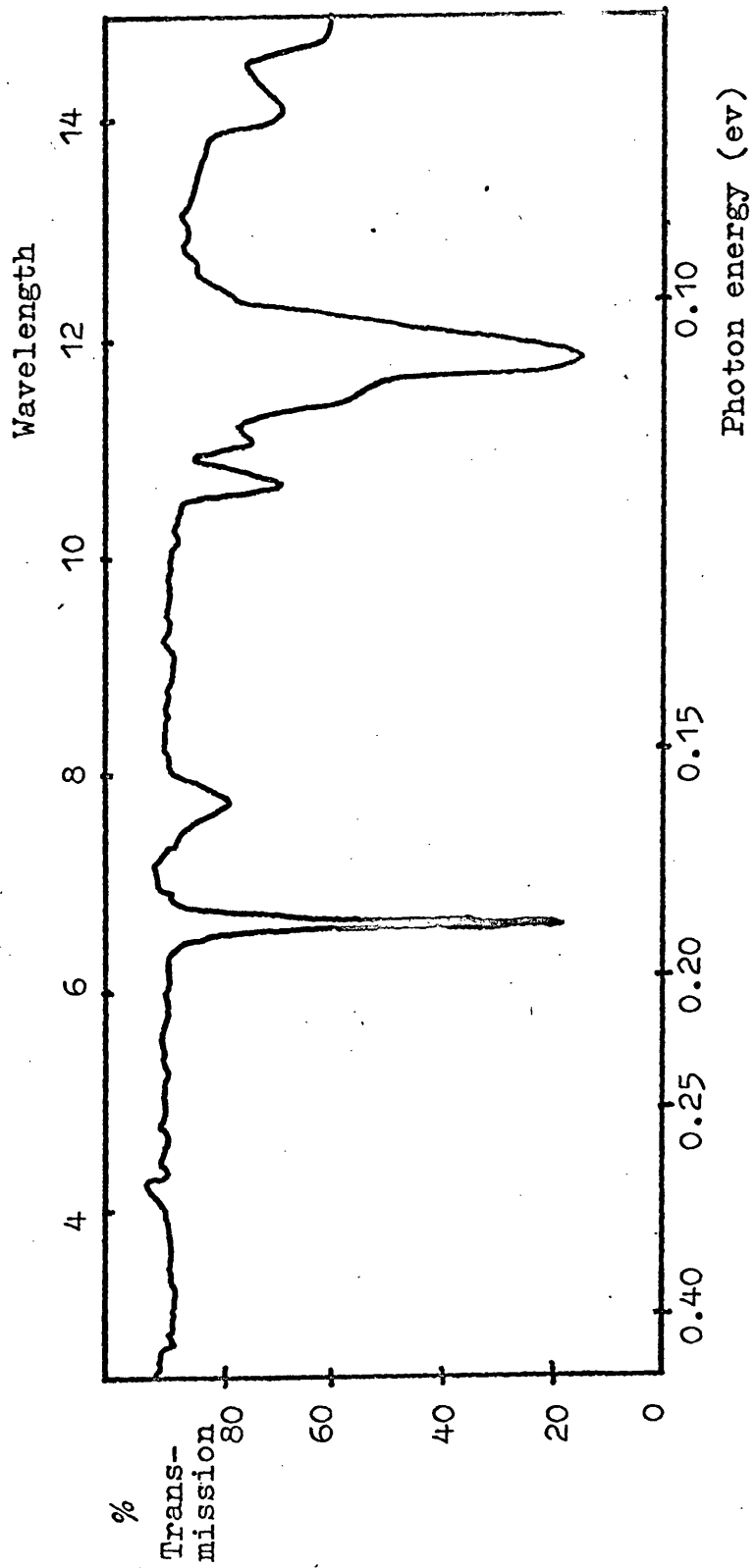


Fig. 7.8 : Infra - red transmission spectrum of sulphur crystal.

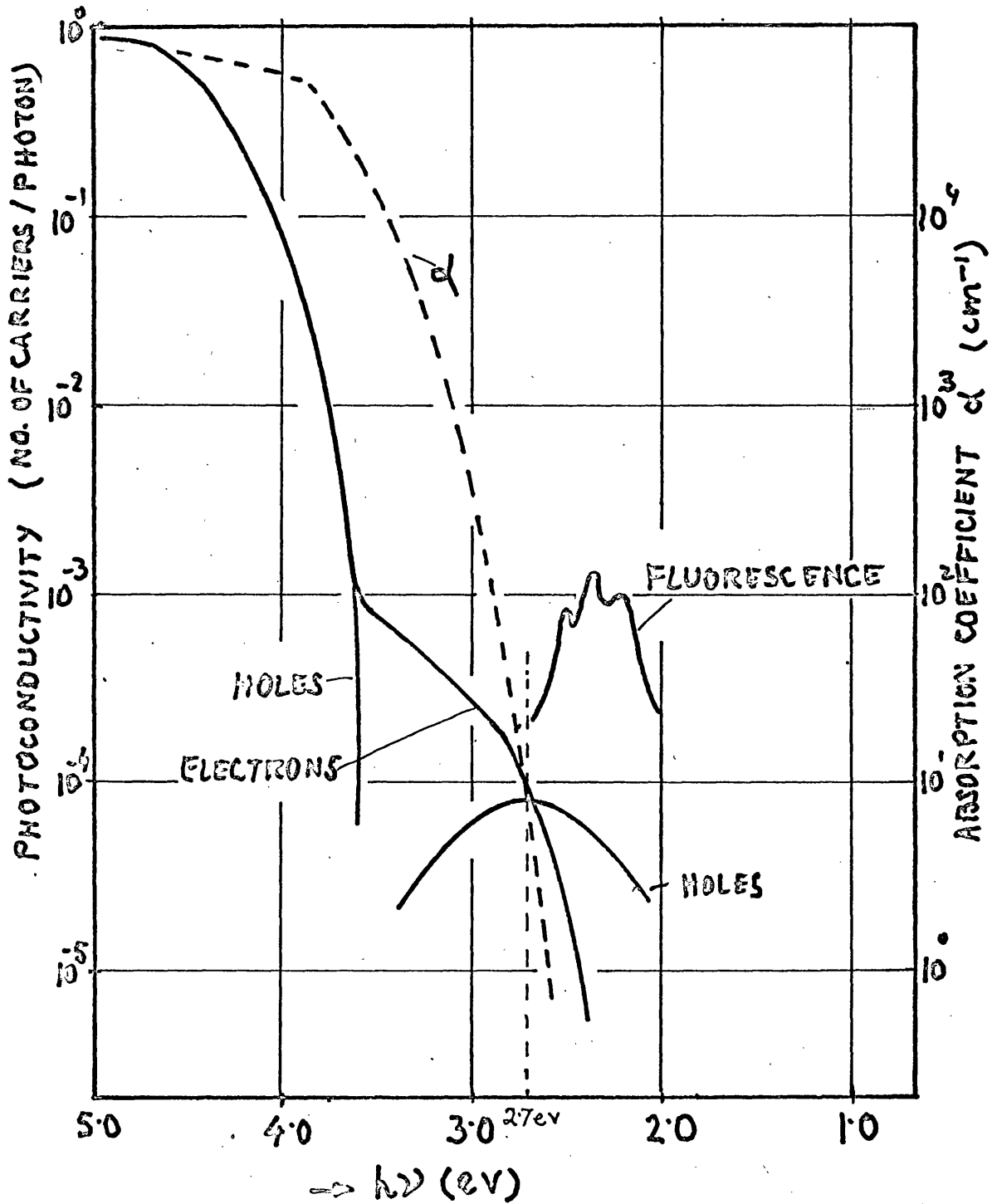


Fig. 7.9 : Photoconductivity and absorption coefficient of solid sulphur are shown with the emission spectrum to indicate the energy of the first excited state of S_8 at 2.7 eV and its association with the hole peak at about the same energy.

ABSTRACT

Specimens of liquid sulphur were obtained by melting orthorhombic sulphur crystals or ultrapure granules of sulphur. Between the melting point (119°C) and 160°C , liquid sulphur is composed of puckered S_8 ring molecules bound by weak van der Waal forces as in the solid. Above 160°C , polymerisation of ring molecules takes place. Drift mobility techniques have been used to study the charge transport during melting and in the liquid up to about 200°C . The specimen cell consisted of two parallel quartz discs separated by glass spacers, 50 to 700 microns thick. Transparent electrodes were applied to the inner surfaces of the discs. Charge carriers were generated close to one of the electrodes by a fast ultraviolet light pulse (~ 10 microsecond duration), and carriers of one polarity were drawn across the specimen in the applied field. Their transit time was measured giving a value for the drift mobility. The results showed that the charge transport is due to both negative and positive charges which move in the liquid by means of phonon - assisted random hopping between neighbouring molecules. From a detailed discussion of the results it is concluded that we are dealing here with an electronic, rather than an ionic charge transport. The electron and hole mobilities at the melting point are 1.0×10^{-4} and 5.5×10^{-5} $\text{cm}^2/\text{volt sec}$ respectively. ^{The} Electron mobility which is ^a hopping transport in the solid, shows a drop of a factor of 30 during change of state. This has been attributed to a decrease of overlap J by a fac-

tor of 5.5. Between 119°C and 160°C the electron mobility increases in the liquid with increasing temperature with an activation energy of 0.15 ± 0.03 ev. Holes have the same activation energy within a larger experimental error. Above 160°C both electron and hole mobilities decrease slowly with increasing temperature. This has been attributed to a decrease in the hopping probability resulting from a loss of ring molecules by polymerisation.

Dark current measurements on liquid sulphur suggested that in less pure specimens impurity ions set up a space charge near each electrode of opposite polarity to that of the electrode which modifies the current in accordance with Thomson's model of conduction in gases.

The measurement of the efficiency of carrier generation in liquid sulphur has been carried out at an applied field of 33 K volt/cm, considerably less than the saturation value. The results show that the ultraviolet photoconductivity reaches a peak at about 2600 \AA with a generation efficiency of 10^{-2} . The recombination lifetime of generated carriers has been estimated to be about 10^{-7} sec.

The visible emission of solid sulphur under x - ray excitation has been studied. The observed emission has an estimated efficiency between $10^{-4} - 10^{-6}$. Three emission peaks at 4900, 5300 and 5700 \AA have been detected. The emission is thought to be due to λ transitions from a molecular excited state, 2.7 ev above the ground state, to the singlet ground state of λ S_8 molecule.